Tectonics, climate, and mountain topography

Jean-Daniel Champagnac,[1] Peter Molnar,[2] Christian Sue,[3] and Frédéric Herman[1]

[1]   By regressing simple, independent variables that describe climate and tectonic processes against measures of topography and relief of 69 mountain ranges worldwide, we quantify the relative importance of these processes in shaping observed landscapes. Climate variables include latitude (as a surrogate for mean annual temperature and insolation, but most importantly for the likelihood of glaciation) and mean annual precipitation. To quantify tectonics we use shortening rates across each range. As a measure of topography, we use mean and maximum elevations and relief calculated over different length scales. We show that the combination of climate (negative correlation) and tectonics (positive correlation) explain substantial fractions (>25%, but <50%) of mean and maximum elevations of mountain ranges, but that shortening rates account for smaller portions, <25%, of the variance in most measures of topography and relief (i.e., with low correlations and large scatter). Relief is insensitive to mean annual precipitation, but does depend on latitude, especially for relief calculated over small (~1 km) length scales, which we infer to reflect the importance of glacial erosion. Larger-scale (averaged over length scales of ~10 km) relief, however, correlates positively with tectonic shortening rate. Moreover, the ratio between small-scale and large-scale relief, as well as the relative relief (the relief normalized by the mean elevation of the region) varies most strongly with latitude (strong positive correlation). Therefore, the location of a mountain range on Earth with its corresponding climatic conditions, not just tectonic forcing, appears to be a key factor in determining its shape and size. In any case, the combination of tectonics and climate, as quantified here, can account for approximately half of the variance in these measures of topography. The failure of present-day shortening rates to account for more than 25% of most measures of relief raises the question: Is active tectonics overrated in attempts to account for present-day relief and exhumation rates of high terrain?

1.   Introduction

[2]   The topography of mountain ranges results from both tectonic processes that elevate the Earth's surface with the rock beneath it, and erosive processes, which depend on climate among several factors (Figure 1). Understanding how tectonics and climate affect topography remains convoluted in part because of the interactions and feedbacks among them and because of the various processes that may affect erosion rates. Perhaps most obvious is the effect of isostatic balance on an eroding landscape. First, the removal of material alters vertical normal stress, and hence the deviatoric stress, which in turn alters the distribution of tectonic deformation [e.g., *Dahlen and Suppe*, 1988]. Second, and simultaneously, uneroded rock rises to compensate for the rock removed, so that as valleys deepen, adjacent ridges and peaks can rise to create more relief, which then facilitates accelerated erosion [e.g., *Holmes*, 1944, 1965; *Wager*, 1937].

[3]   A long tradition in geomorphology associates landscapes with some form of equilibrium, which introduces a second difficulty in understanding how climate and tectonics affect landscapes. As *Strahler* [1950] pointed out, a state of equilibrium underlies the concept of a "graded stream"; *Leopold and Maddock* [1953] used the term "quasi equilibrium," and *Hack* [1960] "dynamic equilibrium." In a state of equilibrium, however, neither cause nor effect can be assigned to any of the constituent parts. Accordingly, insofar as the landscape represents the interface of an equilibrium between tectonic and erosive processes, one cannot assign "cause" to either tectonics or climate (Figure 1), and attempts to determine the extent to which climate or tectonics is responsible for a landscape cannot merely consider the state of a landscape in its present-day tectonic setting and climate [e.g., *Molnar*, 2009]. In principle the landscape will evolve so as to balance the supply of rock provided by tectonic

---
[1]Department of Earth Sciences, Geological Institute, Swiss Federal Institute of Technology, Zürich, Switzerland.
[2]Department of Geological Sciences, Cooperative Institute for Research in Environmental Science, University of Colorado at Boulder, Boulder, Colorado, USA.
[3]Laboratoire Chrono-Environnement, UMR 6249, Université de Franche-Comté, Besançon, France.

Lithosphere   Atmosphere

TECTONICS   6   EROSION & DEPOSITION   1   CLIMATE
          2   10
   3   7   9   5   8
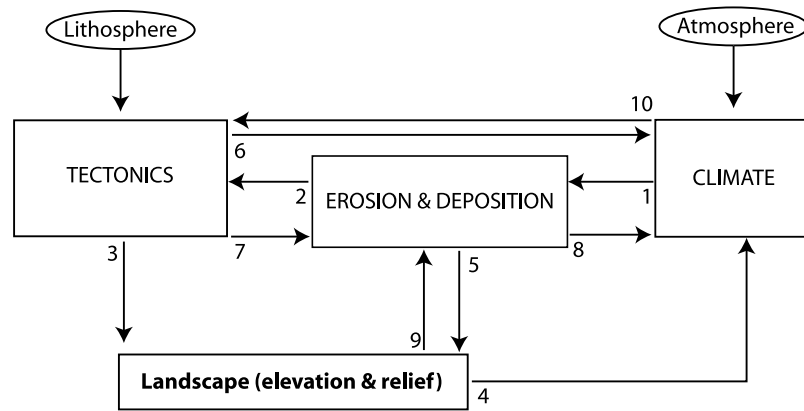   Landscape (elevation & relief)   4

Figure 1. Schematic sketch of the links between the lithosphere and the atmosphere displaying the relationship between tectonics, climate, erosion and the landscape. Many have explored the effect of climate on erosion and landscape, and erosion on tectonics (links 1, 2 and 5). [*Avouac and Burov*, 1996; *Beaumont et al.*, 1992; *Bonnet et al.*, 2007; *Burbank*, 2002; *Grujic et al.*, 2006; *Molnar*, 1990; *Montgomery and Brandon*, 2002; *Roe et al.*, 2008; *Whipple and Meade*, 2006; *Willett et al.*, 1993], and most agree that erosion modifies the pattern of deformation (link 2) [*Beaumont et al.*, 2001; *Calais et al.*, 2010; *Champagnac et al.*, 2008; *Dahlen and Suppe*, 1988; *Herman et al.*, 2010b; *Konstantinovskaia and Malavieille*, 2005; *Koons et al.*, 2003; *Willett et al.*, 1993]. Erosion also affects the thermal structure of the crust [*Batt and Braun*, 1997; *Grasemann and Mancktelow*, 1993; *Stüwe et al.*, 1994; *Zeitler et al.*, 2001] and the mean crustal thickness, which in isostatic equilibrium dictates the maximum elevation of mountain ranges (link 3) [*Abbott et al.*, 1997; *Holmes*, 1965; *Molnar and England*, 1990; *Montgomery*, 1994; *Small and Anderson*, 1998; *Stern et al.*, 2005; *Wager*, 1937; *Whipple et al.*, 1999]. The topography, in turn, affects the climate (link 4) by modifying the atmospheric circulation [*Hoskins and Karoly*, 1981; *Kasahara et al.*, 1973], orographic precipitation [*Roe et al.*, 2002], and global climate [e.g., *Seager et al.*, 2002]. The idea that glacial and peri-glacial condition are able to modify the distribution of the surface elevation and limit the topography of a mountain range (link 5) is as old as *Penck* [1905], later formalized by [*Brocklehurst and Whipple*, 2004; *Broecker and Denton*, 1989; *Brozović et al.*, 1997; *Montgomery et al.*, 2001; *Porter*, 1977; 1989], and named the "glacial buzzsaw" by B. L. Isacks in 1992 [e.g., *Egholm et al.*, 2009; *Mitchell and Montgomery*, 2006; *Spotila et al.*, 2004]. The other links are not directly addressed in this paper, and are the direct tectonic effect on the climate (e.g., volcanism, link 6, [*Zielinski*, 2000]) and on the erosion itself (link 7) by fracturing of rock [*Clarke and Burbank*, 2011; *Dühnforth et al.*, 2010; *Molnar et al.*, 2007], and earthquake-triggered landslides [e.g., *Dadson et al.*, 2003; *Parker et al.*, 2011]. The direct effects of erosion/sedimentation on climate through chemical weathering and carbon burial are depicted by link 8 [*Hay*, 1996; *Volk*, 1987], and the most direct effect of the landscape on erosion is the slope/erosion relationship (link 9) [*Ahnert*, 1970; *Burbank et al.*, 1996; *Dietrich et al.*, 2003; *Montgomery and Brandon*, 2002; *Portenga and Bierman*, 2011; *Roering et al.*, 2007]. Finally, climate affects tectonics by loading or unloading the lithosphere (link 10) [*Bettinelli et al.*, 2008; *Bollinger et al.*, 2010; *Doser and Rodriguez*, 2011; *Hampel et al.*, 2007].

processes and the removal by erosive processes that are intertwined with the prevailing climate [*Beaumont et al.*, 1992; *Dahlen and Suppe*, 1988; *Garcia-Castellanos*, 2007; *Koons*, 1990; *Roe et al.*, 2008; *Willett*, 1999; *Willett and Brandon*, 2002]. How landscapes evolve, however, depends not only on the boundary conditions imposed by tectonics, climate, and their interaction through erosion, but also on how these boundary conditions change with time. Accordingly, a landscape that is not in such a state of equilibrium may owe its morphology more to recent changes in tectonics or in climate than to the states that characterize the present-day (or past 10^4, 10^5, or 10^6 years). In such case, neither climate nor tectonics should be seen as the cause of a landscape, but a change in climate or tectonics can be such a cause.

[4] To understand how climate and tectonics affect the topography of a region, as well as the rates of the erosive processes that shape that topography, two logical strategies present themselves. First, one may quantify changes that have occurred to a landscape and relate them to known changes in either tectonics or climate. Doing so, however, is difficult, because only rarely can we fully quantify changes in the landscape, tectonics, and climate. Second, one may compare regions with different tectonics and different climates and seek correlations with measures of topography and relief that make physical sense. For example, one might imagine that regions with highest rainfall will have the most relief, because of rapid incision, or the least relief, because erosion would remove rock more rapidly than tectonics can supply it. As another example, perhaps regions of rapid horizontal shortening and crustal thickening would show the maximum topography, at least by some sensible measure. We take a first step toward implementing this second approach.

[5] Of course, we are by no means the first to consider the relative roles played by tectonics and climate, or by climate change, in shaping the landscape or altering erosion rates.

Following the insights of *Dahlen and Suppe* [1988], others have sought quantitative understanding of the links among tectonics, climate, and erosion [e.g., *Beaumont et al.*, 1992; *Roe et al.*, 2008; *Stolar et al.*, 2006; *Whipple and Meade*, 2006; *Willett*, 1999]. Most tests of these theoretical inferences using natural data, however, have considered only one (or at most a few different) mountain range(s). For instance, thanks to its very active tectonics, high precipitation gradient and rate, and the occurrence of large temperate glaciers, the South Island of New Zealand was one of the first cases studied [*Adams*, 1980; *Kirkbride and Matthews*, 1997; *Koons*, 1990; *Wellman*, 1979]. In the Andes, *Montgomery et al.* [2001] and *Strecker et al.* [2007] addressed the question of whether climatic or geodynamic processes are more important in shaping that landscape, and concluded that climate has a major impact on the landscape and possibly on the tectonic evolution, but many working in the Central Andes have attributed deep incision to surface uplift beginning near or since 10 Ma [*Barke and Lamb*, 2006; *Hoke et al.*, 2007; *Kober et al.*, 2006; *Schildgen et al.*, 2007; *Schlunegger et al.*, 2006; *von Rotz et al.*, 2005]. Based on Late Pleistocene erosion rates calculated from riverborne cosmogenic [10]Be in SE Tibet, *Henck et al.* [2011] recently postulated that the tectonic setting is more prominent than rainfall or relief to explain erosion rates, but the same method led *Moon et al.* [2011] to the opposite conclusion for the Washington Cascades, where denudation scales with precipitation rate. Several studies have attempted to provide a global (i.e., worldwide) view of the relationship of Earth's topography to snow lines and glaciations [*Broecker and Denton*, 1989; *Egholm et al.*, 2009; *Pedersen et al.*, 2010; *Porter*, 1977], to links between climate and erosion [*Molnar*, 2004; *Willenbring and von Blanckenburg*, 2010; *Zhang et al.*, 2001], to relationships between relief and erosion [*Ahnert*, 1970; *Dietrich et al.*, 2003; *Montgomery and Brandon*, 2002; *Portenga and Bierman*, 2011; *Simoes et al.*, 2010; *von Blanckenburg*, 2005], and to relationships linking all of climate, topography, and erosion [*Pinet and Souriau*, 1988], but to the best of our knowledge, none has tried to relate topography to quantitative measures of both climate and tectonics.

[6] Based on a worldwide data set of mountain belts and regions of high terrain, we attempt to quantify the relative contributions of tectonic and climatic processes in shaping the topography of mountain ranges. We use multiparameter analyses of 69 ranges worldwide distributed over five continents (Figure 2). Our goals include examining plausible general rules that govern average shapes and heights of mountain ranges and presenting a set of data and statistical analyses that will enable readers to decide whether they think that, by some definition, tectonics or climate plays the more important role in shaping the landscape. Although we note a few exceptional or peculiar cases, we try to avoid discussions of specific, individual belts or regions or of detailed processes, either of which could lead to endless digression.

2. Methodology

[7] We considered a set of 69 mountain belts or otherwise high terrain distributed worldwide (Table 1) regardless of their "tectonic ages" (as defined by *Pedersen et al.* [2010]), tectonic setting, the properties of rock exposed at the surface

(in particular the erodibility), or the rheological properties of the crust and mantle lithosphere. We discarded ranges that are obviously high because they overlie hot upper mantle and those with a significant contribution of volcanism to high elevations (e.g., Yellowstone, Cordillera Neovolcanica de Mexico, Japan, etc.). We also discarded mountain ranges related to active extension (e.g., East African Rift system), but we included several inactive regions for which topography may (at least partly) result from rift shoulder tumescence (e.g., Corsica, Australian Alps, Norway, etc.). Finally, we discarded belts with small topographic expression (like the Central Australian Range or the Belgian Ardennes) and avoided mountain ranges with large ice cover (e.g., the Transantarctic Mountains) that would have precluded a proper topographic analysis. For each individual mountain belt, we first determined meaningful boundaries, and we split long belts (e.g., Andes, Himalaya, Tien Shan, etc.) into separate segments, according to geological, hydrographic, or topographic boundaries. For every range, we empirically determined a base level ("BL" in the following, Table 1), above which further calculations have been made, in order to remove large-scale topography that presumably is supported by a hot upper mantle. In the case of asymmetric ranges with different base levels on each side (Himalaya, Qilian Shan, Sierra Nevada, etc.) we determined the two base levels and used their average as BL. For most ranges the base level is close to sea level; for 48 (70%) of 69 ranges, BL < 500 m above sea level (a.s.l.) (Figure A1), but for some it is locally much higher (e.g., ~2000 m in the western United States, or >2000 m in the Himalaya).

[8] For each range, we compiled topographic, climate, and tectonic variables, discussed below (Table 1). Comprehensive statistical analyses require that the degree of knowledge of each parameter be homogeneous. Therefore, we used tectonic, climatic, and topographic parameters that are known with approximately the same accuracy for each mountain ranges, and we ignored parameters that may be more pertinent locally, but poorly known for other ranges, such as thickness of deforming layer (thin- versus thick-skinned tectonics), rock type at the surface, or total shortening that has occurred since the range started to form.

2.1. Topographic Variables

[9] These variables can describe either "elevation" or "relief" (Figure 3). Elevation variables quantify the "presence" of rock above the chosen base level. Relief parameters document the "lack" of rock, due either to "gaps" between tectonic structures or to incision and erosion of material from valleys. Both have been calculated from the Digital Elevation Model (DEM) SRTM30 Plus V6.0 (http://www.dgadv.com/srtm30/), with a pixel dimension of 30″ (~925 m at the equator) [*Becker et al.*, 2009; *Farr et al.*, 2007]. Calculations have been made within the boundaries determined for each range, and above the base level, BL (Figure 2 and Table A1).

[10] Elevation variables are (1) the maximum elevation of range (E_{max}), calculated by isolating the highest elevation of the topography smoothed over sliding window with a 10-km radius (to remove the effect of a high isolated local peak); E_{max} is meant to represent the mean crestline elevation of the range; and (2) the mean elevation of the range (E_{mean}). For most analysis, we use the difference between E_{mean} and the height of regional base level BL, $E_{mean} - BL$, to eliminate
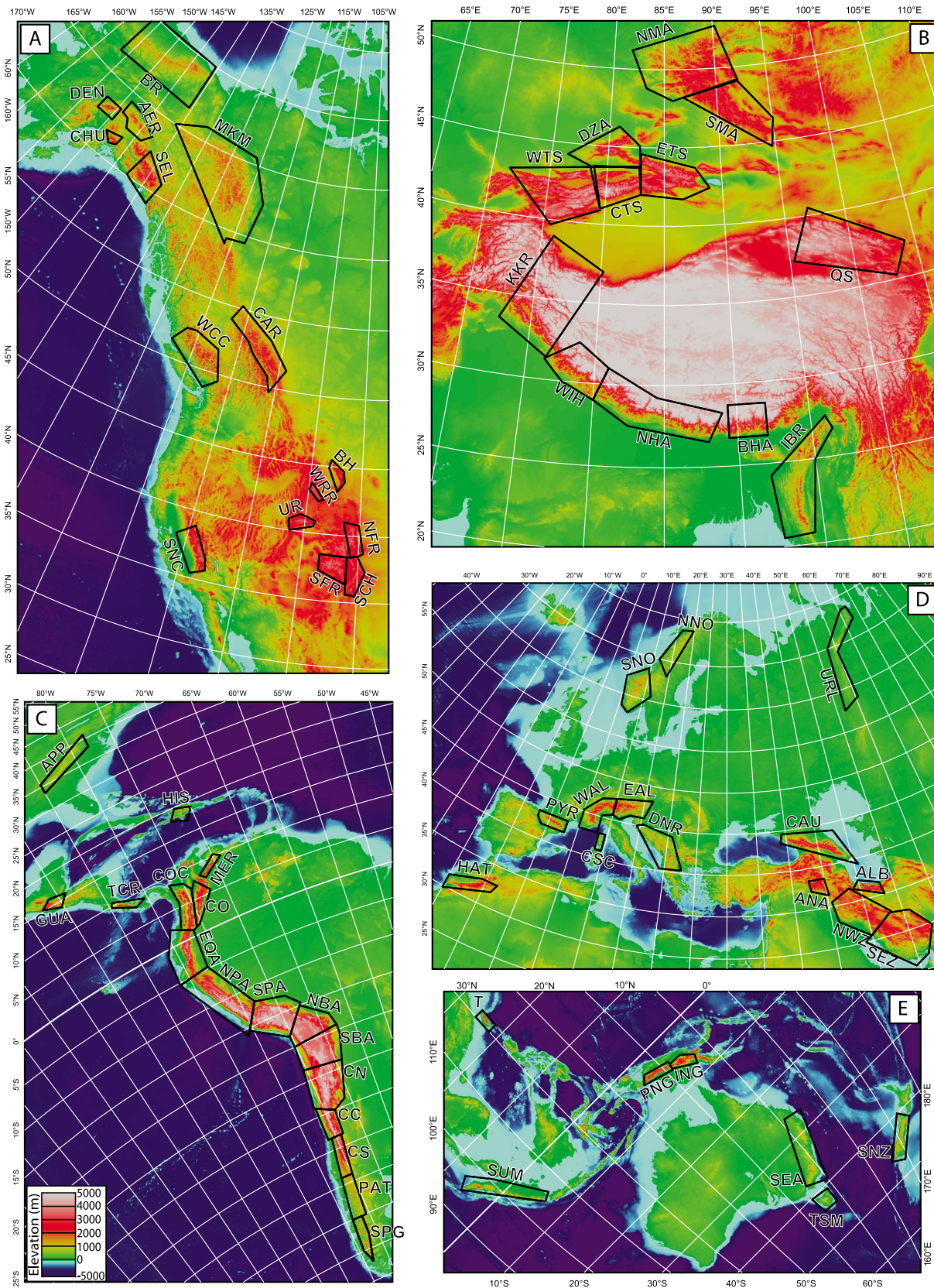
Figure 2. Maps of mountain ranges studied (black polygons and letters codes) on ETOPO DEM (2′ resolution). Note that calculations have been made within these polygons and above base level ("BL") specified in Table 1. The Verkhoyansk Range (VKH) in eastern Russia, as well as Southern India (SI) and Sri Lanka (SL) are not pictured.

Table 1. Schematic Sketch of the Links Between the Lithosphere and the Atmosphere[a]

Range	Code	V_h	Error	Precip	Error	Coslat	E_{max}	$E_{mean} - BL$	GR1	GR5	GR15	nGR1	nGR5	nGR15	GR15/GR1	m
Alaska (Chugach)	CHU	20	5	1126	511	0.477	2603	1187	269	766	1831	0.227	0.645	1.543	6.802	0.426
Alaska (Denali)	DEN	4.1	2.4	512	111	0.454	3470	959	231	726	1889	0.241	0.757	1.968	8.171	0.466
Alaska (Eastern Range)	AER	2	1	320	54	0.448	2236	773	168	510	1291	0.217	0.660	1.670	7.696	0.453
Alaska (Saint Elias)	SEL	41	5	1698	1200	0.491	3444	1072	340	762	1495	0.317	0.710	1.394	4.400	0.329
Alborz	ALB	6	2	604	300	0.809	3320	2179	258	640	1365	0.119	0.294	0.626	5.286	0.370
Alps (Eastern)	EAL	2.2	1	1133	276	0.689	2896	969	223	566	1231	0.230	0.584	1.270	5.519	0.379
Alps (Western)	WAL	0	1	1085	281	0.704	2995	1035	207	546	1228	0.200	0.527	1.186	5.940	0.396
Anatolia	ANA	4.4	0.5	566	128	0.773	3112	1006	219	550	1187	0.217	0.546	1.179	5.430	0.376
Andes (Northern Bolivian)	NBA	6	2	890	958	0.951	4833	2629	104	323	833	0.040	0.123	0.317	8.018	0.462
Andes (Northern Peru)	NPA	6	2	1087	883	0.986	5018	2131	99	370	1112	0.046	0.173	0.522	11.266	0.538
Andes (Southern Bolivia)	SBA	8	3	362	346	0.931	5309	2679	76	272	786	0.028	0.101	0.293	10.323	0.518
Andes (Southern Peru)	SPA	6	2	1063	1178	0.967	5053	3025	166	420	912	0.055	0.139	0.302	5.489	0.378
Appalachians	APP	0	1	1197	176	0.799	1297	338	77	212	495	0.228	0.628	1.463	6.424	0.413
Australia (Southeastern)	SEA	0	1	837	245	0.844	1402	445	33	113	316	0.075	0.255	0.710	9.532	0.501
Baffin	BAF	0	1	223	19	0.332	1628	528	289	603	1117	0.546	1.143	2.115	3.870	0.300
Big Horn (Wyoming)	BH	0	1	309	61	0.715	3177	944	95	294	753	0.101	0.311	0.798	7.917	0.459
Brooks Range (Alaska)	BR	1	2	240	76	0.451	1936	683	145	386	876	0.212	0.566	1.283	6.056	0.400
Canadian Cordillera (Western)	WCC	3.3	1.5	1218	677	0.630	2375	1040	249	583	1186	0.240	0.561	1.141	4.761	0.346
Caucasus	CAU	8	2	796	447	0.737	3426	1097	165	484	1189	0.150	0.441	1.083	7.203	0.438
Chile (33°S–39°S)	CS	1	2	771	409	0.807	5597	1391	177	513	1242	0.128	0.369	0.893	7.001	0.432
Chile (Central, 30°S–33°S)	CC	3	2	176	82	0.854	5613	1934	163	513	1337	0.084	0.265	0.691	8.223	0.468
Chile (Northern, 23°S–30°S)	CN	4	2	290	321	0.906	5625	2516	101	380	1145	0.040	0.151	0.455	11.307	0.538
Cordillera de Merida (Venz.)	MER	5	2	1565	450	0.988	3805	1336	128	465	1363	0.096	0.348	1.020	10.659	0.525
Cord. Occ./Centr. (Colomb.)	COC	0	3	2683	1182	0.997	4050	1348	143	460	1216	0.106	0.341	0.902	8.486	0.475
Cordillera Oriental (Colombia)	COR	8	5	2215	796	0.997	3693	1422	135	429	1125	0.095	0.302	0.791	8.305	0.470
Corsica	CSC	0	2	763	120	0.743	1472	557	158	493	1275	0.284	0.885	2.288	8.065	0.463
Dinarides	DNR	4.5	1	1056	347	0.731	1932	601	120	357	887	0.200	0.594	1.475	7.380	0.444
Ecuadorian Andes	EQA	6	3	1770	1044	1.000	4182	1705	147	461	1198	0.086	0.271	0.703	8.160	0.466
Front Range (S. Colorado)	SFR	0	2	488	140	0.792	3663	947	125	345	801	0.132	0.364	0.845	6.384	0.412
Guatemala Ranges	GUA	6	2	2469	952	0.965	3116	1244	125	405	1080	0.100	0.325	0.868	8.644	0.479
High Atlas	HAT	0.7	0.6	297	115	0.857	3496	1103	168	456	1049	0.153	0.414	0.951	6.233	0.406
Himalayas (Bhutan)	BHA	17	3	1494	983	0.886	5847	973	231	631	1464	0.237	0.649	1.504	6.349	0.410
Himalayas (Nepal)	NHA	19	2.5	1480	632	0.876	6403	554	213	645	1625	0.385	1.164	2.930	7.613	0.451
Himalayas (Western India)	WIH	19	3	1392	379	0.859	6414	665	223	604	1385	0.336	0.908	2.081	6.197	0.405
Hispaniola	HIS	7	4	1144	245	0.949	1951	738	105	352	963	0.143	0.477	1.305	9.133	0.491
Indoburman Ranges	IBR	8	2	2453	711	0.913	1718	809	145	410	974	0.180	0.507	1.203	6.699	0.422
Karakorum	KKR	15	5	482	550	0.817	2673	2668	225	611	1405	0.084	0.229	0.527	6.244	0.407
McKenzie Mountains (Canada)	MKM	5	5	376	76	0.456	3568	785	116	356	912	0.147	0.454	1.163	7.892	0.459
Mongolian Altai (northern)	NMA	4	2	401	189	0.624	2065	1012	147	407	956	0.145	0.403	0.945	6.526	0.416
Mongolian Altai (southern)	SMA	4	2	121	30	0.681	3543	1160	108	346	918	0.093	0.298	0.791	8.524	0.476
New Guinea (Eastern)	PNG	15	5	3173	691	0.995	3105	1305	110	431	1343	0.084	0.330	1.029	12.185	0.555
New Guinea (Western)	WNG	27	5	3456	1228	0.997	3632	1307	100	401	1277	0.076	0.307	0.977	12.769	0.565
Norway (northern)	NNO	0	1	939	348	0.400	1445	570	129	362	856	0.227	0.636	1.503	6.621	0.420
Norway (southern)	SNO	0	1	1278	644	0.491	1718	716	127	281	544	0.178	0.392	0.759	4.267	0.322
Patagonia (northern)	PAT	0	2	1648	799	0.743	2297	661	150	404	926	0.227	0.612	1.402	6.183	0.404
Patagonia (southern)	SPG	0	2	889	692	0.651	2144	742	203	576	1376	0.273	0.776	1.854	6.781	0.425
Pyrenees	PYR	0	0.6	952	308	0.737	2247	766	148	420	1002	0.194	0.548	1.308	6.759	0.424
Qilian Shan	QS	5.5	1.8	256	119	0.789	4879	1328	98	330	913	0.073	0.248	0.687	9.358	0.496
Rockies (Canada)	CAR	2.1	1	587	116	0.611	2725	899	164	445	1023	0.183	0.495	1.138	6.236	0.406

Table 1. (continued)

Range	Code	V_h	Error	Precip	Error	Coslat	E_{max}	$E_{mean} -$ BL	GR1	GR5	GR15	nGR1	nGR5	nGR15	GR15/GR1	m
Rockies (Northern Colorado)	NCR	0	1	491	104	0.771	3870	846	154	453	1119	0.182	0.536	1.323	7.281	0.441
Sangre de Christo (Colorado)	SCH	0	1	377	75	0.800	3337	905	122	385	1003	0.135	0.425	1.108	8.226	0.468
Sierra Nevada (California)	SNC	0		519	226	0.798	3552	1092	137	410	1025	0.125	0.376	0.939	7.491	0.447
Southern Alps (New Zealand)	SNZ	9.1	0.6	1843	1311	0.726	1859	522	118	354	885	0.227	0.679	1.695	7.480	0.447
Southern India	SI	0	2	2091	1019	0.986	1758	656	107	362	1006	0.162	0.552	1.533	9.442	0.498
Sri Lanka	SL	0	2	1793	445	0.993	1732	565	81	299	893	0.143	0.530	1.580	11.050	0.533
Sumatra	SUM	0	3	2665	403	1.000	2326	538	65	267	869	0.121	0.496	1.615	13.375	0.576
Taiwan	T	35	5	2057	368	0.916	2592	771	137	441	1173	0.177	0.572	1.523	8.590	0.477
Talamanca Cord. (Costa Rica)	TCR	20	5	2833	541	0.987	2493	902	127	436	1218	0.141	0.483	1.351	9.579	0.502
Tasmania	TSM	0	1	1257	619	0.749	1187	318	50	194	599	0.159	0.611	1.882	11.865	0.549
Tien Shan (Central)	CTS	14	3	306	136	0.736	5167	1637	178	536	1343	0.109	0.327	0.820	7.535	0.448
Tien Shan (Dzungarian Alatau)	DZA	4	1	255	68	0.714	3622	1263	180	530	1304	0.143	0.420	1.033	7.235	0.439
Tien Shan (Eastern)	ETS	10	3	184	58	0.733	4277	1666	129	431	1177	0.078	0.259	0.706	9.104	0.490
Tien Shan (western)	WTS	19	2	323	112	0.749	4915	1452	153	475	1226	0.105	0.327	0.845	8.025	0.462
Uinta Range (Utah)	UR	0	2	308	88	0.758	4341	692	112	325	793	0.161	0.469	1.146	7.106	0.435
Ural (Russia)	URL	0		635	96	0.435	1136	274	81	238	585	0.295	0.867	2.134	7.232	0.439
Verkhoyansk (Russia)	VKH	0	1	271	67	0.454	1660	614	126	296	602	0.206	0.482	0.979	4.761	0.346
Wind River Range (Wyoming)	WRR	0	1	277	22	0.732	3444	939	134	369	857	0.143	0.392	0.913	6.392	0.412
Zagros (Northwestern)	NWZ	4.5	2	411	193	0.832	3366	1217	145	408	966	0.119	0.335	0.794	6.663	0.421
Zagros (Southeastern)	SEZ	8	2	244	136	0.870	3312	1014	121	367	929	0.119	0.362	0.916	7.696	0.453

[a]V_h: geodetic horizontal tectonic shortening rate (mm yr^{-1}), with error determined from the quality of the data and the location of GPS stations. Precip: average yearly precipitation (mm yr^{-1}) from the GPCC worldwide database (GPCC Normal Version 2010) with a 0.25° grid size (ftp://ftp-anon.dwd.de/pub/data/gpcc/html/gpcc_normals_download.html). Errors express the spatial variability of the precipitation at 1σ. Coslat: The cosine of is the mean latitude of the range. BL: Geometric base level in meters above sea level as defined in section 2. E_{max}: The maximum elevation (m a.s.l.) of the topography averaged over a 10 km circular sliding window. $E_{mean} -$ BL: Mean elevation of the range (in meters above the base level BL). GR1, GR5 and GR15: Mean geophysical relief in meters [i.e., Small and Anderson, 1998] corrected for the dependence of pixel size on latitude. See text and Figure 3 for details. nGR1, nGR5, and nGR15: Relative relief, i.e., geophysical relief normalized by the mean elevation of each range [nGRx = GRx/($E_{mean} -$ BL)]. Note that geophysical relief has also been normalized by the maximum elevation of each range (E_{max}), and are presented in Table A1 (nGRx E_{max}). Those results are similar. See text for details. GR15/GR1: Dimensionless ratio between GR15 and GR1. m: Slope of the least square regression in log-space of GRx value against the area of the circular sliding window within the calculation is made ($\pi*\chi^2$, see Figure 4). This variable has been used to correct GRx values from their raw values (see Table A1).
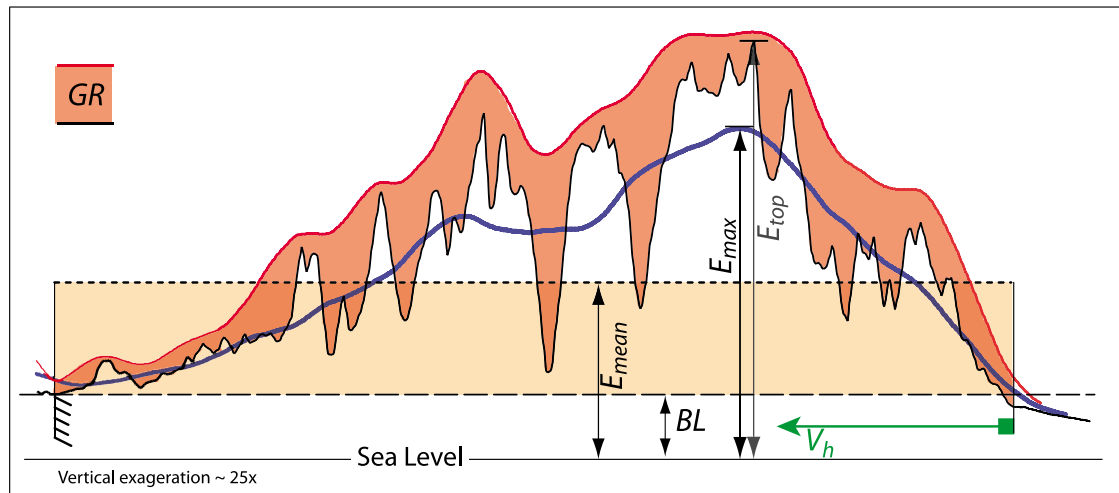
Figure 3. Sketch of the variables used in this paper, based on a topographic profile across the Central Alps (North is to the left). Black curve is the actual topography, with its maximum elevation noted "E_{top}" (not used in this study, but specified in Table A1), blue curve is the topography smoothed over a radius of 10 km (including the region east and west of the profile), and the maximum elevation of this curve is "E_{max}." The overall average topography over the entire range is "E_{mean}." The base level is arbitrarily defined by geometric consideration and is the elevation above sea level of the transition between the mountain front and the foreland basin. The red curve defines a profile through a surface that passes through peaks within a given radius x (in pixels). A pixel is treated as lying within the sliding window if part of it within the considered circle. A sliding window with a "radius" of one pixel is therefore actually a square consisting of a central pixel and 8 surrounding pixels. GRx is the mean value of the difference between this surface envelope (red curve) and the topography, calculated for each pixel. Note that the surface envelope does not intersect the peaks, because the calculation was made in 3D (plotted here as a cross section for which the highest peaks lie outside of the line of the cross section). Thus, GRx is the volume between red and black curve (pink area), divided by the area of the range. "V_h" depicted by an arrow is the geodetic shortening rate across the range. Convergence accommodated by subduction has been ignored, and only the shortening component of oblique convergence has been considered.

the contribution of background elevations not associated with the building of a mountain belt.

[11] For relief variables we use "Geophysical Relief" in the sense of *Small and Anderson* [1998, p. 123], which is "the mean elevation difference between a smooth surface connecting the highest points in the landscape … and the current topography." The smooth surfaces are calculated using sliding windows with radii of 1, 5, and 15 pixels (GR1, GR5, and GR15). Geophysical Relief is therefore the difference between maximum elevations smoothed in this way and the raw present-day elevations (pink area in Figure 3). Geophysical Relief increases with the area over which it is calculated following approximately a power law, with most exponents lying between 0.3 and 0.5 (Figure 4 and Table 1), as previously noted by *Ahnert* [1984] and *Lucazeau and Hurtrez* [1997]. This scaling of relief versus area of calculation window allows a comparison of values from different ranges and computation of values for specified radii. As pixel size decreases with latitude, we calculated values so that GR1, GR5, and GR15 correspond to radii of 0.925, 4.625 and 13.875 km, appropriate for 1, 5, and 15 pixels at the equator (Table 1). (Raw values of GR1, GR5, and GR15 that ignore this latitude dependence of pixel size are presented in Table A1.) Because mountain belts of high mean elevation offer greater potential for creating relief than ranges with moderate or low mean elevation, we also examined normalizations of relief, obtained by dividing the relief value

(GR1, GR5, and GR15) by (E_{mean} − BL). These represent the "relative relief" of a mountain range and are noted below as "nGR1," "nGR5" and "nGR15." Normalization by (E_{max}) yields similar results (Table A1) and will not be discussed here. Note that in most cases, neither GR5 nor nGR5 is discussed in detail, because values and patterns are intermediate between those for GR1 and GR15.

2.2. Climate Variables

[12] To address climate differences, we used the mean annual precipitation and the mean latitude of each range, as a surrogate for mean annual temperature and insolation. The elevation of the mean snow line, hence the potential for glaciers to develop and erode, depends mostly on temperature and precipitation. Since mean annual insolation is highest at the equator, and decreases toward the poles as the cosine of the mean latitude of each range, we use "coslat," rather than latitude itself. This parameter is therefore independent of the topography that affects glaciation (higher mountains should have more glaciers), and also independent of precipitation, that also affects glaciation. Obviously, the best quantity assessing the role of glaciation would be present-day equilibrium line elevations (ELAs), and comparably good might be snow line elevations lines, which *Egholm et al.* [2009] and *Pedersen et al.* [2010] have used in their analysis of the role of glaciation at high altitudes. Unfortunately, we do not know either ELAs or snow line altitudes for most of the belts
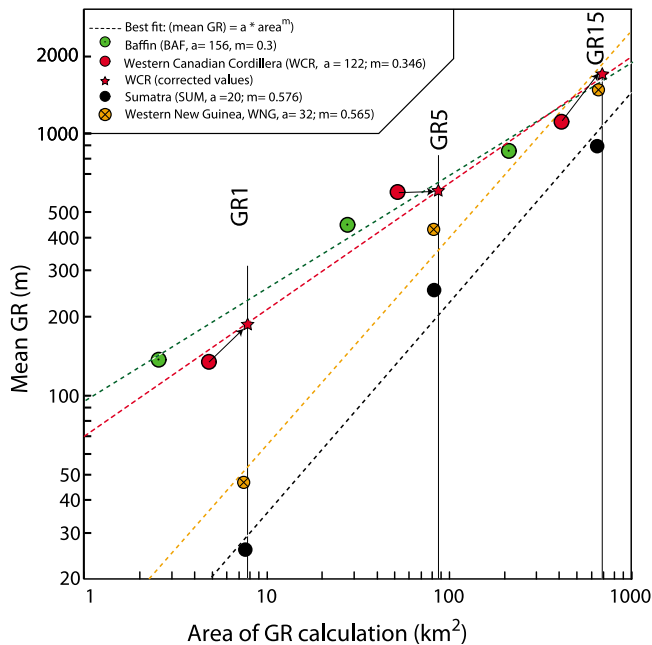
Figure 4. Log-log plot of five end-member examples of relief (Geophysical Relief, GR on the *y*-axis) calculated over different circular sliding windows ("Area of GR calculation" on the *x*-axis). Linear fits ($R^2 > 0.95$) in log-log space indicate power law functions, with an exponent ("*m*") ranging from 0.3 to 0.6 (slopes of the dashed lines). These linear relationships in log-log space have been used to correct relief calculations made at different latitudes, because the dimension of a pixel decreases with latitude (see text for details); for example, for the Western Canadian Cordillera (WCR), raw GR values are shown as red circles, and corrected values as red stars. Ranges undergoing severe glacial conditions tend to have small exponents (here Baffin Island, BAF, and the Western Canadian Cordillera, WCR, in green and red, respectively). Ranges with no glacial imprint tend to have large exponents (here Western New Guinea, WNG, and Sumatra, SUM, in orange and black, respectively). This dependence on latitude is particularly exploited further in Figure 9 and section 3.2.3.

that we consider here, for the present or the Late Glacial Maximum (LGM). In fact, we found that published values of ELAs from the same ranges can differ by as much as 1000 m, mostly because of the climate characteristics, the hypsometry, and the orientation of the glaciated basins [*Allen*, 1998; *Flint*, 1971; *Gilbert*, 1904; *Huybers and Roe*, 2009]. Hence we are forced to use a less direct measure of glaciation, but one that takes into account other periglacial processes, such as frost shattering [*Delunel et al.*, 2010; *Hales and Roering*, 2009], which may affect topography at high latitude/high elevation. Note that when coslat increases, the latitude decreases. Therefore, a negative correlation between coslat and another variable means that the other variable increases toward the equator. We compiled precipitation from the Global Precipitation Climatology Centre worldwide database (GPCC Normal Version 2010, 1951–2000) with a 0.25° grid size (ftp://ftp-anon.dwd.de/pub/data/gpcc/html/gpcc_normals_download.html) to quantify the role of

mean annual precipitation (precip) in shaping the topography of mountain ranges. We used the average of values within the boundary of each range and its standard deviation over the region to describe spatial variability of precipitation. We did not take into account geographic (leeward versus windward flanks) and temporal (storminess) distributions of precipitation or precipitation phase (rain versus snow) that have been shown to be important in geomorphology [*Anders et al.*, 2008, 2006; *Barros et al.*, 2006; *Bookhagen and Burbank*, 2006; *Snyder et al.*, 2003], because we do not have this information for most of the mountain ranges used.

2.3. Tectonic Variables

[13] To quantify the relative contribution of tectonics in shaping mountain ranges, we used geodetically (i.e., decadal), or in a few cases geologically, measured shortening rates (V_h) across ranges (see Appendix A for details). We tried to avoid any geological complications that would have jeopardized internal consistency of the database, which is the backbone of this study. We acknowledge that the shortening rate imperfectly describes geometric and geologic constraints on mountain belt evolution, with two main pitfalls: (1) Neither the duration of shortening, nor variations of shortening rates through time are considered, and hence we do not try to quantify total amounts of shortening across different belts (though we do discuss this source of error for some ranges in the text). (2) The initial thickness of deforming layer(s) is also not taken into account, and hence we do not distinguish between thin- and thick-skinned belts. We also assume for all ranges that the decadal observations reflect the long-term rates of shortening across the belts (i.e., many millennia to millions of years). Most relative plate motions measured geodetically [e.g., *Argus et al.*, 2010] and with magnetic anomalies spanning seafloor younger than ∼2 Ma [e.g., *DeMets et al.*, 2010] match one another within uncertainties. Across mountain ranges, geodetically measured rates on decadal time scales match those measured geologically over millennial times scales for instance in Asia [*England and Molnar*, 2005; *Thompson et al.*, 2002], in New Zealand [*Beavan et al.*, 1999; *Sutherland et al.*, 2006], and elsewhere, as well as for most of the inactive ranges used in this study, that have been tectonically quiet for (at least) several Ma. In regions where recent major earthquakes have displaced GPS control points, we used studies that considered intervals of time that preceded the earthquakes or that demonstrated no affect of the earthquakes.

[14] We base the analyses in this study on bi- and multi-variable linear regressions among the aforementioned variables (summarized in Figure 3 and Table 1). Most of the correlations shown in this paper are rather poor ($R < 0.5$, Tables 2a–2c). This is due in part to the poor signal/noise ratio of data averaged over large areas and to internal variability within the belts themselves (e.g., strain localization, rain shadows, etc.). Regardless of the traditions in statistics, we labeled the quality of correlation depending on the value of R^2 of a linear regression at the 95% confidence level: "no correlation" for $R^2 < 0.1$ ($|R| < 0.3$), "weak correlation" for $0.1 < R^2 < 0.25$ ($0.3 < |R| < 0.5$), "fair correlation" for $0.25 < R^2 < 0.5$ ($0.5 < |R| < 0.7$ and "good correlation" for $R^2 > 0.5$ ($|R| > 0.7$). All of the correlations are summarized when the entire data set was used (Table 2a), and when

Table 2a. Pearson Correlation Matrix for the Entire Data Set[a]

	Precip	Coslat	E_{max}	$E_{mean} - BL$	GR1	GR5	GR15	Gr15/GR1	m	nGR1	nGR5	nGR15
V_h												
R	*0.376*	0.153	*0.312*	0.177	*0.356*	*0.444*	*0.494*	0.078	0.060	0.059	0.067	0.013
P-value	*0.001*	0.210	*0.009*	0.147	*0.003*	*0.000*	*0.000*	0.525	0.625	0.633	0.586	0.914
Precip												
R		**0.509**	−0.126	−0.132	−0.111	−0.009	0.138	*0.403*	*0.351*	−0.030	0.070	*0.334*
P-value		**0.000**	0.303	0.279	0.366	0.943	0.258	*0.001*	*0.003*	0.806	0.566	*0.005*
Coslat												
R			*0.407*	*0.378*	−0.370	−0.203	0.024	**0.575**	**0.590**	*−0.573*	*−0.471*	−0.254
P-value			*0.001*	*0.001*	0.002	0.095	0.844	**0.000**	**0.000**	**0.000**	0.000	0.036
E_{max}												
R				**0.626**	0.199	0.335	0.430	0.091	0.125	*−0.306*	*−0.331*	**−0.651**
P-value				**0.000**	0.102	0.005	0.000	0.458	0.306	*0.011*	*0.005*	**0.000**
$E_{mean} - BL$												
R					0.097	0.178	0.248	0.114	0.118	**−0.614**	**−0.703**	**−0.524**
P-value					0.428	0.143	0.040	0.350	0.336	**0.000**	**0.000**	**0.000**
GR1												
R						*0.936*	*0.721*	−0.647	−0.669	**0.560**	*0.421*	0.109
P-value						*0.000*	*0.000*	0.000	0.000	**0.000**	*0.000*	0.374
GR5												
R							*0.917*	−0.403	−0.402	*0.422*	*0.358*	0.121
P-value							*0.000*	*0.001*	*0.001*	*0.000*	*0.003*	0.322
GR15												
R								−0.036	−0.022	0.208	0.233	0.137
P-value								0.767	0.856	0.087	0.054	0.260
GR15/GR1												
R									*0.984*	−0.528	*−0.329*	0.095
P-value									*0.000*	0.000	*0.006*	0.437
m												
R										−0.562	*−0.344*	0.054
P-value										0.000	*0.004*	0.660
nGR1												
R											*0.955*	**0.542**
P-value											*0.000*	**0.000**
nGR5												
R												0.633
P-value												0.000

[a]Bold italic values indicate high correlation, $|R| > 0.7$; bold values indicate fair correlation $0.5 < |R| < 0.7$; italic values indicate weak correlation, $0.3 < |R| < 0.5$; regular values indicate no correlation, $|R| < 0.3$.

inactive (Table 2b) and active (Table 2c) belts were treated separately.

3. Bivariate Data Analysis

[15] We examine bivariate statistical relations among the aforementioned variables using linear regressions (Tables 2a–2c). To avoid overwhelming readers with too many plots, we show only those yielding meaningful regressions and/or offering significant insights (Figures 5–10).

3.1. Topography (Elevation and Relief) Versus Tectonics

3.1.1. Elevation Versus Tectonics

[16] We first regress the topography of ranges against shortening rates to document the links between the maximum elevation above sea level (E_{max}) and the mean elevation above base level(s) ($E_{mean} - BL$) of mountain ranges against tectonic shortening rates (V_h) (Figure 5). Plots of all data give hints of trends but show a large scatter. This scatter may be intrinsically related to our limited knowledge of tectonic geometry and history (different durations or ages of mountain building, thick- versus thin-skin tectonics, etc.), but it appears, at least qualitatively, that this scatter derives from external processes. Specifically, different erosion rates

in different climates are an important source of scatter (discussed below). For instance, some ranges with low mean elevations above base level (low $E_{mean} - BL$) and significantly rapid tectonic shortening (large V_h) are known for their high erosion rates: e.g., the Southern Alps of New Zealand (SNZ) [*Herman and Braun*, 2006; *Herman et al.*, 2010a; *Hovius et al.*, 1997], Taiwan (T) [*Dadson et al.*, 2003], and the St Elias Range (SEL) [*Berger et al.*, 2008]. The mean elevations of these belts seem to be limited by rapid erosion, controlled by rock uplift, climate, and the type of rock at the surface, which controls the angles of critical slopes and therefore valley spacing and elevation [e.g., *Perron et al.*, 2009]. Oppositely, ranges with high mean elevation (large $E_{mean} - BL$) appear to be related to plateau conditions, such as most of the high Andes of Peru (SPA and NPA), Bolivia (SBA and NBA), and Northern Chile (CN), or the Karakorum (KKR) and Alborz (ALB), where there are large arid portions and a bimodal distribution of precipitation (see section 3.2.1).

3.1.2. Relief Versus Tectonics

[17] Relief results from (1) inhomogeneous surface uplift due to slip on discrete faults and to folding, plus (2) the spatially varying amount of rock that has been removed from the range by inhomogeneous erosion (incision) [e.g., *Champagnac et al.*, 2007; *Kirkbride and Matthews*, 1997; *Montgomery*, 1994; *Shuster et al.*, 2005; *Small and Anderson*,

Table 2b. Pearson Correlation Matrix for the Inactive Ranges Only[a]

	Precip	Coslat	$E_{\max}$	$E_{\mean}$ − BL	GR1	GR5	GR15	Gr15/GR1	m	nGR1	nGR5	nGR15
Precip												
R		**0.588**	−0.141	0.018	−0.264	−0.105	0.115	**0.561**	**0.511**	−0.271	−0.123	0.299
P-value		**0.003**	0.511	0.933	0.212	0.624	0.592	**0.004**	**0.011**	0.200	0.568	0.155
Coslat												
R			*0.351*	0.287	*−0.437*	−0.174	0.143	***0.710***	***0.753***	**−0.669**	**−0.506**	−0.164
P-value			*0.093*	0.174	*0.033*	0.312	0.374	***0.000***	***0.000***	**0.000**	**0.012**	0.443
$E_{\max}$												
R				***0.822***	0.186	*0.312*	*0.374*	−0.076	0.000	*−0.406*	**−0.505**	***−0.652***
P-value				***0.000***	0.384	0.138	0.072	0.724	1.000	*0.049*	**0.012**	**0.001**
$E_{\mean}$ − BL												
R					0.356	0.487	**0.528**	−0.191	−0.121	*−0.372*	**−0.510**	*−0.485*
P-value					0.088	0.016	**0.008**	0.370	0.572	*0.074*	**0.011**	*0.016*
GR1												
R						***0.930***	***0.717***	**−0.647**	**−0.667**	**0.696**	**0.525**	0.270
P-value						***0.000***	***0.000***	**0.001**	**0.000**	**0.000**	**0.008**	0.203
GR5												
R							***0.921***	*−0.418*	*−0.401*	**0.522**	*0.450*	*0.308*
P-value							***0.000***	*0.042*	*0.052*	**0.009**	*0.027*	*0.143*
GR15												
R								−0.072	−0.034	0.279	*0.328*	*0.345*
P-value								0.738	0.874	0.187	*0.118*	*0.098*
GR15/GR1												
R									***0.980***	**−0.506**	−0.226	0.200
P-value									***0.000***	**0.012**	0.288	0.350
m												
R										**−0.573**	−0.277	0.125
P-value										**0.003**	0.190	0.560
nGR1												
R											***0.929***	**0.615**
P-value											***0.000***	**0.001**
nGR5												
R												***0.792***
P-value												***0.000***

[a]Bold italic values indicate high correlation, $|R| > 0.7$; bold values indicate fair correlation $0.5 < |R| < 0.7$; italic values indicate weak correlation, $0.3 < |R| < 0.5$; regular values indicate no correlation, $|R| < 0.3$.

1998; *Stern et al.*, 2005; *Valla et al.*, 2011]. In this section, we discuss the links between relief and shortening rates, in order to isolate the source of relief that is directly linked to tectonic processes (faulting/folding). At small scale (GR1), the correlation of relief with tectonic shortening is weak ($R = 0.36$, Figure 6a and Tables 2a–2c); GR1 spans almost one order of magnitude, regardless the shortening rate. The correlation with shortening rate, however, increases with calculation size of the relief (GR5 and GR15, Figures 6b and 6c), and is best ($R = 0.5$, p < 0.01%) for larger averaging areas (GR15). Thus, GR15 values depend in part on rates of crustal shortening (with a large scatter), but GR1 does not; large-scale relief is more sensitive to tectonics than is small-scale relief.

[18] These results differ from those of *Pedersen et al.* [2010], who reported a clear relationship between tectonic activity and relief above snow line. Despite similarities in the terminology used in the present study and in Pedersen's study ("relief" and "tectonic activity"), the definitions of the variables used are different; i.e., they used relief above the mean snow line, whereas we used mean geophysical relief, and they used three groups of tectonic activity (active, almost active and inactive), whereas we use GPS shortening rates. Therefore, these apparently different conclusions appear to result from different definitions.

3.1.3. Topography Versus Relief

[19] For active ranges ($V_h > 0$ mm/yr), relief, as defined by GR1, GR5 and GR15, appears not to correlate with the mean elevation above base level ($E_{\mean}$ − BL) of ranges (gray dots on Figures 7a and 7b). One might expect that the mean relief of high-elevation ranges would be larger than relief of low-elevation ranges, simply because incision has greater potential to cut deep valleys in higher than in lower ranges. If anything, however, relief decreases slightly with mean elevation (Table 2c). These poor correlations suggest that the relief of a belt is not strongly linked to its mean elevation, at least where tectonic shortening occurs across the belt. In contrast, for inactive ranges ($V_h = 0$ mm/yr; red dots in Figure 7) fair correlations do exist between relief (GR1, GR5 and GR15) and ($E_{\mean}$ − BL) (Table 2b). The correlation is higher ($R = 0.53$) for GR15 versus ($E_{\mean}$ − BL) than for GR1 versus ($E_{\mean}$ − BL) ($R = 0.36$). Interestingly, two ranges located at high latitude with only moderate mean elevation (Denali, DEN, and Baffin, BAF) show a large relief (especially for GR1).

3.2. Topography (Elevation and Relief) Versus Climate

3.2.1. Topography Versus Precipitation

[20] To address climate, we consider two independent measures of climate, both imperfect, but easily quantified. As a surrogate for a general climatic influence on erosion, we use mean annual precipitation, and for likelihood of glaciation, we use the mean latitudes of belts.

[21] Measures of elevation ($E_{\max}$ and $E_{\mean}$ − BL) do not show linear correlations with mean annual precipitation (Figures 8a and 8b). Very high precipitation (more than

Table 2c. Pearson Correlation Matrix for the Active Ranges Only[a]

	Precip	Coslat	E_{max}	E_{mean} − BL	GR1	GR5	GR15	Gr15/GR1	m	nGR1	nGR5	nGR15
V_h												
R	*0.487*	0.099	0.086	−0.131	*0.315*	*0.364*	*0.395*	0.061	0.011	*0.301*	*0.304*	0.260
P-value	*0.001*	0.523	0.581	0.396	*0.037*	*0.015*	*0.008*	0.695	0.941	*0.047*	*0.045*	0.089
Precip												
R		*0.495*	−0.173	−0.220	−0.065	0.009	0.143	*0.317*	0.261	0.106	0.166	*0.420*
P-value		*0.001*	0.262	0.152	0.676	0.955	0.354	*0.036*	0.087	0.495	0.281	*0.005*
Coslat												
R			*0.391*	*0.388*	−0.453	−0.382	−0.200	*0.497*	*0.485*	−0.481	−0.417	−0.283
P-value			*0.009*	*0.009*	*0.002*	*0.010*	0.193	*0.001*	*0.001*	*0.001*	*0.005*	0.063
E_{max}												
R				*0.478*	0.033	0.120	0.212	0.151	0.154	−0.146	−0.147	***−0.690***
P-value				*0.001*	0.831	0.436	0.167	0.328	0.317	0.346	0.340	**0.000**
E_{mean} − BL												
R					−0.136	−0.141	−0.106	0.185	0.156	***−0.712***	***−0.768***	***−0.621***
P-value					0.377	0.360	0.494	0.228	0.311	**0.000**	**0.000**	**0.000**
GR1												
R						*0.942*	**0.690**	***−0.726***	***−0.768***	**0.660**	**0.533**	0.133
P-value						*0.000*	**0.000**	**0.000**	**0.000**	**0.000**	**0.000**	0.388
GR5												
R							*0.891*	**−0.503**	**−0.534**	**0.622**	**0.557**	0.199
P-value							*0.000*	**0.001**	**0.000**	**0.000**	**0.000**	0.196
GR15												
R								−0.079	−0.101	*0.443*	*0.468*	0.255
P-value								0.610	0.513	*0.003*	*0.001*	0.095
GR15/GR1												
R									*0.988*	**−0.553**	*−0.394*	0.011
P-value									*0.000*	**0.000**	*0.008*	0.945
m												
R										**−0.557**	*−0.382*	0.011
P-value										**0.000**	*0.011*	0.944
nGR1												
R											*0.973*	*0.431*
P-value											*0.000*	*0.003*
nGR5												
R												**0.501**
P-value												**0.001**

[a]Bold italic values indicate high correlation, |R| > 0.7; bold values indicate fair correlation 0.5 < |R| < 0.7; italic values indicate weak correlation, 0.3 < |R| < 0.5; regular values indicate no correlation, |R| < 0.3.

2 m/yr, pale gray dots in Figure 8), however, seem limited to belts with moderate (2000–4000 m), not high (>4000 m), maximum elevations. The average E_{max} is 2944 ± 707 m for the 10 wettest ranges, but is 3327 ± 1417 m for the 59 others. Similarly, the average E_{mean} − BL is 1030 ± 328 m for the 10 wettest ranges, but is 1120 ± 638 m for the 59 others. One should note, however, that precipitation and elevation variables (E_{max} and E_{mean} − BL) are not independent of one another, because of orographic effects on precipitation [e.g., *Roe*, 2005; *Smith*, 1979], and because precipitation tends to be maximum not at the highest elevations, but commonly below ∼2000 m, as, for example, in the Himalaya [*Anders et al.*, 2006]. Hence precipitation, when averaged over the entire area of the range, may be less for high than lower ranges. If rainfall at lower elevations leads to greater erosion there than at high elevations, the isostatic response to the removal of material might raise the high parts and enhance the contrast in rainfall between high and low parts of the range.

[22] Overall, measures of relief (GR1 and GR15, Figures 8c and 8d) show no correlations with mean annual precipitation. The average GR1 is 119 ± 24 m for the 10 wettest ranges, but it is 154 ± 60 m for the 59 other ones, hence overlapping at 1σ. For *GR15*, the difference is also negligible between mean values (1128 ± 146 m versus 1069 ± 308 m). Precipitation rates seem unlikely to depend on relief; hence a correlation between these variables would carry more sense than that between precipitation rates and elevation. For small to moderate rainfall, relief is insensitive to precipitation, but relief in ranges with rainfall above a threshold (∼2 m/yr) appears to be relatively small. One may conclude that if erosion rates depended on precipitation, relief must depend on erosion patterns that do not scale with mean annual precipitation amounts. High precipitation rates do not increase the relief, in agreement with results from [*Bonnet and Crave*, 2003; *Stolar et al.*, 2007; *Whipple et al.*, 1999] that show that relief decreases when precipitation increases.

3.2.2. Topography Versus Latitude

[23] As shown by *Herman et al.* [2010a] and *Koppes and Montgomery* [2009], the rate of fluvial erosion can keep pace with glacial erosion, at least in regions where both are high. Fluvial erosion, however, appears to be more homogeneously distributed over a wider area than glacial erosion, which tends to carve valleys with steep sides [e.g., *Haeuselmann et al.*, 2007; *Shuster et al.*, 2005; *Valla et al.*, 2011]. Moreover, ice can protect high and especially cold summits where glaciers are frozen to their beds, where ice deforms without sliding over the rock, and/or where debris in the ice is sparse [*Anderson*, 2005; *Foster et al.*, 2008; *Griffiths*, 1952; *Herman et al.*, 2011; *Pedersen et al.*, 2010; *Thomson et al.*, 2010; *Tomkin and Braun*, 2002], and hence increase the relief.
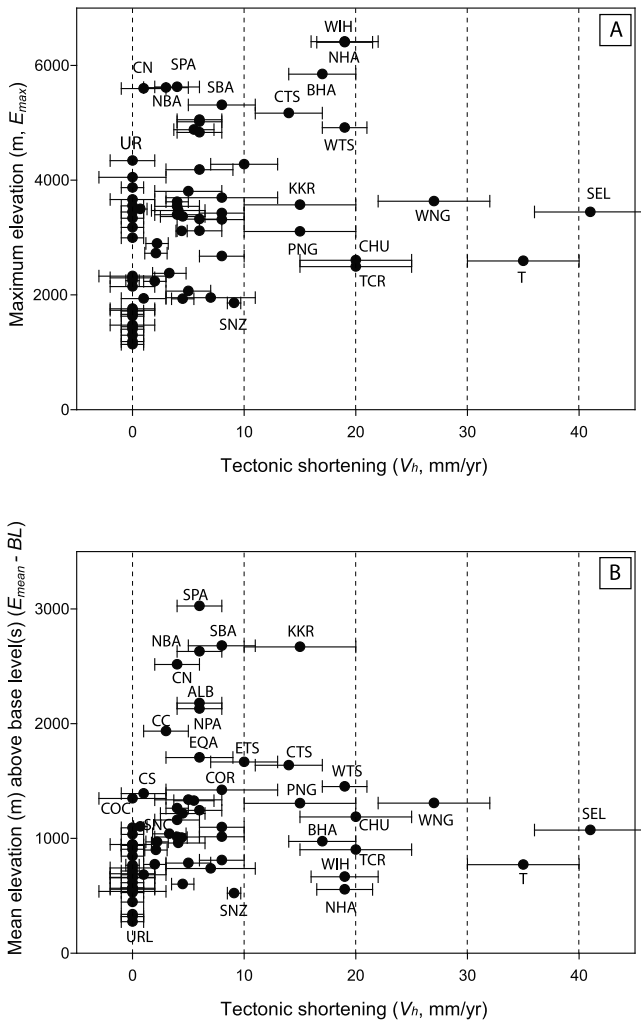
Figure 5. Topographic parameters (elevation, E_{max} and mean elevation above base level, $E_{mean} - BL$) plotted against tectonic shortening rate (V_h).

[24] The correlations between average maximum elevation (E_{max}) and mean elevation ($E_{mean} - BL$) with cosine of latitude (Figure 9) confirm what others have noted before: mean elevation is limited at relatively high latitudes [*Brocklehurst and Whipple*, 2004; *Egholm et al.*, 2009; *Montgomery et al.*, 2001; *Pedersen et al.*, 2010; *Porter*, 1989]. Low values of E_{max} and $E_{mean} - BL$ are common at high and low latitude, but the scatter is much larger in the tropics (coslat > 0.9, latitude < 25°), and becomes greatly reduced at mid to high latitudes (i.e., coslat < 0.7, latitude > 45°). Overall correlations between E_{max} and $E_{mean} - BL$ with coslat remain poor, $R = 0.16$ and 0.1, respectively, and the latter is not statistically significant for inactive ranges ($p = 17\%$).

[25] Relief calculated using small averaging areas (*GR1*, Figure 9c) appears to correlate with coslat; GR1 increases as latitude increases ($R = -0.37$, -0.44 and -0.45 for the entire data set, and for inactive and active ranges only, respectively, see Tables 2a–2c). Note that this trend might be improved if it were possible to take into account the hidden part of the relief at high latitude (coslat < 0.5, latitude > 60°), that due to valley floors submerged beneath glaciers, beneath

water in fjords and lakes, and beneath sediment, but such information is not currently available for enough regions. Thus, bedrock topography partly covered by these features biases the analysis proposed here toward lower relief. We
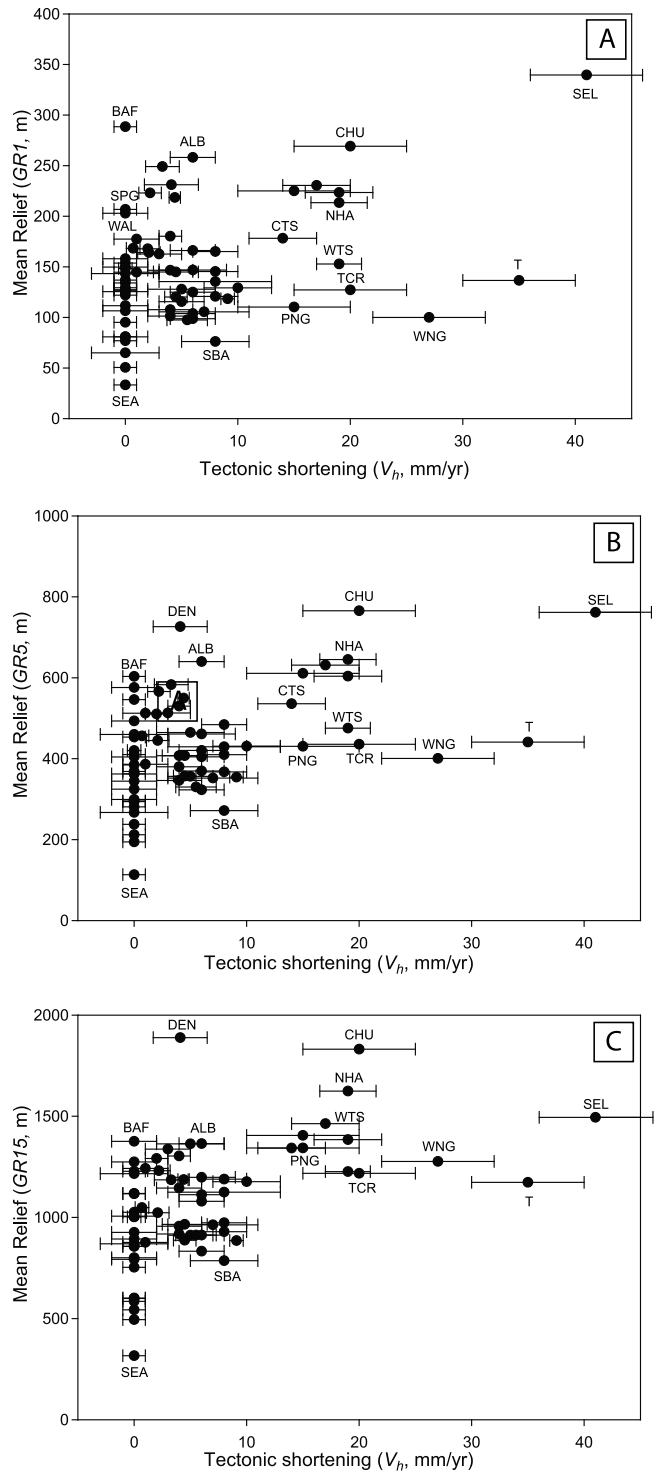
Figure 6. Topographic parameters (relief, GR1, GR5 and GR15) plotted against tectonic shortening (V_h). Note particularly high relief, GR1, for three high latitude ranges (Baffin, BAF, Chugach, CHU, and St Elias, SEL), and exceptionally high relief, GR15, of Denali (DEN).
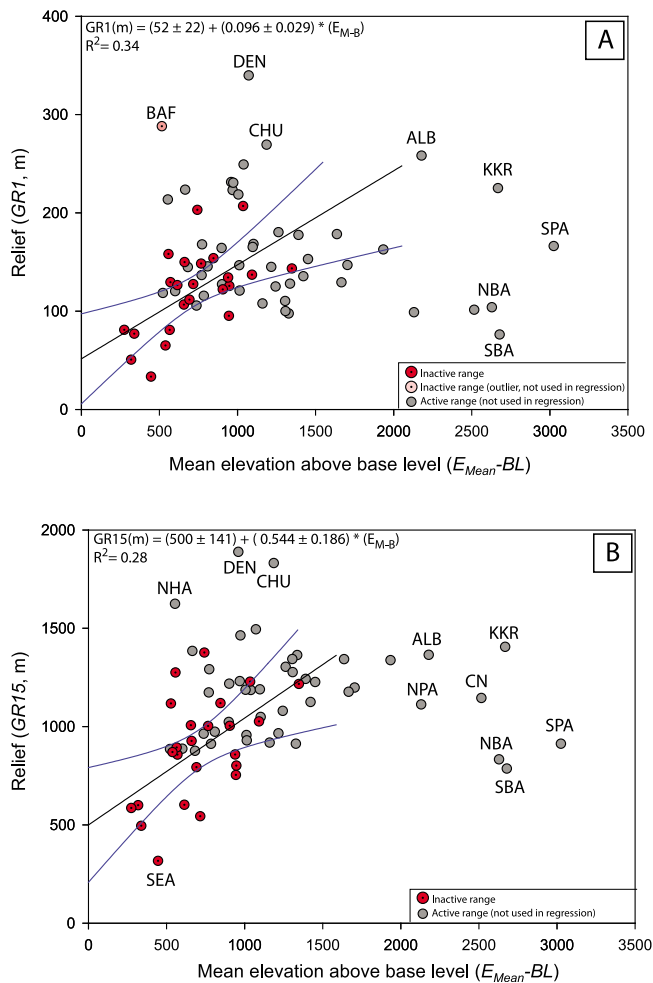
Figure 7. Relief plotted against mean elevation above base level(s) ($E_{mean} - BL$). (a) GR1 versus ($E_{mean} - BL$): Inactive ranges are pictured in red (pink for the outlier not used in the regression, Baffin, BAF), and active ranges are displayed in gray, and not used in the regression (correlations for the entire data set and for active ranges only not statistically significant, see Tables 2a and 2c). Regressions shown in this paper are least squares linear regressions with 95% confidence bands and p-value < 1%. (b) GR15 versus ($E_{mean} - BL$): Same color coding than in Figure 7a, with regression using only inactive ranges (correlations for the entire data set and for active ranges only not statistically significant, see Tables 2a and 2c).

tried to select regions where ice sheets, fjords, and lakes were sparse, but their effects cannot be avoided at high latitude. Relief calculated over a larger averaging length scale (GR15) shows no correlation for either inactive or active ranges (Figure 9d).

[26] As demonstrated in section 3.1.3 and illustrated in Figure 7, the relationship between relief and the mean elevation of the range ($E_{mean} - BL$) differs for active and inactive ranges. To take this difference into account, we normalized relief (GR1 and GR15) by the mean elevation of each range ($E_{mean} - BL$). This leads to two new variables, nGR1 and nGR15, that quantify "relative relief." Not only does nGR1 appear to correlate positively and well with

coslat ($R = 0.6$) (Figure 9e), but the relation also applies comparatively well for active and inactive ranges. The relation of the larger-scale relative relief (nGR15) with coslat is much weaker, with almost no correlation between them (Figure 9f). By contrast, the relation between nGR1 and coslat is one of the strongest we found ($R = 0.71$ for inactive ranges, Tables 2a–2c). This suggests (1) not only do the data in Table 1 allow such correlations, but also the generally poor correlations shown in previous sections are also meaningful, and not due simply to low signal/noise ratios, and therefore inaccurate data; and (2) a process that is latitude-dependent seems to exert a strong control on small-scale relief, and tends to increase it toward the poles. Furthermore, this correlation between normalized relief (nGR1) and latitude is not an artifact due to the decrease of the mean elevation toward the pole: normalization of other variables (e.g., GR15 or GR15/GR1) by the mean elevation ($E_{mean} - BL$) yields insignificant, negligibly small correlations.

3.2.3. Scaling Factor of Relief Versus Climate

[27] As described in the previous section, relief averaged over areas with different dimensions carries different information regarding climate and tectonics. To investigate this difference we use both the simple ratio between GR15 and GR1 (GR15/GR1) and the exponent that describes the slope of [log GRx versus log (averaging area)] in Figure 4 ("m" in the following). These two parameters measure the relative importance of different horizontal length scales on the total relief. As suggested by the examples shown in Figure 4, ranges with high values of GR15/GR1 (>10) and large exponents ($m > 0.4$) lie close to the equator, and ranges with low ratios GR15/GR1 (<5) and small exponents ($m < 0.3$) are located at higher latitudes (Figures 10a and 10b), despite the fact that part of the small-scale relief is hidden by ice, fjords, lakes, and thick sediment. Correlations between GR15/GR1 and coslat are positive ($R = 0.57$) for the entire data set. Consideration of active and inactive ranges separately, however, reveals different patterns: for active ranges (gray dots in Figure 10a) the correlation between GR15/GR1 and coslat is weaker ($R = 0.5$, not plotted), and for inactive ranges it is larger ($R = 0.71$, red dots in Figure 10a). The same pattern is observed for the regression between m and coslat, with an even better correlation for inactive ranges ($R = 0.75$, red dots on Figure 10b).

[28] The correlation of GR15/GR1 with precip is positive but small ($R = 0.4$), with higher values of GR15/GR1 for wetter ranges. The correlation is larger for inactive ($R = 0.56$, Figure 10c) than active ranges ($R = 0.32$). Similarly, the correlation of m with precip is positive but small ($R = 0.35$) when all ranges are considered. Again, the correlation is larger for inactive ($R = 0.51$, Figure 10d) than active ranges ($R = 0.26$).

[29] Correlations between (GR15/GR1) and m with climatic variables are much larger for latitude than for precipitation. Moreover, these correlations are fair to good for inactive ranges ($R = 0.56$ and 0.51 for precip, and $R = 0.71$ and 0.75 for coslat) but not statistically significant for active ranges ($p > 5\%$, see Table 2c). This indicates that the climate signal (here represented by latitude and precipitation rate) is recorded in the topography, and expresses itself more clearly without tectonics. In general, relief averaged over large distances tends to be relatively large for low latitudes and high precipitation rates, whereas relief averaged over smaller
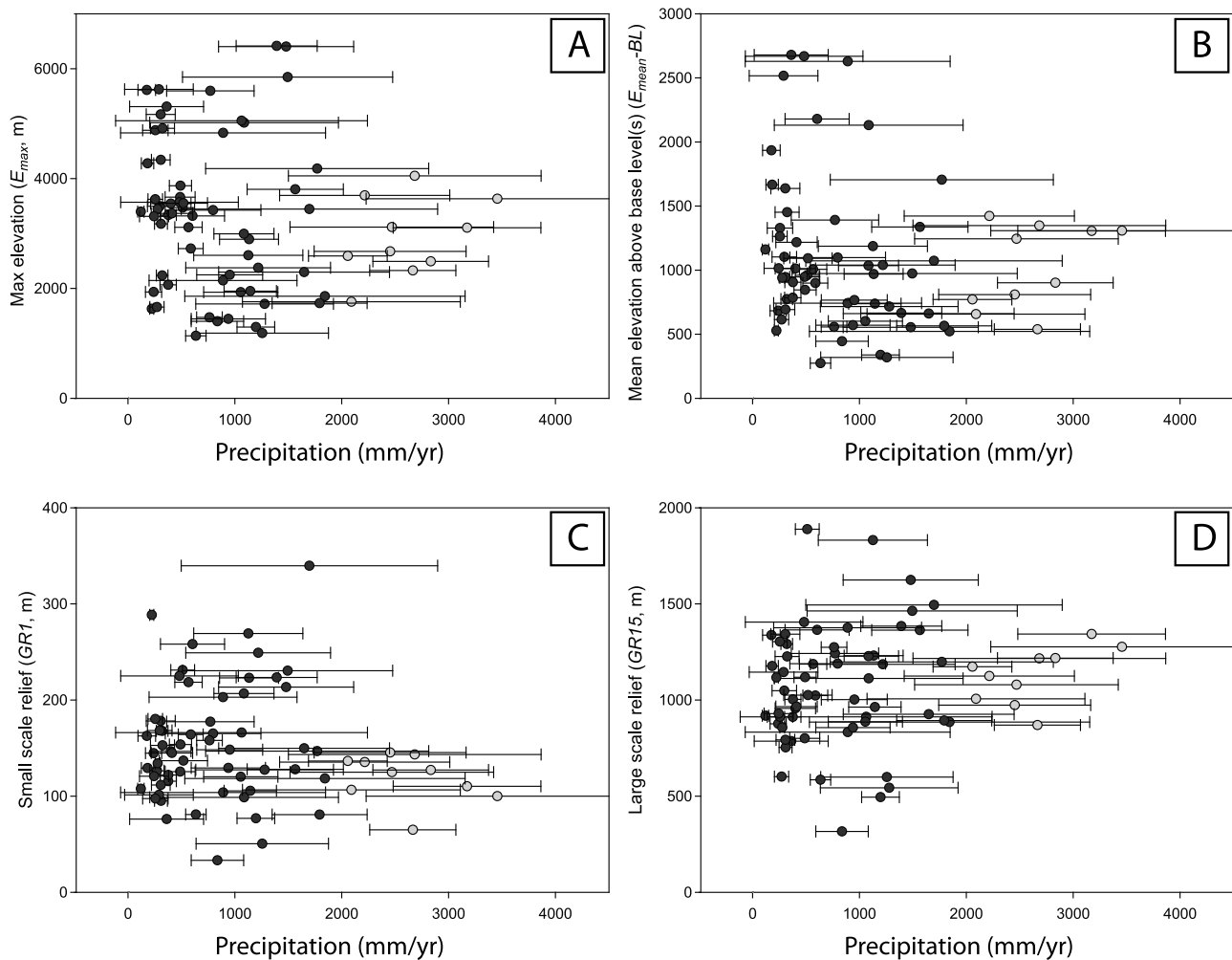
Figure 8. Topographic parameters (elevation: E_{max} and $E_{mean} - BL$, and relief: GR1 and GR15) plotted against mean annual precipitation (precip). Pale gray dots depict ranges with average precipitation >2000 mm/yr. Error bars give one standard deviation of the spatial variability of precipitation. Correlation between precipitation and the four topographic variables used is negligible in all cases (see Tables 2a–2c).

scales tends to be relatively large at high latitudes and where precipitation rates are low [e.g., *Sugden and John*, 1969].

4. Multivariate Regressions

[30] In section 3 we have arrived at the unsurprising result that both climate and tectonics correlate with various aspects of topography, and we have tried to determine the relative importance of both in shaping and modifying mountainous landscapes by examining different parameters (e.g., relief, mean elevation, etc.) represented by different variables. The previous analysis, however, is limited to a series of bivariate analyses, using linear regressions (Figures 5–10) and their correlation coefficients (summarized in Tables 2a–2c). These analyses document the existence (or absence) of statistical correlations between pairs of variables. Some relations are stronger than others, but the different dimensions of the variables, as well as multiple relations among these variables, prevent the calculation of their relative importance in shaping topography.

[31] To explore this further, we use multivariate linear regressions that give relative contributions of "independent"

variables (climate and tectonics) to topographic variables (Figures 11–13 and Figure A3, summarized in Tables 3a–3c and Tables 4a–4c). All variables (*A*) have been normalized using $A_{norm} = (A - \mu)/\sigma$, where μ is the mean of the population and σ the standard deviation of this population, so that the average of the A_{norm} is 0 with a standard deviation of 1. Independent (external) variables are V_h, precip, and coslat, and dependent variables are topographic variables (see section 2.1). In Tables 3a–3c and Tables 4a–4c, statistically significant results (*p* value < 0.02) are in bold.

[32] Regressions of E_{max} and of $E_{mean} - BL$ show a classical result (Figures 11a and 11b): tectonic shortening (V_h) raises the mountains (positive correlations), and the impact of climate on erosion, parameterized by mean annual precipitation (precip) and latitude (coslat), decreases mean elevations. Correlations are negative for precip, but positive for coslat, which increases as latitude decreases.

[33] Relief (GR1 and GR15), however, is not affected much by mean annual precipitation rates (Figures 11c and 11d), but depends on coslat (negative correlation), at least for small length-scale relief (GR1), and on tectonic shortening
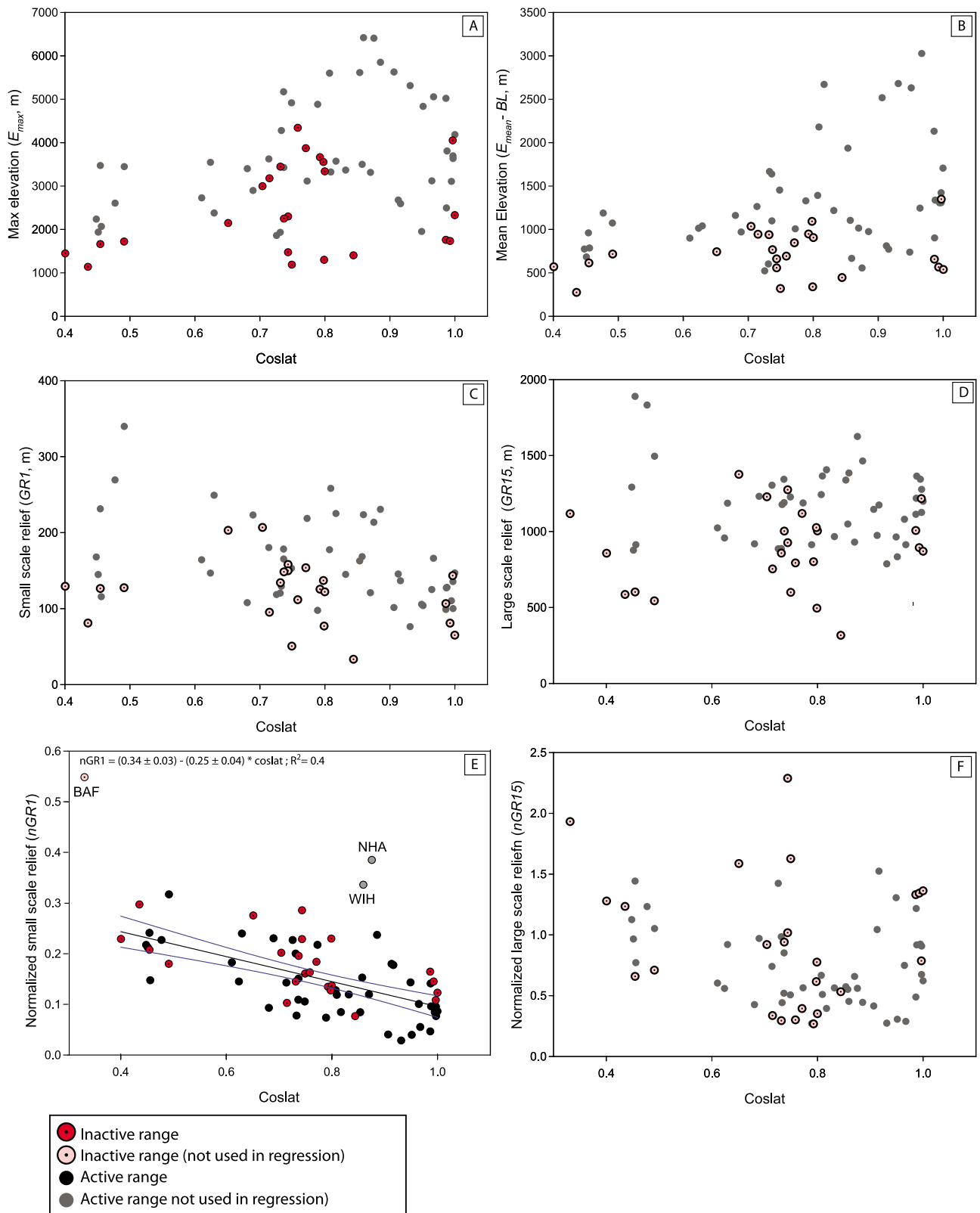
Figure 9. Topographic parameters (elevation: E_{max} and $E_{mean} - $ BL, relief: GR1 and GR15, and normalized relief: nGR1 and nGR15) plotted against cosine of latitude (coslat). Red dots show inactive ranges used in the regression, pink dots show inactive ranges not used in the regression. Black dots show active ranges used in the regression and gray dots active ranges not used in the regression. Note that for small-scale relief (GR1), active and inactive ranges show similar relationships, but for larger-scale relief (GR15), they differ, with a weak or null correlation with latitude for inactive ranges.
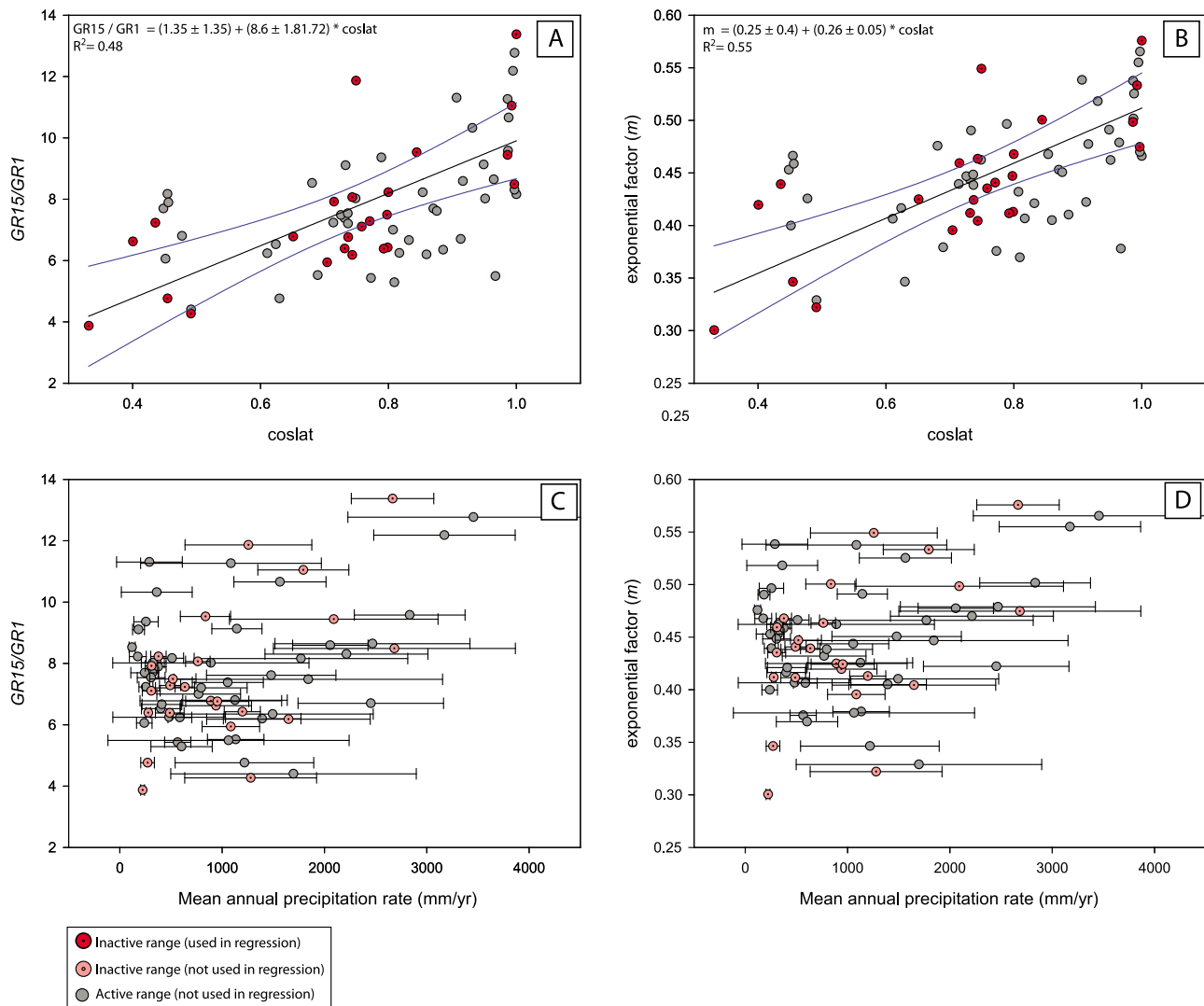
Figure 10. The scaling ratios of relief (GR15/GR1 and m) plotted against cosine of latitude (coslat). See section 3.2.3 and Figure 4 for further explanation of how m is calculated. Red dots show inactive ranges used in the regression, and gray dots show active ranges not used in the regressions. For precipitation error bars, see caption of Figure 8.

rate (positive correlation). Although large-scale relief (GR15) appears to be controlled only by tectonic shortening, the overall quality of the regression is poor ($R^2 = 0.25$).

[34] This latter correlation is probably not independent of the relation between relief and elevation (see section 3.1.3 and Figure 7), an inference corroborated by the poor quality of the correlation when relief is normalized by mean elevation ($E_{mean} - BL$), namely nGR1 and nGR15 (Figures 11e and 11f, respectively). Specifically, and not surprisingly, V_h does not explain nGR1 and nGR15 (large error bars, small coefficients and high p-values). nGR1 is better explained by a combination of precip (slight positive contribution) and coslat (large negative contribution). nGR15 is explained as well by the climate variable, that act together more equally (Figure 11f). The normalized relief (nGR1 and nGR15) therefore appears to be largely explained by climatic factors, and latitude plays an important role to control small-scale normalized relief, that is higher at high latitude. One cannot exclude, however, that part of this correlation may come

from the normalization procedure, because of the weak correlation between coslat and the mean elevation ($E_{mean} - BL$) used to normalize relief ($R^2 = 0.14$, see Table 2a). The scaling factor of the relief (GR15/GR1 and m, see section 3.2.3) correlates only with latitude (decrease toward the poles, Figures 11g and 11h), which confirms the observations presented in Figure 10. Contributions of the other independent variables (V_h and precip) are not statistically significant. These results confirm the global analysis and are summarized in Tables 3b and 3c, and presented in Figure A3.

[35] What Figure 11 does not show well is the quality of each regression (Table 3a), and thus the importance of tectonics or climate variables in explaining the topographic variables. Recall that R^2 defines the fraction of the variance in the data that has been accounted for, and there remains a fraction, $1 - R^2$, that has not been accounted for. The fraction of the variance in the various topographic variables that V_h, precip, and coslat explain ranges from $\sim$1/4 to 1/2 (Figure 12 and Tables 4a–4c), the larger of which might
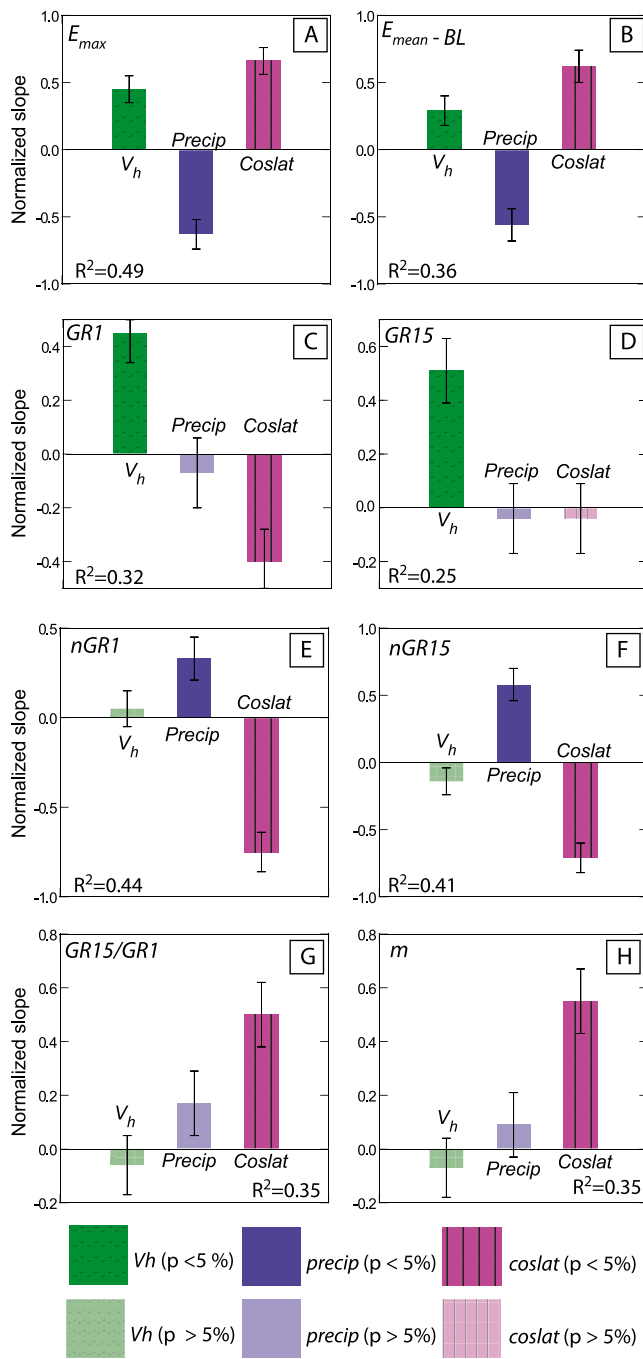
seem to be surprisingly large given the scatter observed in the various topographic variables when plotted against only one of V_h, precip, and coslat (Figures 5–10), and consideration of only these three variables. The interpretations of the different panels of Figure 12 are similar to those of Figure 11. Convergence rates V_h, our measure of tectonics, accounts for, at most, only ∼20% of the variance in all measures of topography (for large scale relief, GR15, Figure 12d), and

Figure 11. Histograms of "raw" factors of the normalized multivariate linear regressions of topographic variables against V_h, precip, and coslat, with 1σ error bars, from Tables 3a–3c. Note that positive correlations between topography and coslat correspond to negative correlations with latitude. Significant factors (p-values < 5%) are pictured in bright colors, insignificant factors (p-values > 5%) are pictured in pale colors. Color coding corresponds to that used in Tables 1 (green for V_h, blue for precip, and violet for coslat).
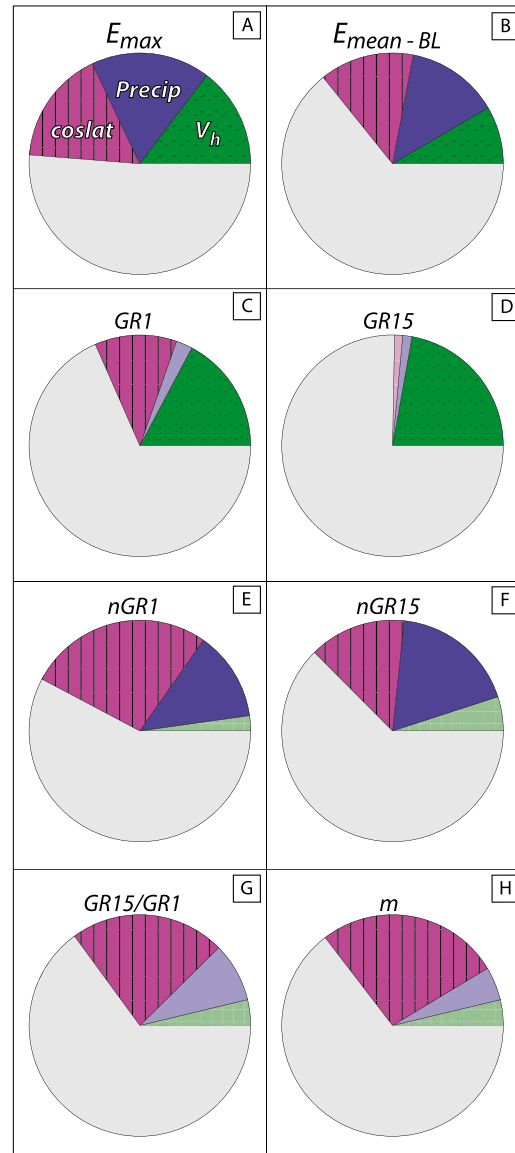

Figure 12. Pie charts of the relative contributions of each external variable – V_h (tectonic forcing), precip (mean annual precipitation), and coslat – to the observed variance of the topographic variables, as summarized in Table 4a. As in Figure 11, significant factors (p-values < 5%) are pictured in bright colors, and insignificant factors (p-values > 5%) are pictured in pale colors (same color coding as in Figure 11). The gray shading is the unexplained part of the variance that is due to unused variables and natural scatter. Similar pie charts calculated for inactive and active ranges separately are presented in Figure 13 (from Tables 4b and 4c, respectively).
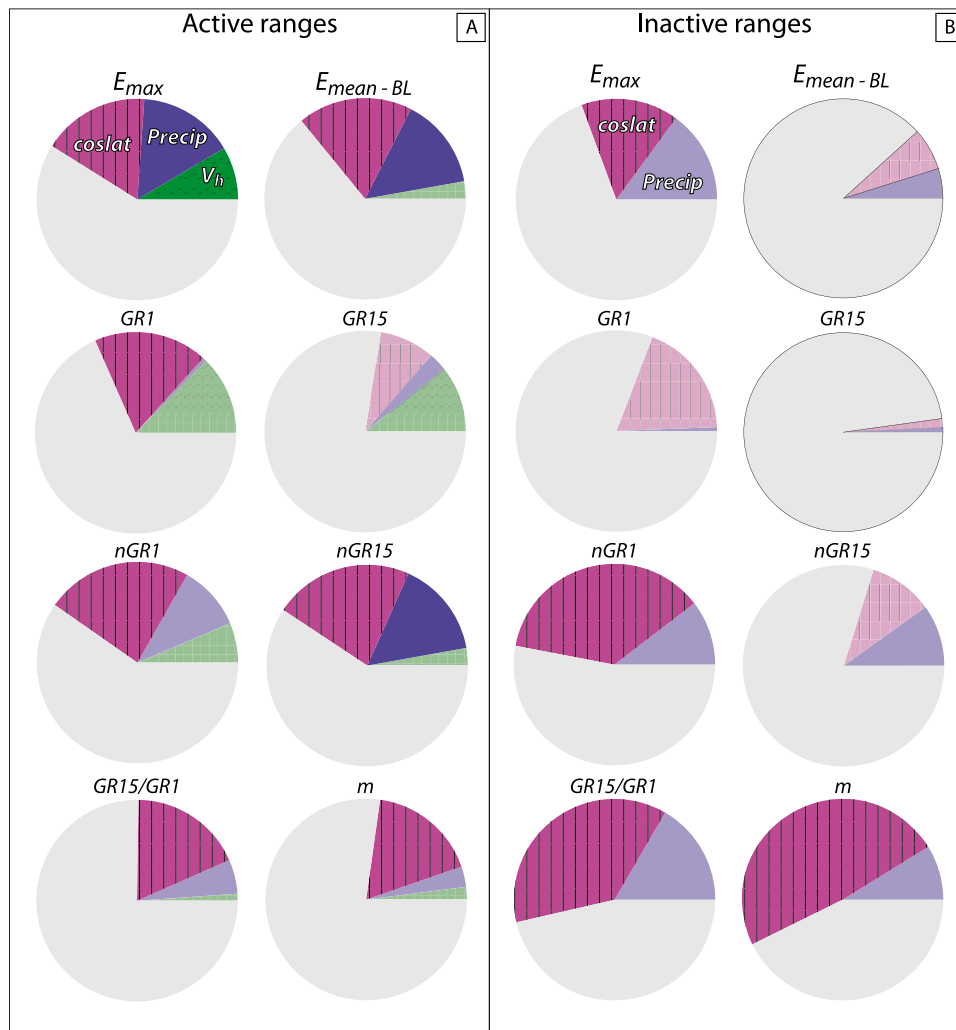
Figure 13. Pie charts similar to those in Figure 12, calculated for active ranges only (Figure 13a) and for inactive ranges only (Figure 13b) related to Tables 4b and 4c, respectively. As in Figures 11 and 12, significant factors (p-values < 5%) are pictured in bright colors, and insignificant factors (p-values > 5%) are pictured in pale colors. These data confirm, for instance, that GR15 is not well explained by climatic variables, since most of the variance of GR15 remains unexplained for inactive ranges (Figure A3b). This also confirms that the scale length of the relief (GR15/GR1 and m, i.e., the ratio between large scale relief and small scale relief) mostly depends on climatic factors, especially latitude, for both active and inactive ranges.

accounts for a negligible fraction of the normalized relief and relief length scale (Figures 12e–12h). It accounts for only 7–12% of the variance of the maximum and mean elevation of the ranges. Mean annual precipitation (precip) accounts for a significant fraction (20–25%) of the elevation of ranges (Figures 12a and 12b), but a negligible fraction of relief (<5%). The mean latitude of the range (coslat) is a large contributor (up to 41% for nGR1) to almost all of the topographic variables, but not GR15 (Figure 12d), which appears to be most strongly controlled by tectonics.

[36] When active and inactive ranges are treated separately (Tables 3b and 4c, Figure 13), the same patterns are clear. For active ranges only (Figure 13a), V_h, precip, and coslat explain less of the variance of the maximum elevations of ranges than when the entire data set is used (only 8.5%, instead of 12.6%). These variables fail to explain the mean

Table 3a. Multivariate Normalized Slope Values of Active and Inactive Ranges Depicted in Figure 11[a]

	E_{max}	Error	$E_{mean} - BL$	Error	GR1	Error	GR15	Error	nGR1	Error	nGR15	Error	GR15/GR1	Error	m	Error
V_h	**0.45**	**0.10**	**0.29**	**0.11**	**0.45**	**0.11**	**0.51**	**0.12**	0.05	0.10	−0.14	0.10	−0.06	0.11	−0.07	0.11
Precip	**−0.63**	**0.11**	**−0.56**	**0.12**	−0.07	0.13	−0.04	0.13	**0.33**	**0.12**	**0.58**	**0.12**	0.17	0.09	−0.12	0.12
Coslat	**0.66**	**0.10**	**0.62**	**0.12**	**−0.40**	**0.12**	−0.04	0.13	**−0.75**	**0.11**	**−0.71**	**0.11**	**0.50**	**0.12**	**0.55**	**0.12**
R/R^2	0.70	0.49	0.60	0.36	0.56	0.32	0.50	0.25	0.67	0.44	0.64	0.41	0.59	0.35	0.60	0.35

[a]Bold values indicate p < 0.02.

Table 3b. Multivariate Normalized Slope Values of Active Ranges Depicted in Figure A3a[a]

	E_{max}	Error	E_{mean} − BL	Error	GR1	Error	GR15	Error	nGR1	Error	nGR15	Error	GR15/GR1	Error	m	Error
V_h	**0.33**	**0.13**	0.11	0.15	**0.33**	**0.14**	**0.31**	**0.13**	0.17	0.13	−0.10	0.10	−0.03	0.14	−0.05	0.14
Precip	−**0.60**	**0.14**	−**0.57**	**0.16**	−0.02	0.16	0.08	0.15	0.28	0.14	**0.55**	**0.11**	0.12	0.16	0.08	0.16
Coslat	**0.67**	**0.12**	**0.71**	**0.16**	−**0.48**	**0.14**	−0.26	0.14	−**0.63**	**0.14**	−**0.80**	**0.10**	**0.41**	**0.16**	**0.42**	**0.15**
Constant	0.14	0.12	0.23	0.14	0.14	0.14	0.26	0.13	−0.16	0.12	−0.03	0.09	−0.01	0.14	0.02	0.14
R/R^2	0.64	0.41	0.60	0.36	0.56	0.32	0.47	0.22	0.63	0.40	0.64	0.41	0.50	0.25	0.48	0.23

[a]Bold values indicate p < 0.02.

Table 3c. Multivariate Normalized Slope Values for Inactive Ranges Depicted in Figure A3b[a]

	E_{max}	Error	E_{mean} − BL	Error	GR1	Error	GR15	Error	nGR1	Error	nGR15	Error	GR15/GR1	Error	m	Error
Precip	−**0.46**	**0.19**	−0.11	0.12	0.01	0.26	0.05	0.28	0.23	0.24	0.59	0.33	0.28	0.23	0.14	0.23
Coslat	**0.48**	**0.16**	0.17	0.10	−0.39	0.22	0.10	0.24	−**0.80**	**0.20**	−**0.61**	**0.27**	**0.62**	**0.19**	**0.74**	**0.19**
Constant	−**0.55**	**0.14**	−**0.62**	**0.09**	−**0.48**	**0.19**	−**0.63**	**0.20**	0.13	0.17	0.17	0.24	0.09	0.17	0.08	0.16
R/R^2	0.55	0.31	0.34	0.12	0.44	0.19	0.15	0.02	0.69	0.47	0.45	0.20	0.73	0.54	0.76	0.57

[a]Bold values indicate p < 0.02.

Table 4a. Corrected Variance Coefficients of Multivariate Regression for Active and Inactive Ranges Depicted in Figure 12a[a]

	E_{max}	Error	E_{mean} − BL	Error	GR1	Error	GR15	Error	nGR1	Error	nGR15	Error	GR15/GR1	Error	m	Error
V_h (%)	**12.6**	**2.7**	**7.1**	**2.6**	**15.3**	**3.8**	**21.7**	**4.9**	1.9	4.0	4.0	2.9	3.0	5.2	3.4	5.3
Precip (%)	**17.7**	**3.1**	**13.6**	**3.0**	2.5	4.4	1.6	5.6	**13.1**	**4.6**	**16.6**	**3.4**	8.3	5.9	4.6	5.8
Coslat (%)	**18.5**	**2.9**	**15.1**	**2.8**	**13.7**	**4.1**	1.5	5.3	**29.3**	**4.3**	**20.1**	**3.2**	**23.7**	**5.6**	**27.4**	**5.8**
Unexplained variance (%)	51.3		64.2		68.5		75.3		55.8		59.3		65.0		64.6	

[a]Percentage the observed variance has been calculated by using the slope values (Table 3a) that have been normalized so that their sum equals R^2 * 100, without taking account of possible nonzero "constant" values in the regressions. Bold font is used for statistically significant values, with p < 2%.

Table 4b. Corrected Variance Coefficients of Multivariate Regression for Active Ranges Depicted in Figure A3a[a]

	E_{max}	Error	E_{mean} − BL	Error	GR1	Error	GR15	Error	nGR1	Error	nGR15	Error	GR15/GR1	Error	m	Error
V_h (%)	**8.5**	**3.3**	2.8	3.8	**12.7**	**5.3**	**10.7**	**4.6**	6.4	4.7	2.8	2.7	1.1	6.3	2.0	6.0
Precip (%)	**15.4**	**3.6**	**14.7**	**4.2**	0.6	6.0	2.9	5.1	10.4	5.2	**15.5**	**3.0**	5.5	6.8	3.3	6.7
Coslat (%)	**17.2**	**3.2**	**18.4**	**4.1**	**18.3**	**5.2**	8.9	5.0	**23.5**	**5.1**	**22.4**	**2.9**	**18.2**	**6.8**	**17.5**	**6.5**
Unexplained variance (%)	58.9		64.1		68.5		77.5		59.7		59.3		75.3		77.2	

[a]Bold font is used for statistically significant values, with p < 2%.

Table 4c. Corrected Variance Coefficients of Multivariate Regression for Inactive Ranges Depicted in Figure A3b[a]

	E_{max}	Error	E_{mean} − BL	Error	GR1	Error	GR15	Error	nGR1	Error	nGR15	Error	GR15/GR1	Error	exp	Error
Precip (%)	**14.9**	**4.0**	4.6	1.6	0.6	5.6	0.7	0.8	10.4	9.7	9.9	4.8	16.6	12.6	8.8	13.4
Coslat (%)	**15.7**	**3.4**	7.1	1.3	18.6	4.8	1.5	0.7	**36.6**	**8.2**	10.3	4.6	**37.0**	10.6	**48.5**	**11.3**
Unexplained variance (%)	69.3		88.3		80.9		97.8		53.0		79.8		46.4		42.7	

[a]Bold font is used for statistically significant values, with p < 2%.

elevation (E_{mean} − BL) of the ranges used in our data set. For the inactive ranges (Figure 13b), with tectonic shortening rates not considered, the results give insights of the relative contribution of latitude and precipitation to shape a mountain range after its death, but given the small number of cases (n = 24), these results should be treated with caution. For half of the topographic variables (E_{mean} − BL, GR1, GR15 and nGR15), the results are not statistically significant. The analysis of inactive ranges, however, corroborates the important contribution of physical parameters that depend on latitude (most likely glaciation) in shaping the topography, which we observed earlier (Figures 9–12), and which is even more pronounced than for ranges undergoing of tectonic shortening. coslat explains more than 1/3 (37%) of the total variance of nGR1, and almost 1/2 (48%) of the scaling ratio m of the relief.

5. Discussion

[37] The landscape reflects a quasi-equilibrium (perhaps in a transient state progressing toward a new equilibrium) between processes that raise or lower it and that shape it, tectonics and climate (through its impact on erosion). The present paper quantifies plausible sets of parameters that describe landscapes and that characterize a subset of processes by which tectonics and climate affect landscapes. Despite a large scatter inherent to the kinds of data used, we show that some significant correlations exist between independent variables (e.g., convergence rate, V_h, and maximum elevations of the ranges, E_{max}), and that correlations between some of the parameters is high enough to justify a posteriori the quality of the database.

[38] One noteworthy result of this study is the contrasting insensitivity of small scale relief (GR1 and nGR1) to mean annual precipitation to its high correlation with latitude. We have used coslat as a surrogate for the likelihood of glaciations (and periglacial processes), and we note the apparent importance of glaciation in reducing mean elevation and in increasing relief at small but not large, scales. This reflects the more inhomogeneous distribution of glacial and periglacial erosion than fluvial incision, and in particular its ability to deeply carve valleys with steep slopes, while also protecting other parts of the landscape [*Anderson*, 2005; *Herman et al.*, 2011; *Thomson et al.*, 2010; P. Sternai et al., The pre-glacial topography of the Alps, submitted to *Geology*, 2012]. Glacial erosion appears to be the main agent of relief creation at small scale. Furthermore, the relations between the topographic parameters and latitude indicate that glacial and periglacial not only act to reduce the overall elevation but also to increase the "roughness" of the topography toward the poles [*Molnar and England*, 1990].

[39] Another implication from our study derives from the relatively weak importance of tectonics, at least active tectonics, in controlling topographic parameters (see correlation coefficients in Tables 4a–4c). For active ranges (V_h > 0 mm/yr), tectonics explains a statistically insignificant part of the variance in mean elevation (E_{mean} − BL) (Figure 13a and Tables 3b and 4b). Obviously, only tectonic processes are capable of building thick crust and high mean elevations, and where convergence occurs, tectonic shortening is unlikely to reduce mean elevations. This process, however, may be limited to the first stages of mountain building [e.g., *Abbott et al.*, 1997], and we consider it noteworthy that active tectonics, widely treated as the most important process that has created present-day topography and relief accounts for only 25%, or less, of the variance in most of the measures topography or relief considered here. This observation poses the question: Is the role of tectonics in the creation of relief overrated? An affirmative answer would be consistent with the suggestion that climate change via its impact on erosion is responsible for juvenile landscapes that have traditionally be ascribed to "uplift" and recent tectonics [e.g., *Molnar and England*, 1990; *Zhang et al.*, 2001].

[40] We recognize that we have ignored relevant processes responsible for present-day topography, and we hope that as the knowledge base grows, it will be possible to include other relevant processes, such as the storminess of a climate (not just mean annual precipitation), past geologic history including total amounts of crustal shortening and thickening (not just present-day rates) and the erodibility of rock types that crop out in mountain belts, accurate measures of both present-day and Quaternary glaciation, etc. Surely, our failure to include such processes accounts for the failure of the three parameters that we have considered – convergence rate, mean annual precipitation, and latitude – to account for more than half of the variance in most measures of topography and relief that we have considered (Figure 12).

6. Conclusions

[41] From results of section 3 (bivariate analyses) and section 4 (multivariate analyses), the following points are of particular importance, and are summarized in Figures 11–13 and A3:

[42] 1. Elevations of ranges directly reflect the interaction between tectonics, which thickens the crust, and therefore increases elevations, and climate (through erosion), which thins the crust, and hence decreases the elevation (Figures 12a and 12b). This statement may seem trivial, but this is, as far as we know, the first quantitative demonstration of this over such a large geologic database. The importance of tectonics appears to be modest in most cases, and although tectonics is obviously essential for mountain building, the shapes of mature ranges appear to be controlled mostly by climate factors, which cause the large scatter observed in Figure 5.

[43] 2. Relief is not sensitive to mean annual precipitation amounts (Figures 12c and 12d, but increases with shortening rates and latitude (hence glacial erosion). Relief averaged over large areas (GR15, ∼600 km^2) is not obviously affected much by climatic factors, and more by tectonics, but relief measured on short distance scales (GR1, ∼8 km^2, Figures 11c and 12c) correlates best with a combination of tectonics and latitude. Relief in high-latitude mountain ranges result largely from glacial excavation at valley scale of the topography created by tectonics.

[44] 3. The location of a mountain range on Earth appears to be a key factor in determining its elevation, as already showed by others [e.g., *Egholm et al.*, 2009, and references therein; *Porter*, 1977]. Latitude also correlates with relief measured on short distance scales (GR1, ∼8 km^2) and the relative relief (the amount of relief scaled to the mean elevation of the range) (Figures 12e and 12f). Presumably, the

climatic differences that vary with latitude, glaciers in particular, play a crucial role in shaping that relief (Figures 12g and 12h).

Appendix A

[45] This appendix provides additional figures (Figures A1, A2, and A3), as well as additional (raw) data (Table A1) not directly used in the manuscript, but potentially useful for more curious readers.

Appendix B: Summary of Geodetic and Other Constraints on Shortening Rates

[46] Alaska (Chugach) (CHU): *Freymueller et al.* [2008] reported velocities of several points north and south of the range, and differences between those north and south of the range suggest a north–south shortening rate of ∼25 mm/yr. *Suito and Freymueller* [2009], however, showed that 5 mm/yr (or perhaps more) of this convergence results from the viscoelastic response to the 1964 Alaska earthquake. Some might also be associated with subduction of the Pacific plate beneath southern Alaska, if not along the margins of the range itself. Accordingly we allow for a relatively large uncertainty: 20 ± 5 mm/yr.

[47] Alaska (Denali) (DEN): We rely on GPS measurements summarized by *Freymueller et al.* [2008]. We use the difference in components of velocity perpendicular to the Denali Fault at Mount Denali between the stations WOND and HURR to obtain 4.1 ± 2.4 mm/yr. We recognize that post-seismic slip following the 1964 Alaskan earthquake might contribute to the velocities at these two sites, but we ignore it here.

[48] Alaska (Eastern Range) (EAR): We rely on measurements along the Richardson Highway presented by *Fletcher* [2002], which were made before the earthquake of 2001. The scatter and differences between stations on both sides of the range makes choosing which points to use difficult, and we rely on the component perpendicular to the Denali Fault along this profile: 2 ± 1 mm/yr.
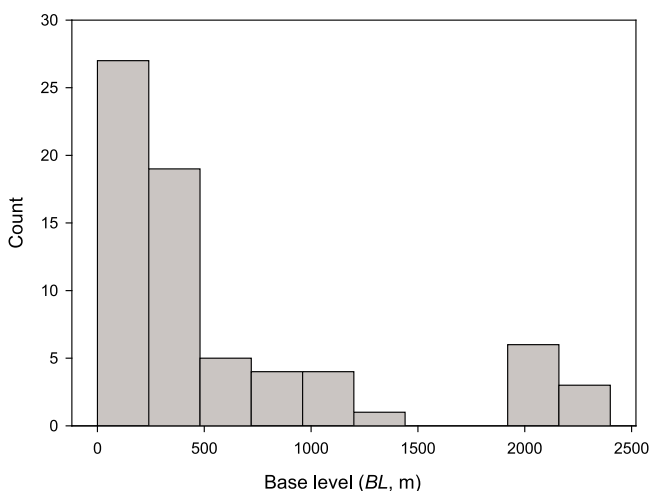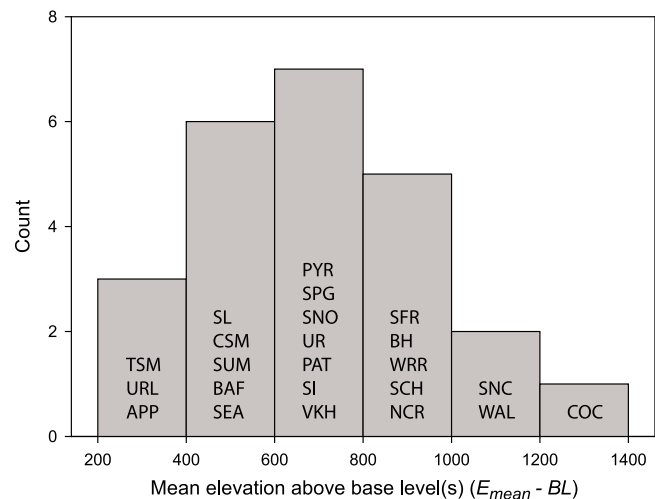
Figure A2. Histograms of the mean elevation above base level (E_{mean} − BL) of the 24 inactive ranges, with their names.

[49] Alaska (Saint Elias) (SE): We use the result of *Elliott et al.* [2010] that the Yakutat block south of the Saint Elias Range moves at ∼45 mm/yr NNW toward the Southern Alaska block of *Fletcher* [2002], which lies north of the range. With an east–west orientation of the Saint Elias Range and convergence at approximately N20°W, we use a shortening rate of 42 ± 5 mm/yr, where the uncertainty is meant to include not only errors and scatter in GPS rates, but also variation in convergence rates along the range and errors in orientations of both it and movement of the two blocks.

[50] Alborz (ALB): We use the GPS result of 6 ± 2 mm/yr of *Djamour et al.* [2010], which replace the rates of 8 ± 2 mm/yr given by *Vernant et al.* [2004b] and 5 ± 2 mm/yr given by *Vernant et al.* [2004a].

[51] Alps (Eastern) (EAL): We rely on GPS results showing that the Apulian peninsula rotates about an axis in or near the western Po Basin and converges with Eurasia at 2.2 ± 1 mm/yr [*Calais et al.*, 2002b], which agree sufficiently well with GPS results of *Battaglia et al.* [2004] and *Serpelloni et al.* [2005], and with the rate of shortening measured by *Benedetti et al.* [2000] for the bounding thrust fault of the Alps in southern Italy.

[52] Alps (Western) (WAL): We rely on the GPS results of *Calais et al.* [2002a], and corroborated by several other studies [*Calais et al.*, 2002a; *D'Agostino et al.*, 2008; *Serpelloni et al.*, 2005; *Weber et al.*, 2010], which show essentially no present-day convergence across the western Alps, but extension and strike-slip movement parallel to the belt and internal deformation of it. This range may be a singular case, because active shortening is null but recent geological history shows that shortening across the range occurred during the Pliocene, and has apparently stopped since then. We use 0 ± 1 mm/yr.

[53] Anatolia (ANA): We rely on the GPS results of *Reilinger et al.* [2006], which supersede those of *McClusky et al.* [2000]. *Reilinger et al.* [2006] divided the region into blocks, and they showed 4.4 ± 0.5 (1σ) mm/yr of shortening across this region, with a much larger component of left-lateral shear (∼15 mm/yr) across it.
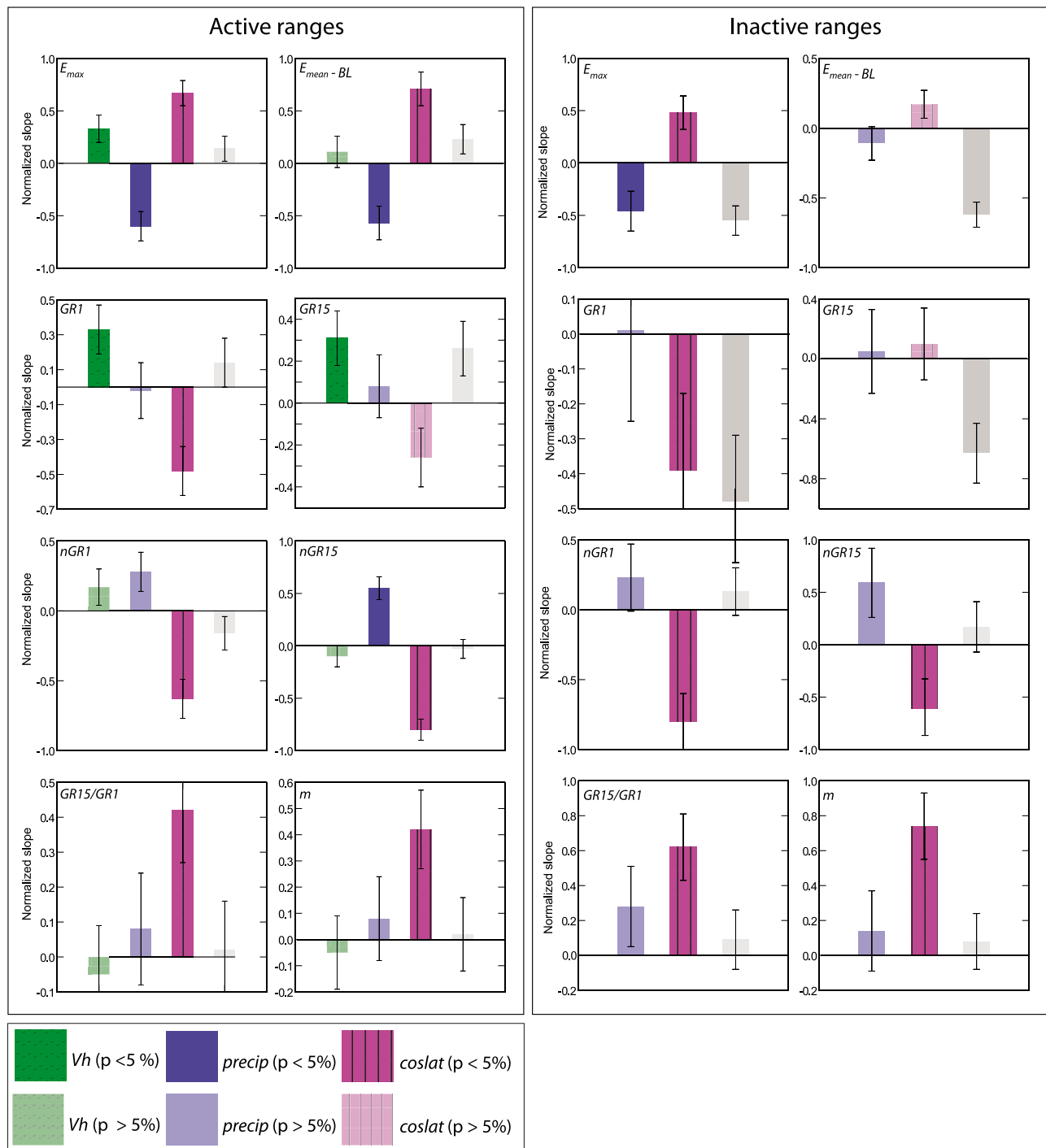
Figure A1. Histogram of the base level (BL) chosen for each range. 70% of the base levels are below 500 m a.s.l.

Figure A3. Histograms of "raw" factors of the normalized multivariate linear regressions of topographic variables against V_h, precip, and coslat, with 1σ error bars, from Tables 3b and 3c (active and inactive ranges taken separately). Significant factors (p-values < 5%) are pictured in bright colors, insignificant factors (p-values > 5%) are pictured in pale colors. Color coding corresponds to that used in Table 1 and Figure 11 (green for V_h, blue for precip, and violet for coslat).

[54] Andes (Northern Bolivia and Southern Peru) (NBA and SPA): We rely on the GPS results of *Bevis et al.* [2001] and *Kendrick et al.* [2001], and the analysis by *Allmendinger et al.* [2007], which shows convergence rate of 6 ± 2 mm/yr. These results supersede those of *Norabuena et al.* [1998], who reported a somewhat higher rate.

[55] Andes (Northern Peru) (NPA): Again, we rely on the GPS results of *Bevis et al.* [2001] and *Kendrick et al.* [2001] showing a convergence rate of 6 ± 2 mm/yr and superseding those of *Norabuena et al.* [1998].

[56] Andes (Southern Bolivia) (SBA): We use the GPS results of *Bevis et al.* [2001], showing a convergence rate of

Table A1. Parameters Not Shown in Table 1[a]

Range	Code	E_{top} (m)	a	GR1i	GR5i	GR15i	Bl_low	BL_high	BL	nGR1_E_{max}	nGR5_E_{max}	nGR15_E_{max}	Area (× 10^3 km²)	Latitude (deg)	Coordinates (longitude1, latitude1; longitude2, latitude2 …)
Alaska (Chugach)	CHU	3779	112.94	178.9	662.4	1159.2	0	600	300	0.103	0.294	0.704	7.5	61.525	(−149.1, 61.7; −146.5, 62; −146.7, 61.3; −147.7, 61.1)
Alaska (Denali)	DEN	6098	89.219	149.7	548.0	1150.9	200	500	350	0.067	0.209	0.544	13.2	63	(−149.5, 63.5; 149.5, 62.5; −152.5, 62.5; −152.5, 63.5)
Alaska (Eastern Range)	AER	3850	66.561	107.7	407.7	789.6	150	600	375	0.075	0.228	0.577	32.9	63.4	(−149, 64.4; −146.4, 64.2; −142.85, 63.3; −144, 62.6; −147, 62.7; −147.8, 63.3; −149, 63.4)
Alaska (Saint Elias)	SEL	5800	173.57	139.3	569.4	1131.6	0	700	350	0.099	0.221	0.434	66.2	60.6	(−141.8, 62.4; −137.7, 60.8; −138.3, 59.1; −142.8, 60.1)
Alborz	ALB	5587	121.42	225.6	649.8	1148.1	0	1000	500	0.078	0.193	0.411	32.8	36	(50, 37.4; 53, 36.5; 53.3, 35; 49, 37.4)
Alps (Eastern)	EAL	3628	102.85	177.6	575.2	938.5	100	500	300	0.077	0.195	0.425	94.1	46.44	(10, 47.6; 16.5, 48.2; 15.4, 46; 13, 46; 11.2, 45.25; 10, 45.6)
Alps (Western)	WAL	4536	92.206	175.2	488.0	1004.5	200	400	300	0.069	0.182	0.410	94.3	45.27	(10, 47.6; 10 45.6; 8.2, 45.2; 8.2, 43; 5, 43; 5, 45.3; 7.5, 47.2)
Anatolia	ANA	4078	101.52	187.1	549.4	977.4	600	1600	1100	0.070	0.177	0.381	34.8	39.42	(42.6, 38.5; 45, 38.5; 45.3, 36.4; 42.8, 37.2)
Andes (Northern Bolivian)	NBA	6194	40.437	94.4	356.1	721.2	0	200	100	0.021	0.067	0.172	246.8	−18	(−70.25, −20; −70.34, −18.43; −67, −15; −63.27, −17.5; −62.75, −19.3)
Andes (Northern Peru)	NPA	6710	32.949	90.1	421.7	960.2	0	300	150	0.020	0.074	0.222	350.2	−9.5	(−77, −4.75; −73, −12; −76, −16; −81.7, −5.3)
Andes (Southern Bolivia)	SBA	6010	26.436	68.3	294.1	668.9	0	400	200	0.014	0.051	0.148	322.7	−21.4	(−64, −24; −62.75, −20.5; −62.75, −19.3; −70.3, −20; −75.5, −23.36)
Andes (Southern Peru)	SPA	6278	76.82	157.8	438.4	835.8	0	300	150	0.033	0.083	0.181	323.8	−14.7	(−73, −12; −68.5, −13; −68.7, −14.7; −70.35, −18.46; −75.6, −15.36)
Appalachians	APP	1981	33.139	65.5	217.3	402.9	300	300	300	0.059	0.164	0.381	139.7	37	(−78, 41; −78, 38; −85, 33.5; −85, 35.5)
Australia (Southeastern)	SEA	2431	11.95	28.7	114.1	260.6	50	250	150	0.024	0.081	0.226	319.3	−32.45	(151, −26; 145, −37.6; 150, −39.5; 155, −26.7)
Baffin	BAF	1807	156.27	197.8	466.9	742.3	0	100	50	0.177	0.371	0.686	44.3	70.675	(−75.5, 72.9; −65.6, 69.8; −67, 68.6; −76.9, 71.4)
Big Horn (Wyoming)	BH	3401	37.253	76.5	279.0	578.5	1300	1300	1300	0.030	0.092	0.237	10.9	44.4	(−108.1, 45.5; −106.8, 44.7; −106.65, 43.9; −107.3, 43.2; −108.3, 44.9)
Brooks Range (Alaska)	BR	2621	63.97	96.8	326.2	560.9	150	300	225	0.075	0.199	0.453	178.1	63.2	(−140.5, 56.5; −156.5, 56.5; −156.5, 70; −140.5, 70)
Canadian Cordillera (Western)	WCC	3375	122.82	193.9	587.7	885.7	0	500	250	0.105	0.246	0.499	86.7	51	(−125.3, 52.5; −122.3, 51.7; −121.35, 49.5; −122.75, 48.8; −127.75, 51.35; −126.5, 52.45)
Caucasus	CAU	5483	67.471	134.4	477.7	924.7	300	300	300	0.048	0.141	0.347	146.0	42.57	(39.3, 44.6; 49.5, 43.8; 50.7, 39.3; 39.3, 44.6)
Chile (33°S–39°S)	CS	5980	73.46	150.8	525.4	1009.6	250	700	475	0.032	0.092	0.222	104.9	−36.2	(−70, −39; −72.2, −39; −70.8, −33.4; −69, −33.4)
Chile (Central, 30°S–33°S)	CC	6813	62.606	140.5	537.0	1101.3	200	600	400	0.029	0.091	0.238	120.0	−31.4	(−68.6, −33.4; −71.5, −33.4; −71.3, −28.8; −68.3, −30)
Chile (Northern, 23°S–30°S)	CN	6668	33.751	89.2	405.8	955.8	100	400	250	0.018	0.068	0.204	360.9	−25	(−68.3, −30; −66, −29; −64, −24; −70.5, −23.4; −71.5, −28.7)
Cordillera de Merida (Venz.)	MER	4991	43.773	116.6	533.9	1176.6	100	200	150	0.034	0.122	0.358	34.6	8.9	(−69.9, 10.3; −69, 9.7; −71.9, 7.4; −72.6, 8.1)
Cordillera Occ./Central (Colomb.)	COC	5217	54.389	134.1	509.0	1085.2	100	300	200	0.035	0.114	0.300	148.0	4.7	(−78, 1.8; −76.6, 5.5; −76.8, 8.7; −75 8; −74.3, 6.7; −75.85, 1.2; −76.3 1)
Cordillera Oriental (Colombia)	COR	4114	51.912	125.7	484.4	994.9	100	400	250	0.037	0.116	0.305	94.5	4.4	(−75.85, 1.2; −74.37, 6.44; −73.55, 7.7; −72 5.4; −75.3, 1.4)
Corsica	CSC	2463	61.368	125.7	505.1	963.2	0	0	0	0.107	0.335	0.866	8.2	42	(43, 9; 43.9, 9.6; 41, 9.6; 8.5, 41.9)

Table A1. (continued)

Range	Code	E_{top} (m)	a	GR1i	GR5i	GR15i	BIlow	BLhigh	BL	nGR1_E_{max}	nGR5_E_{max}	nGR15_E_{max}	Area ($\times 10^3$ km^2)	Latitude (deg)	Coordinates (longitude1, latitude1; longitude2, latitude2 …)
Dinarides	DNR	2626	48.579	96.9	354.2	682.5	0	600	300	0.062	0.185	0.459	124.6	43.02	(15.5, 45.25; 20.75, 44.25; 22.75, 40.3; 19.2, 40.3; 14.4, 45)
Ecuadorian Andes	EQA	6074	56.723	137.5	512.5	1070.2	50	400	225	0.035	0.110	0.287	152.3	37.6	(−77, −4.7; −81.7, −5.3; −1.3, −1; −79.3, 2.5; −76.5, 1)
Front Range (Southern Colorado)	SFR	4280	54.163	105.6	358.0	644.5	1800	2300	2050	0.034	0.094	0.219	27.1	15.29	(−108.4, 38.5; −108.4, 37.3; −106, 36.35; −106, 38.4)
Guatemala Ranges	GUA	3987	46.998	121.9	389.4	1013.5	150	250	200	0.040	0.130	0.346	45.4	31	(−91.2, 16.25; −89, 15.7; −90.3, 14; −92.6, 15.2)
High Atlas	HAT	4057	73.423	149.0	471.6	891.0	500	1100	800	0.048	0.130	0.300	40.0	27.7	(−10, 31.5; −5.7, 32.8; −3.3, 32.8; −3.8, 31.8; −10, 29.8)
Himalayas (Bhutan)	BHA	7461	99.767	203.0	687.6	1233.2	150	4500	2325	0.039	0.108	0.250	54.2	28.91	(89.4, 28.7; 92, 28.7; 92, 26.7; 89.4, 26.7)
Himalayas (Nepal)	NHA	8752	85.054	186.4	690.3	1354.3	200	4500	2350	0.033	0.101	0.254	182.3	30.76	(81, 31; 80, 29; 82.5, 27.5; 88, 26.5; 89, 28.25; 84.5, 29.25)
Himalayas (Western India)	WIH	7409	97.774	195.0	647.1	1156.6	300	4500	2400	0.035	0.094	0.216	90.9	18.4	(81, 31; 80, 29; 77.7, 30; 76.3, 31.3; 78.8, 32.5)
Hispaniola	HIS	2928	38.707	97.3	371.7	847.9	0	0	0	0.054	0.181	0.494	29.2	24.1	(−72, 19.8; −70, 19; −71, 17; −73, 18)
Indoburman Ranges	IBR	3464	61.391	129.2	452.6	827.2	100	150	125	0.054	0.153	0.364	118.2	35.23	(96, 27.5; 96.4, 26.7; 95, 25; 94.4, 20.65; 92.5, 20.5; 92, 24.25)
Karakorum	KKR	8238	98.149	190.8	652.6	1138.7	400	1400	900	0.063	0.171	0.394	286.5	62.9	(76, 39; 80.2, 37; 76.4, −31.4; 72.6, 33.5)
McKenzie Mountains (Canada)	MKM	2939	45.319	72.6	300.6	544.1	200	600	400	0.056	0.173	0.442	339.0	51.42	(−136, 66; −141, 65; −126, 59; −126, 59.4; −123.3, 59.5; −122.5, 62.5; −126, 65.5)
Mongolian Altai (northern)	NMA	4280	62.644	112.0	379.0	699.6	400	1000	700	0.041	0.115	0.270	222.7	47.13	(81.8, 51.2; 90.2, 52.7; 92.1, 49.2; 85.8, 48; 83.3, 48.8)
Mongolian Altai (southern)	SMA	4165	40.778	83.8	321.9	680.6	800	1200	1000	0.032	0.102	0.270	119.6	−5.92	(92.1, 49.1; 95.1, 46.5; 94.7, 44.7; 86.8, 48.2)
New Guinea (Eastern)	PNG	4437	35.507	100.9	494.3	1161.6	50	250	150	0.036	0.139	0.433	100.0	−4.27	(141.5, −4.7; 144.3, −4.8; 146.5, −6.5; 145.75, −8; 141.4, −5.6)
New Guinea (Western)	WNG	5179	31.529	92.4	452.5	1115.1	50	150	100	0.028	0.110	0.352	107.9	66.425	(136.5, −2.9; 141.7, −4.2; 141.3, −5.8; 135, −4.2)
Norway (northern)	NNO	1955	54.93	80.8	288.3	510.5	0	200	100	0.090	0.251	0.593	88.3	60.62	(11.6, 65; 16.5, 68.7; 19.9, 68.8; 14.4, 63.2)
Norway (southern)	SNO	2292	65.999	98.7	300.1	484.0	0	100	50	0.074	0.164	0.316	131.5	−42	(9.5, 63.7; 11.6, 60.5; 7.3, 58; 5.5, 58.7; 4.7, 62.2)
Patagonia (northern)	PAT	3556	65.612	121.9	419.0	720.1	0	500	250	0.065	0.176	0.403	138.6	−49.4	(−70, −39; −72.2, −39; −73.6, −45.1; −70.7, −45.1)
Patagonia (southern)	SPG	3809	85.224	153.6	570.9	992.5	0	250	125	0.095	0.269	0.642	90.7	42.54	(−73.6, −45.1; −71.6, −45.1; −71.8, −47.9; −73.3, −52; −74.2, −49.9; −73.6, −45.1)
Pyrenees	PYR	3153	62.383	121.6	414.9	785.9	200	400	300	0.066	0.187	0.446	45.0	37.93	(−2, 43.25; 3, 43.25; 3, 41.8; −1, 41.8; −2, 42.6)
Qilian Shan	QS	5713	35.407	81.0	326.8	721.3	1400	2700	2050	0.020	0.068	0.187	272.0	52.4	(97, 40.5; 104.2, 37.25; 103, 35.25; 95.3, 37.25; 92.2, 39.4)
Rockies (Canada)	CAR	3610	71.579	122.1	433.0	726.6	800	800	800	0.060	0.163	0.375	94.9	39.6	(−121, 55.2; −116.6, 53.3; −114.2, 51.4; −115.7, 49.65; −116.2, 50.75; −118.37, 52.1; −119.25, 52.9; −121.9, 54.1)
Rockies (Northern Colorado)	NCR	4328	62.499	132.4	420.7	926.3	1500	2500	2000	0.040	0.117	0.289	47.9	36.9	(−107.5, 41; −105.2, 40.5; −105.2, 38.4; −107.5, 38.5)
Sangre de Christo (Colorado)	SCH	4210	46.934	101.4	397.0	794.5	1600	2300	1950	0.037	0.115	0.301	13.9	37.1	(−105.9, 35.4; −105.2, 35.45; −104.56, 37.15; −105.17, 38.5; −105.9, 38.2)
Sierra Nevada (California)	SNC	4314	54.968	115.5	415.7	826.2	50	1100	575	0.039	0.116	0.289	46.8	−43.5	(−119.5, 38.9; −121, 38; −119, 35.35; −117.8, 35.8; −118, 36.65; −118.85, 38)

Table A1. (continued)

Range	Code	E_{top} (m)	a	GR1i	GR5i	GR15i	Bl$_{low}$	Bl$_{high}$	BL	nGR1_E_{max}	nGR5_E_{max}	nGR15_E_{max}	Area ($\times 10^3$ km^2)	Latitude (deg)	Coordinates (longitude1, latitude1; longitude2, latitude2 ...)
Southern Alps (New Zealand)	SNZ	3173	47.548	94.2	356.3	671.2	0	200	100	0.064	0.191	0.476	151.3	9.57	(172.5, −40; 165.5, −46; 169, −47.5; 175, −42)
Southern India	SI	2533	38.523	96.3	423.7	861.7	0	200	100	0.061	0.206	0.572	17.7	7	(76.2, 10.7; 78, 10.5; 77.5, 8.1; 76.5, 9)
Sri Lanka	SL	2490	27.215	73.3	350.2	765.7	0	200	100	0.047	0.173	0.516	12.6	0.7	(80, 5; 82, 5; 82, 9; 80, 9)
Sumatra	SUM	3633	20.071	59.9	305.1	755.8	0	200	100	0.028	0.115	0.374	189.7	23.6	(94.5, 5.5; 104.7, −6.3; 106.5, −5.5; 100.5, 3; 97, 6.7)
Taiwan	T	3743	51.55	121.5	480.0	993.1	0	0	0	0.053	0.170	0.453	35.3	9.25	(122, 25.4; 120, 25.4; 120, 21.8; 122, 21.8)
Talamanca Cordillera (Costa Rica)	TCR	3688	45.663	117.7	484.7	1072.0	0	200	100	0.051	0.175	0.488	35.1	−41.5	(−84.5, 10.5; −80.4, 8.7; −81.9, 8; −84.8, 9.8)
Tasmania	TSM	1522	16.461	39.6	190.5	444.2	0	100	50	0.043	0.164	0.505	63.7	42.59	(144, −40.2; 148.5, −40.7; 148.5, −43.8; 144.5, −43.6)
Tien Shan (Central)	CTS	7169	71.368	145.7	517.9	1049.4	600	1300	950	0.034	0.104	0.260	64.8	44.48	(78.8, 43.7; 82.8, 43.7; 83, 42; 79.6, 41)
Tien Shan (Eastern)	ETS	5039	73.508	144.9	513.5	1001.7	450	550	500	0.050	0.146	0.360	88.6	42.88	(82.9, 44.6; 87.7, 43.7; 88.9, 42.4; 86.6, 41.7; 83, 42)
Tien Shan (Dzungarian Alatau)	DZA	4337	47.501	104.2	408.0	903.6	800	1200	1000	0.030	0.101	0.275	62.3	−0.6	(82.7, 43.8; 78.7, 43.6; 76.4, 44.3; 80.9, 46.3; 82.8, 45.1; 82.7, 43.8)
Tien Shan (western)	WTS	5604	59.469	125.3	461.5	959.5	750	1200	975	0.031	0.097	0.249	280.3	41.55	(78.5, 43.8; 80, 40.5; 89, 43; 86.7, 44.5; 82, 45)
Uinta Range (Utah)	UR	4340	45.877	92.3	323.4	626.7	1700	2200	1950	0.026	0.075	0.183	14.7	40.71	(−111.5, 40.85; −110.45, 41.3; −109.1, 40.9; −109.2, 40.5; −111.3, 40)
Ural	URL	1775	33.002	51.9	189.2	357.9	50	350	200	0.071	0.209	0.515	92.1	64.22	(65.5, 68.5; 57.8, 65; 56.8, 57.5; 60.6, 58.6; 61, 64.3; 67.9, 67.1; 67.4, 68.6)
Verkhoyansk (Russia)	VKH	2207	62.298	90.4	263.0	413.8	250	350	300	0.076	0.178	0.362	146.5	63	(126, 71; 131, 71; 131, 63.5; 125.5, 63.5)
Wind River Range (Wyoming)	WRR	3988	57.851	109.4	368.8	669.1	1750	2200	1975	0.039	0.107	0.249	6.2	43	(−109.8, 43.65; −109.5, 43.5; −108.5, 42.5; −109, 42.4; −110, 43.2)
Zagros (Northwestern)	NWZ	4200	61.377	126.8	412.2	810.2	200	800	500	0.043	0.121	0.287	245.3	33.72	(53.4, 32.8; 48.4, 36.7; 45.5, 35.5; 46, 33; 50, 30.6)
Zagros (Southeastern)	SEZ	4468	47.899	106.7	379.4	785.4	0	800	400	0.036	0.111	0.281	329.4	29.53	(56.5, 26.7; 58.2, 29.75; 55.9, 32.3; 53.2, 32.65; 49, 30; 54.5, 25.8)

[a] E_{top} is the absolute maximum elevation on the DEM used, not shown in the paper, because of its very similar behavior to that of "E_{max}." Note that because of relatively large pixel size (~900 m), this value is lower than absolute peak elevation of each range. a is the pre-factor in the equation used in the correction (see Figure 4 and text for details). GR1i, GR5i and GR15i are raw mean values for the geophysical relief, not corrected for the latitudinal decrease of pixel size. nGR1_max, nGR5_max and nGR15_max are relative relief normalized to E_{max}. Area is the area within the polygon defined in row "coordinates" and displayed in Figure 2 and above the base level "BL." Latitude is the mean latitude of each range. Negative latitude are West of Greenwich, negative longitude are southern hemisphere.

8 ± 3 mm/yr, which is similar to the 6–7 mm/yr reported by *Kendrick et al.* [2006].

[57] Appalachians (APP): Using continuously recording GPS stations in eastern and central USA, *Gan and Prescott* [2001] report stability of the region spanning the Appalachians. We assume 0 ± 1 mm/yr.

[58] Australia (Southeastern) (SEA): Using nine continuously recording GPS stations spanning the Australian continent, *Tregoning* [2003, p. 41] reported: "within the resolution of the technique (∼2 mm/y at 95% confidence level), there are no significant changes in the dimensions of the Australian Plate across the Australian continent." We therefore use 0 ± 2 mm/yr.

[59] Baffin (BAF): Sparse continuously recording GPS sites on Greenland are moving southwest relative to North America at ∼2 mm/yr, and ∼1 mm/yr with respect to stations in northern and eastern Canada [*Argus et al.*, 2010]. This movement is almost surely associated with post-glacial rebound, but existing models of ice sheet history and of the viscosity structure cannot match these and other relevant data well [*Argus and Peltier*, 2010]. Nevertheless, we assume this deformation is a transient, and the convergence rate is only 0 ± 1 mm/yr.

[60] Big Horn (Wyoming) (BH): Although he did not discuss them, *Berglund* [2010] showed essentially no movement between GPS sites spanning the range. We assume 0 ± 1 mm/yr.

[61] Brooks Range (Alaska) (BR): *Freymueller et al.* [2008] showed that north–south relative movement of GPS points north and south of the Brooks Range imply ∼2 (±2) mm/yr of divergence. *Suito and Freymueller* [2009], however, show that visco-elastic deformation following the 1964 Alaska earthquake can contribute 2–3 mm/yr of divergence. Accordingly, we use 1 ± 2 mm/yr.

[62] Canadian Cordillera (Western) (WCC): By dividing the region into blocks, which allows them to exclude elastic strain from differences in GPS velocities, *McCaffrey et al.* [2007] inferred 3.3–3.4 mm/yr of shortening across the region. Their formal error is small, <1 mm/yr, but we use 3.3 ± 1.5 mm/yr to allow for some of this rate to be due to internal deformation west of the Cordillera. This accords with an estimate farther northwest of $\sim 2 \pm 2$ mm/yr given by *Mazzotti et al.* [2003].

[63] Caucasus (CAU): We rely on the GPS results of *McClusky et al.* [2000] and *Reilinger et al.* [2006] showing 8 ± 2 mm/yr of shortening across the range.

[64] Chile (Southern, 33°S–39°S) (CS): In the southern part of this region, GPS points on the east side of the Andes show slow movement with respect to stable South America, and *Kendrick et al.* [2006] inferred slow shortening across this area (from ∼1 mm/yr in the southern part to ∼2 mm/yr in the north). Inferring shortening across the Andes in the southern part of this region is made difficult by post-seismic deformation following the 1960 Chile earthquake (whose rupture terminated near 37.5°S) [*Khazaradze et al.*, 2002; *Klotz et al.*, 2001], but *Klotz et al.* [2001] inferred 6 ± 2 mm/yr of shortening in northern edge of this region from 39°S to 34°S. In the latitude band of 35°N to 37°N, some GPS data suggest that essentially all relative movement among points can be explained by elastic strain due to slip at the subduction zone [*Moreno et al.*, 2008; *Ruegg et al.*, 2002, 2009], but uncertainties in their reported measurements allow for

1–2 mm/yr. Complicating matters further, *Melnick et al.* [2006b] demonstrated that the high part of this segment of the Andes is undergoing normal faulting and approximately east–west extension. *Melnick et al.* [2006a], in fact, argued that shortening across this part of the Andes ceased at ∼6 Ma. Guided by these most recent studies and allowing for differences among them and differences along the belt, we assume an average convergence rate of 1 ± 2 mm/yr.

[65] Chile (Central, 30°S–33°S) (CC): Using GPS data *Brooks et al.* [2003] estimated ∼4.5 mm/yr of shortening in the Andes back-arc region, but revisions by *Kendrick et al.* [2006] suggest a lower rate. We assume 3 ± 2 mm/yr.

[66] Chile (Northern, 23°S–30°S) (CN): We rely on *Klotz et al.* [1999] who inferred 3–4 mm/yr of shortening across the northern part of this region and on *Brooks et al.* [2003] who estimated ∼4.5 mm/yr across the southern part. They found that by subtracting 3.4 mm/yr from the Nazca-South America convergence rate, they could fit the rest of the GPS data assuming elastic strain along the plate margin, and allowing for post-seismic deformation following the 1960 Chilean earthquake. *Khazaradze and Klotz* [2003] later reported the result of *Klotz et al.* [1999] as 3.4 ± 2 mm/yr. These rates seem consistent with the summary by *Kendrick et al.* [2006]. We assume 4 ± 2 mm/yr.

[67] Cordillera de Merida (Venezuela) (MER): Sparse GPS velocities given by *Trenkamp et al.* [2002] suggest shortening at 5 ± 3 mm/yr.

[68] Cordillera Occidental/Central Colombia (COC): Sparse GPS velocities given by *Trenkamp et al.* [2002] suggest negligible, but poorly constrained, present-day shortening, and we assume 0 ± 3 mm/yr.

[69] Cordillera Oriental (Colombia) (COR): Sparse GPS velocities given by *Trenkamp et al.* [2002] suggest rapid, but uncertain, present-day shortening, of 8 ± 5 mm/yr.

[70] Corsica (CRC): No resolvable movement of one continuously recording site on Corsica with respect to Europe [*Nocquet and Calais*, 2003; *Oldow et al.*, 2002] suggests little deformation of the region surrounding this point, and we assume that shortening does not occur across the island: 0 ± 2 mm/yr.

[71] Talamanca Cordillera (Costa Rica) (TCR): We rely on both GPS measurements [*LaFemina et al.*, 2009; *Norabuena et al.*, 2004] and slip rates on faults active in Quaternary time [*Fisher et al.*, 2004; *Sitchler et al.*, 2007]. In particular, with corrections for elastic strain along the subduction zone, *LaFemina et al.* [2009] show 25 ± 5 mm/yr of shortening across the region above sea level. Although the geologic bounds on Quaternary shortening, 10–40 mm/yr [*Fisher et al.*, 2004; *Sitchler et al.*, 2007] are less precisely constrained than those based on GPS measurements, they support the evidence for rapid shortening.

[72] Dinarides (DNR): We use the GPS rate of 4.5 ± 1 mm/yr given by *Bennett et al.* [2008], which supersedes the rates of 6 ± 1 mm/yr of *Battaglia et al.* [2004] and *Serpelloni et al.* [2005].

[73] Ecuadorian Andes (EQA): Using the data of *Trenkamp et al.* [2002] and correcting for elastic strain along the subduction zone, *White et al.* [2003] reported slip rates of 3 mm/yr on two thrust faults on the eastern margin of the range. So, we use 6 ± 3 mm/yr.

[74] Front Range (Southern Colorado) (SFR): From three years of data from 11 continuously recording GPS

instruments spanning a distance of ~900 km, *Berglund* [2010] inferred extensional strain spanning the region from east of the Front range, across the Sangre de Christo Range, the San Juan Mountains to southeastern Utah at 1.26 ± 0.21 nanostrain/yr. This corresponds to 0.126 ± 0.021 mm/yr across a region 100 km wide. We assume 0 ± 0.2 mm/yr for the Front Range, the Sangre de Christo Range, and the San Juan Mountains.

[75] Guatemala (GUA): We rely on the GPS measurements of *Lyon-Caen et al.* [2006]. Using the northeastern-most point and the two southwestern-most points and assuming an orientation of the range of N120°E, we calculate that shortening occurs at 6.1 mm/yr. This ignores possible elastic strain along the subduction zone and along the northern margin of the range. We assume 6 ± 2 mm/yr.

[76] High Atlas (Morocco) (HA): We rely on GPS measurements presented by *Fadil et al.* [2006], who reported 0.4 ± 0.6 mm/yr across the western part of the range and 1.0 ± 0.6 across the eastern part. We use the average: 0.7 ± 0.6 mm/yr.

[77] Himalaya (Bhutan) (BHA): We rely on the demonstration by *Jade et al.* [2004] that the rate of shortening along the Himalaya varies little, and GPS measurements of *Jade et al.* [2007] to infer 17 ± 3 mm/yr.

[78] Himalaya (Nepal) (NHA): GPS measurements of *Bilham et al.* [1997], *Bettinelli et al.* [2006], and *Feldl and Bilham* [2006] and *Lavé and Avouac*'s [2000] estimate of the slip rate on the main frontal thrust fault agree with one another. We use 19 ± 2.5 mm/yr from *Bettinelli et al.* [2006].

[79] Himalaya (Western India) (WIH): We use the rate based on GPS measurements and given by *Jade et al.* [2004]: 19 ± 3 mm/yr.

[80] Hispaniola (HIS): From GPS velocities of *Calais et al.* [2002b] and *Mann et al.* [2002], we use the NNE-SSW component of relative movement across the island: 7 ± 4 mm/yr.

[81] Indoburman Ranges (IBR): Using GPS data presented later by *Simons et al.* [2007], *Socquet et al.* [2006] inferred 7 to 9 mm/yr of shortening across the ranges; we use 8 ± 2 mm/yr.

[82] Karakorum (KKR): To estimate a convergence rate across this region, we use the angular velocities of India [*Argus and Peltier*, 2010] and of Tarim [*Reigber et al.*, 2001] with respect to Eurasia, both of which are based on GPS measurements. At the longitude of the Karakorum, these yield ~15 mm/yr of convergence between India and Tarim. This rate is lower than the convergence rates across the Himalaya farther east, presumably because east–west extension, by strike-slip and normal faulting, within Tibet nullifies some of the shortening at the Himalaya. We assume 15 ± 5 mm/yr.

[83] McKenzie Mountains (Canada) (MKM): From sparse continuously recording GPS measurements at sites SW of the mountains, *Leonard et al.* [2007] reported a rate of convergence between them and North America of 3–10 mm/a, little different from ~5 mm/yr given by *Mazzotti and Hyndman* [2002]. The wide range of possible rates derives in part from inconsistent velocities of campaign-style GPS measurements. Using seismic moments of moderate earthquakes, *Leonard et al.* [2008] inferred rates of 1.8 to

4.0 mm/yr. Recognizing the large uncertainties associated with such estimates, we use a rate at the low end of what *Leonard et al.* [2007] suggested: 5 ± 2 mm/yr.

[84] Mongolian Altai, northwestern and southeastern parts (NMA and SMA): We rely on GPS results of *Calais et al.* [2006, 2003] and also *England and Molnar*'s [2005] analysis of them. GPS points are sparse, and these authors have calculated smoothed deformation fields across the Mongolian Altai. Abundant evidence of strike-slip faulting along the Mongolian Altai accounts for part of the deformation within the belt [e.g., *Baljinnyam et al.*, 1993], but a convergent component also is present. The analyses of *Calais et al.* [2003, 2006] and *England and Molnar* [2005] suggest 4 ± 2 mm/yr of shortening.

[85] Rockies (Canada) (CAR): Few GPS data seem to span this area, and contamination by post-glacial rebound makes it difficult to separate transient deformation from longer-term tectonic strain. From the velocity of the continuously recording site at Penticton [*Argus et al.*, 2010], we infer 2.1 ± 1.0 mm/yr.

[86] New Guinea (Western, Indonesia) (WNG): Only one GPS site (SENT) lies north of the axial range of Irian Jaya. Using the latest rate for it relative to Australia [*Bock et al.*, 2003], the component trending N160°W, perpendicular to the range, is ~27 ± 2 mm/yr. With only one station, we assume a larger uncertainty of 5 mm/yr. Thus we use 27 ± 5 mm/yr.

[87] New Guinea (Eastern, Papua) (PNG): The complicated tectonics of this region makes it difficult to determine a precise shortening rate from the sparse GPS measurements. We rely on *Wallace et al.* [2004, p. 14], who state: "The New Guinea Highlands Fold and Thrust Belt is probably accommodating up to 15 mm/yr of convergence between the New Guinea Highlands and Australian Plates." We assume an uncertainty of 5 mm/yr, and we use 15 ± 5 mm/yr.

[88] Southern Alps, New Zealand (SNZ): We rely on the thorough treatment and presentation of GPS measurements by *Beavan et al.* [2007, 2002], who reported convergence across the South Island of 9.1 ± 0.6 mm/yr.

[89] Norway (Northern, NNO, and southern, SNO): This region is commonly treated as tectonically inactive, and we assume 0 ± 1 mm/yr for both NNO and SNO. Velocities of a few GPS stations along the west coast of Norway, as well as many others in Sweden and Finland, can be matched assuming that they reflect post-glacial rebound of an ice sheet centered farther east [*Lidberg et al.*, 2007]. Hence they are consistent with tectonic inactivity.

[90] Patagonia (northern) (39°N–45°N, PAT): *Khazaradze and Klotz* [2003] showed that points on the east side of Patagonia move west relative to stable South America, but they argued that this movement is due to viscous relaxation after the 1960 Chile earthquake, an inference confirmed by *Wang et al.* [2007]. Active tectonics of this segment of the Andes seems to include a rapid component of right-lateral strike slip parallel to the belt along the Liquiñe-Ofqui fault zone [*Cembrano et al.*, 1996; *Rosenau et al.*, 2006], which is seismically active [*Lange et al.*, 2008]. *Rosenau et al.* [2006] inferred rates of strike slip of more than 10 mm/yr and conceivably as much as 30 mm/yr, but recent GPS work suggest a rate of 6.5 mm/yr [*Wang et al.*, 2007]. Thus,

although shortening might be slow, active deformation is not negligible. We assume convergence at 0 ± 2 mm/yr.

[91] Patagonia (southern) (45°N–52°N, SPG): We are not aware of GPS data that constrain this rate. The Liquiñe-Ofqui fault zone continues into this region [e.g., *Cembrano et al.*, 1996]. Seismicity demonstrates that it is active [*Lange et al.*, 2008; *Mora et al.*, 2010], but GPS coverage seems to be too sparse to define a rate. *Lagabrielle et al.* [2004] argued that crustal shortening ended in Miocene time, perhaps earlier than *Melnick et al.* [2006a] inferred for a part of the Chilean Andes farther north, but they contend that the range rose only in the past 3 Ma, which *Lagabrielle et al.* [2007] ascribed to the insertion of a hot upper mantle beneath the region when the Chile Ridge passed to the north. *Lagabrielle et al.* [2007] and *Scalabrino et al.* [2010] demonstrated recent and active normal faulting, if on steep faults and perhaps not with rapid slip, and accordingly, we assume the same as for the region to the north, 0 ± 2 mm/yr.

[92] Pyrenees (France, PYR): No resolvable movement of continuously recording GPS sites in Western Europe [*Nocquet and Calais*, 2003; *Nocquet et al.*, 2001] puts a maximum rate of movement across the Pyrenees of 0.6 mm/yr. We assume that no shortening across the range: 0 ± 0.6 mm/yr.

[93] Qilian Shan (China, QS): GPS measurements across the region suggest shortening at 5.5 ± 1.8 mm/yr [*Gan et al.*, 2007; *Zhang et al.*, 2004].

[94] Rockies (Northern Colorado) (NCR): From three years of data from eight continuously recording GPS instruments spanning a distance of 400 km, *Berglund* [2010] inferred extensional strain across the region from east of the Front Range to western Colorado at 0.631 ± 0.21 nanostrain/yr. This corresponds to 0.0621 ± 0.021 mm/yr across a region 100 km wide. We assume 0 ± 0.1 mm/yr.

[95] Sangre de Christo (Colorado) (SCH): See Front Range above.

[96] San Juan Mountains (southwestern Colorado) (SJM): See Front Range above.

[97] Sierra Nevada (California) (SNC): Although small earthquakes occur with the Sierra Nevada, the range is commonly treated as a micro-plate undergoing negligibly slow deformation [e.g., *Argus and Gordon*, 1991; *Argus and Gordon*, 2001]As GPS measurements do not show evidence of deformation [e.g., *McCaffrey*, 2005], we use 0 ± 1 mm/yr.

[98] Southern India (SI): *Bettinelli et al.* [2006] showed that GPS and DORIS stations on India, Sri Lanka, and the Chagos-Laccadive island chain move with respect to one other at <2 (± 1–2) mm/yr, and hence suggest negligible deformation 0 ± 2 mm/yr.

[99] Sri Lanka (SL): We are aware of only one DORIS, and no GPS, station on Sri Lanka. Hence, deformation cannot be constrained well, but the consistency of the velocity of that DORIS site with others on the Indian plate to the north and south suggests little deformation [*Bettinelli et al.*, 2006]. We assume 0 ± 2 mm/yr.

[100] Sumatra (SUM): A major strike-slip fault, the Sumatran fault, follows the line of volcanoes, and as a result GPS stations on the two sides of move rapidly with respect to one another. Only a few stations lie to the northeast, and apparently velocities of the most recent measurements are quite uncertain [*Bock et al.*, 2003]. We assume no shortening: 0 ± 3 mm/yr, but with a relatively large uncertainty.

[101] Taiwan (T): GPS data show rapid oblique convergence between the Philippine Sea plate and South China at 80 mm/yr, but the majority is absorbed by thrust slip east of the island [*Hsu et al.*, 2003; *Yu et al.*, 1997]. Deformation on the island seems to be complex and not described well as two-dimensional. *Hsu et al.* [2003] show that the GPS data along two profiles call for convergence across the island at 30–40 mm/yr. The remaining portion is absorbed at the eastern margin of the island and offshore. Uplifted terraces on the east side of the island corroborate the large faction of shortening there [*Huang et al.*, 2010]. Geological constraints on slip rates for major faults suggest somewhat slower slip that GPS data do [*Shyu et al.*, 2006], but because of the complexity, both are uncertain. We assume a rate of 35 ± 5 mm/yr.

[102] Tasmania (TSM): Employing the same logic as for Southeast Australia (SEA), we use 0 ± 2 mm/yr.

[103] Tien Shan (Central) (CTS): GPS measurements demonstrate 15 ± 3 mm/yr of convergence between the Tarim Basin and Eurasia along the western edge of this region [*Zubovich et al.*, 2010]. Recognizing the decreasing rate toward the east [*Avouac et al.*, 1993], we infer that the average rate should be closer to 14 mm/yr. We thus assume that 10 ± 3 mm/yr. is absorbed in the Tien Shan, and the remaining 4 ± 1 mm/yr is absorbed across the Dzungarian Alatau.

[104] Dzungarian Alatau (DZA): GPS measurements demonstrate 4 ± 1 mm/yr of convergence across this region [*Zubovich et al.*, 2011]. (See also the discussion of the Central Tien Shan.)

[105] Tien Shan (Eastern) (ETS): Again by exploiting rates farther west, across the Western Tien Shan [*Zubovich et al.*, 2011], and assuming an eastward decrease [*Avouac et al.*, 1993] we use 10 ± 3 mm/yr. This rate accords with GPS data of *Yang et al.* [2008].

[106] Tien Shan (Western) (WTS): GPS measurements demonstrate 19 ± 2 mm/yr across this region [*Zubovich et al.*, 2011], consistent with earlier studies of *Abdrakhmatov et al.* [1996] and *Reigber et al.* [2001].

[107] Uinta Range (Utah) (UR): Although neither discussed this area, *Bennett et al.* [1999] and *Berglund* [2010] presented GPS velocities for points on both sides of the range that move slowly (1–2 ± 2 mm/yr) with respect to the stable parts of North America. We assume 0 ± 2 mm/yr.

[108] Ural (URL): GPS measurements from sites in Europe and Asia show negligible motion between them [*Kogan et al.*, 2000; *Steblov et al.*, 2003]. We assume 0 ± 1 mm/yr.

[109] Verkhoyansk (Russia) (VKH): GPS measurements from sites east of the southern part of this range show negligible motion with respect to Europe and Asia [*Steblov et al.*, 2003]. We assume 0 ± 1 mm/yr.

[110] Wind River Range (Wyoming) (WRR): Although he did not discuss them, *Berglund* [2010] showed essentially no movement between GPS sites spanning the range. We assume 0 ± 1 mm/yr.

[111] Zagros (Northwestern) (NWZ): GPS measurements spanning the range of *Hessami et al.* [2006], *Vernant et al.* [2004b], and *Walpersdorf et al.* [2006] yield an average convergence rate of 4.5 ± 2 mm/yr.

[112] Zagros (Southeastern) (SEZ): GPS measurements spanning the range of *Hessami et al.* [2006], *Tatar et al.*

[2002], *Vernant et al.* [2004a], and *Walpersdorf et al.* [2006] yield an average convergence rate of 8 ± 2 mm/yr.

References

Abbott, L. D., E. A. Silver, R. S. Anderson, R. Smith, J. C. Ingle, S. A. Kling, D. Haig, E. Small, J. Galewsky, and W. Sliter (1997), Measurement of tectonic surface uplift rate in a young collisional mountain belt, *Nature*, *385*, 501–507, doi:10.1038/385501a0.

Abdrakhmatov, K. Y., et al. (1996), Relatively recent construction of the Tien Shan inferred from GPS measurements of present-day crustal deformation rates, *Nature*, *384*, 450–453, doi:10.1038/384450a0.

Adams, J. (1980), Contemporary uplift and erosion of the Southern Alps, New Zealand, *Geol. Soc. Am. Bull.*, *91*, 1–114.

Ahnert, F. (1970), Functional relationship between denudation, relief, and uplift in large mid-latitude drainage basins, *Am. J. Sci.*, *268*, 243–263, doi:10.2475/ajs.268.3.243.

Ahnert, F. (1984), Local relief and the height limits of mountain ranges, *Am. J. Sci.*, *284*, 1035–1055, doi:10.2475/ajs.284.9.1035.

Allen, T. R. (1998), Topographic context of glaciers and perennial snowfields, Glacier National Park, Montana, *Geomorphology*, *21*, 207–216, doi:10.1016/S0169-555X(97)00059-7.

Allmendinger, R. W., R. Reilinger, and J. Loveless (2007), Strain and rotation rate from GPS in Tibet, Anatolia, and the Altiplano, *Tectonics*, *26*, TC3013, doi:10.1029/2006TC002030.

Anders, A. M., G. H. Roe, B. Hallet, D. R. Montgomery, N. J. Finnegan, and J. Putkonen (2006), Spatial patterns of precipitation and topography in the Himalaya, *Spec. Pap. Geol. Soc. Am.*, *398*, 39–53.

Anders, A. M., G. H. Roe, D. R. Montgomery, and B. Hallet (2008), Influence of precipitation phase on the form of mountain ranges, *Geology*, *36*, 479–482, doi:10.1130/G24821A.1.

Anderson, R. S. (2005), Teflon peaks: The evolution of high local relief in glaciated mountain ranges, *Eos Trans. AGU*, *86*(52), Fall Meet. Suppl., Abstract H33F-04.

Argus, D. F., and R. G. Gordon (1991), Current Sierra-Nevada North-America motion from very long base-line interferometry: Implications for the kinematics of the western United-States, *Geology*, *19*, 1085–1088, doi:10.1130/0091-7613(1991)019<1085:CSNNAM>2.3.CO;2.

Argus, D. F., and R. G. Gordon (2001), Present tectonic motion across the Coast Ranges and San Andreas fault system in central California, *Geol. Soc. Am. Bull.*, *113*(12), 1580–1592, doi:10.1130/0016-7606(2001) 113<1580:PTMATC>2.0.CO;2.

Argus, D. F., and W. R. Peltier (2010), Constraining models of postglacial rebound using space geodesy: A detailed assessment of model ICE-5G (VM2) and its relatives, *Geophys. J. Int.*, *181*(2), 697–723.

Argus, D. F., R. G. Gordon, M. B. Heflin, C. Ma, R. J. Eanes, P. Willis, W. R. Peltier, and S. E. Owen (2010), The angular velocities of the plates and the velocity of Earth's centre from space geodesy, *Geophys. J. Int.*, *180*(3), 913–960, doi:10.1111/j.1365-246X.2009.04463.x.

Avouac, J. P., and E. B. Burov (1996), Erosion as a driving mechanism of intracontinental mountain growth, *J. Geophys. Res.*, *101*, 17,747–17,769, doi:10.1029/96JB01344.

Avouac, J. P., P. Tapponnier, M. Bai, H. You, and G. Wang (1993), Active thrusting and folding along the northern Tien Shan, and Late Cenozoic rotation of the Tarim relative to Dzungaria and Kazakhstan, *J. Geophys. Res.*, *98*, 6755–6804, doi:10.1029/92JB01963.

Baljinnyam, I., et al. (1993), *Ruptures of Major Earthquakes and Active Deformation in Mongolia and Its Surroundings*, *Mem. Geol. Soc. Am.*, *181*, 62 pp.

Barke, R., and S. Lamb (2006), Late Cenozoic uplift of the Eastern Cordillera, Bolivian Andes, *Earth Planet. Sci. Lett.*, *249*, 350–367, doi:10.1016/j.epsl.2006.07.012.

Barros, A. P., S. Chiao, T. J. Lang, D. Burbank, and J. Putkonen (2006), From weather to climate—Seasonal and interannual variability of storms and implications for erosion processes in the Himalaya, *Spec. Pap. Geol. Soc. Am.*, *398*, 17–38.

Batt, G. E., and J. Braun (1997), On the thermomechanical evolution of compressional orogens, *Geophys. J. Int.*, *128*(2), 364–382, doi:10.1111/j.1365-246X.1997.tb01561.x.

Battaglia, M., M. H. Murray, E. Serpelloni, and R. Bürgmann (2004), The Adriatic region: An independent microplate within the Africa-Eurasia collision zone, *Geophys. Res. Lett.*, *31*, L09605, doi:10.1029/2004GL019723.

Beaumont, C., P. Fullsack, and J. Hamilton (Eds.) (1992), Erosional control of active compressional orogens, in *Thrust Tectonics*, pp. 1–18, Chapman and Hall, London.

Beaumont, C., R. A. Jamieson, M. H. Nguyen, and B. Lee (2001), Himalayan tectonics explained by extrusion of a low-viscosity crustal channel coupled to focused surface denudation, *Nature*, *414*, 738–742.doi:10.1038/414738a.

Beavan, J., et al. (1999), Crustal deformation during 1994–1998 due to oblique continental collision in the central Southern Alps, New Zealand, and implications for seismic potential of the Alpine fault, *J. Geophys. Res.*, *104*, 25,233–25,255.

Beavan, J., P. Tregoning, M. Bevis, T. Kato, and C. Meertens (2002), Motion and rigidity of the Pacific Plate and implications for plate boundary deformation, *J. Geophys. Res.*, *107*(B10), 2261, doi:10.1029/2001JB000282.

Beavan, J., S. Ellis, L. Wallace, and P. Denys (2007), Kinematic constraints from GPS on oblique convergence of the Pacific and Australian plates, central South Island, New Zealand, in *A Continental Plate Boundary: Tectonics at South Island, New Zealand*, *Geophys. Monogr. Ser.*, vol. 175, edited by D. Okaya, T. Stern, and F. Davey, pp. 75–94, AGU, Washington, D. C.

Becker, J. J., et al. (2009), Global bathymetry and elevation data at 30 arc seconds resolution: SRTM30_PLUS, *Mar. Geod.*, *32*(4), 355–371, doi:10.1080/01490410903297766.

Benedetti, L., P. Tapponnier, G. C. P. King, B. Meyer, and I. Manighetti (2000), Growth folding and active thrusting in the Montello region, Veneto, northern Italy, *J. Geophys. Res.*, *105*, 739–766, doi:10.1029/1999JB900222.

Bennett, R. A., J. L. Davis, and B. P. Wernicke (1999), Present-day pattern of Cordilleran deformation in the western United States, *Geology*, *27*, 371–374, doi:10.1130/0091-7613(1999)027<0371:PDPOCD>2.3.CO;2.

Bennett, R. A., S. Hreinsdóttir, G. Buble, T. Baši, Z. Bai, M. Marjanovi, G. Casale, A. Gendaszek, and D. Cowan (2008), Eocene to present subduction of southern Adria mantle lithosphere beneath the Dinarides, *Geology*, *36*, 3–6, doi:10.1130/G24136A.1.

Berger, A. L., et al. (2008), Quaternary tectonic response to intensified glacial erosion in an orogenic wedge, *Nat. Geosci.*, *1*, 793–799, doi:10.1038/ngeo334.

Berglund, H. T. (2010), *Geodetic Measurements of Deformation in the Rio Grande Rift Region*, 126 pp., Univ. of Colo., Boulder.

Bettinelli, P., J. P. Avouac, M. Flouzat, F. Jouanne, L. Bollinger, P. Willis, and G. R. Chitrakar (2006), Plate motion of India and interseismic strain in the Nepal Himalaya from GPS and DORIS measurements, *J. Geod.*, *80*, 567–589, doi:10.1007/s00190-006-0030-3.

Bettinelli, P., J. P. Avouac, M. Flouzat, L. Bollinger, G. Ramillien, S. Rajaure, and S. Sapkota (2008), Seasonal variations of seismicity and geodetic strain in the Himalaya induced by surface hydrology, *Earth Planet. Sci. Lett.*, *266*(3–4), 332–344.

Bevis, M., E. Kendrick, R. Smalley Jr., B. A. Brooks, R. W. Allmendinger, and B. L. Isacks (2001), On the strength of interplate coupling and the rate of back arc convergence in the central Andes: An analysis of the interseismic velocity field, *Geochem. Geophys. Geosyst.*, *2*, 1067, doi:10.1029/2001GC000198.

Bilham, R., et al. (1997), GPS measurements of present-day convergence across the Nepal Himalaya, *Nature*, *386*, 61–64, doi:10.1038/386061a0.

Bock, Y., L. Prawirodirdjo, J. F. Genrich, C. W. Stevens, R. McCaffrey, C. Subarya, S. S. O. Puntodewo, and E. Calais (2003), Crustal motion in Indonesia from Global Positioning System measurements, *J. Geophys. Res.*, *108*(B8), 2367, doi:10.1029/2001JB000324.

Bollinger, L., M. Nicolas, and S. Marin (2010), Hydrological triggering of the seismicity around a salt diapir in Castellane, France, *Earth Planet. Sci. Lett.*, *290*(1–2), 20–29.

Bonnet, C., J. Malavieille, and J. Mosar (2007), Interactions between tectonics, erosion, and sedimentation during the recent evolution of the Alpine orogen: Analogue modeling insights, *Tectonics*, *26*, TC6016, doi:10.1029/2006TC002048.

Bonnet, S., and A. Crave (2003), Landscape response to climate change: Insights from experimental modeling and implications for tectonic versus climatic uplift of topography, *Geology*, *31*, 123–126, doi:10.1130/0091-7613(2003)031<0123:LRTCCI>2.0.CO;2.

Bookhagen, B., and D. Burbank (2006), Topography, relief, and TRMM-derived rainfall variations along the Himalaya, *Geophys. Res. Lett.*, *33*, L08405, doi:10.1029/2006GL026037.

Brocklehurst, S. H., and K. X. Whipple (2004), Hypsometry of glaciated landscapes, *Earth Surf. Processes Landforms*, 29(7), 907–926, doi:10.1002/esp.1083.

Broecker, W. S., and G. H. Denton (1989), The role of ocean–atmosphere reorganizations in glacial cycles, *Geochim. Cosmochim. Acta*, 53(10), 2465–2501, doi:10.1016/0016-7037(89)90123-3.

Brooks, B. A., M. Bevis, R. J. Smalley, E. Kendrick, R. Manceda, E. Lauría, R. Maturana, and M. Araujo (2003), Crustal motion in the southern Andes (26°–36°S): Do the Andes behave like a microplate?, *Geochem. Geophys. Geosyst.*, 4(10), 1085, doi:10.1029/2003GC000505.

Brozović, N., D. W. Burbank, and A. J. Meigs (1997), Climatic limits on landscape development in the northwestern Himalaya, *Science*, 276, 571–574, doi:10.1126/science.276.5312.571.

Burbank, D. W. (2002), Rates of erosion and their implications for exhumation, *Mineral. Mag.*, 66(1), 25–52, doi:10.1180/0026461026610014.

Burbank, D. W., J. Leland, E. Fielding, R. S. Anderson, N. Brozovic, M. R. Reid, and C. Duncan (1996), Bedrock incision, rock uplift and threshold hillslopes in the northwestern Himalayas, *Nature*, 379, 505–510, doi:10.1038/379505a0.

Calais, E., J. M. Nocquet, F. Jouanne, and M. Tardy (2002a), Current strain regime in the Western Alps from continuous Global Positioning System measurements, 1996–2001, *Geology*, 30, 651–654, doi:10.1130/0091-7613(2002)030<0651:CSRITW>2.0.CO;2.

Calais, E., Y. Mazabraud, B. Mercier de Lepinay, P. Mann, G. Mattioli, and P. Jansma (2002b), Strain partitioning and fault slip rates in the northeastern Caribbean from GPS measurements, *Geophys. Res. Lett.*, 29(18), 1856, doi:10.1029/2002GL015397.

Calais, E., M. Vergnolle, V. San'kov, A. Lukhnev, A. Miroshnitchenko, S. Amarjargal, and J. Deverchere (2003), GPS measurements of crustal deformation in the Baikal-Mongolia area (1994–2002), Implications for current kinematics of Asia, *J. Geophys. Res.*, 108(B10), 2501, doi:10.1029/2002JB002373.

Calais, E., L. Dong, M. Wang, Z. Shen, and M. Vergnolle (2006), Continental deformation in Asia from a combined GPS solution, *Geophys. Res. Lett.*, 33, L24319, doi:10.1029/2006GL028433.

Calais, E., A. M. Freed, R. Van Arsdale, and S. Stein (2010), Triggering of New Madrid seismicity by late-Pleistocene erosion, *Nature*, 466(7306), 608–611.

Cembrano, J., F. Hervé, and A. Lavenu (1996), The Liquine–Ofqui fault zone: A long-lived intra-arc fault system in southern Chile, *Tectonophysics*, 259, 55–66, doi:10.1016/0040-1951(95)00066-6.

Champagnac, J. D., P. Molnar, R. S. Anderson, C. Sue, and B. Delacou (2007), Quaternary erosion-induced isostatic rebound in the western Alps, *Geology*, 35, 195–198, doi:10.1130/G23053A.1.

Champagnac, J.-D., P. van der Beek, G. Diraison, and S. Dauphin (2008), Flexural isostatic response of the Alps to increased Quaternary erosion recorded by foreland basin remnants, SE France, *Terra Nova*, 20(3), 213–220.

Clarke, B. A., and D. W. Burbank (2011), Quantifying bedrock-fracture patterns within the shallow subsurface: Implications for rock mass strength, bedrock landslides, and erodibility, *J. Geophys. Res.*, 116, F04009, doi:10.1029/2011JF001987.

Dadson, S. J., et al. (2003), Links between erosion, runoff variability and seismicity in the Taiwan orogen, *Nature*, 426, 648–651, doi:10.1038/nature02150.

D'Agostino, N., A. Avallone, D. Cheloni, E. D'Anastasio, S. Mantenuto, and G. Selvaggi (2008), Active tectonics of the Adriatic region from GPS and earthquake slip vectors, *J. Geophys. Res.*, 113, B12413, doi:10.1029/2008JB005860.

Dahlen, F. A., and J. Suppe (1988), Mechanics, growth, and erosion of mountain belts, *Processes Cont. Lithospheric Deformation*, 218, 161–178.

Delunel, R., P. A. van der Beek, J. Carcaillet, D. L. Bourles, and P. G. Valla (2010), Frost-cracking control on catchment denudation rates: Insights from in situ produced Be-10 concentrations in stream sediments (Ecrins-Pelvoux massif, French Western Alps), *Earth Planet. Sci. Lett.*, 293, 72–83, doi:10.1016/j.epsl.2010.02.020.

DeMets, C., R. G. Gordon, and D. F. Argus (2010), Geologically current plate motions, *Geophys. J. Int.*, 181(1), 1–80, doi:10.1111/j.1365-246X.2009.04491.x.

Dietrich, W. E., D. G. Bellugi, L. S. Sklar, J. D. Stock, A. M. Heimsath, and J. J. Roering (2003), Geomorphic transport laws for predicting landscape form and dynamics, in *Prediction in Geomorphology*, *Geophys. Monogr. Ser.*, vol. 135, edited by P. R. Wilcock and R. M. Iverson, pp. 103–132, AGU, Washington, D. C.

Djamour, Y., et al. (2010), GPS and gravity constraints on continental deformation in the Alborz mountain range, Iran, *Geophys. J. Int.*, 183(3), 1287–1301, doi:10.1111/j.1365-246X.2010.04811.x.

Doser, D. I., and H. Rodriguez (2011), A seismotectonic study of the Southeastern Alaska Region, *Tectonophysics*, 497(1–4), 105–113.

Dühnforth, M., R. S. Anderson, D. Ward, and G. M. Stock (2010), Bedrock fracture control of glacial erosion processes and rates, *Geology*, 38, 423–426, doi:10.1130/G30576.1.

Egholm, D. L., S. B. Nielsen, V. K. Pedersen, and J. E. Lesemann (2009), Glacial effects limiting mountain height, *Nature*, 460, 884–887, doi:10.1038/nature08263.

Elliott, J. L., C. F. Larsen, J. T. Freymueller, and R. J. Motyka (2010), Tectonic block motion and glacial isostatic adjustment in southeast Alaska and adjacent Canada constrained by GPS measurements, *J. Geophys. Res.*, 115, B09407, doi:10.1029/2009JB007139.

England, P., and P. Molnar (2005), Late Quaternary to decadal velocity fields in Asia, *J. Geophys. Res.*, 110, B12401, doi:10.1029/2004JB003541.

Fadil, A., P. Vernant, S. McClusky, R. Reilinger, F. Gomez, D. Ben Sari, T. Mourabit, K. Feigl, and M. Barazangi (2006), Active tectonics of the western Mediterranean: Geodetic evidence for rollback of a delaminated subcontinental lithospheric slab beneath the Rif Mountains, Morocco, *Geology*, 34, 529–532, doi:10.1130/G22291.1.

Farr, T. G., et al. (2007), The Shuttle radar topography mission, *Rev. Geophys.*, 45, RG2004, doi:10.1029/2005RG000183.

Feldl, N., and R. Bilham (2006), Great Himalayan earthquakes and the Tibetan plateau, *Nature*, 444, 165–170, doi:10.1038/nature05199.

Fisher, D. M., T. W. Gardner, P. B. Sak, J. D. Sanchez, K. Murphy, and P. Vannucchi (2004), Active thrusting in the inner forearc of an erosive convergent margin, Pacific coast, Costa Rica, *Tectonics*, 23, TC2007, doi:10.1029/2002TC001464.

Fletcher, H. J. (2002), Crustal deformation in Alaska measured using the Global Positioning System, PhD thesis, 135 pp., Univ. of Alaska, Fairbanks.

Flint, R. F. (1971), *Glacial and Quaternary Geology*, John Wiley, New York.

Foster, D., S. H. Brocklehurst, and R. L. Gawthorpe (2008), Small valley glaciers and the effectiveness of the glacial buzzsaw in the northern Basin and Range, USA, *Geomorphology*, 102, 624–639, doi:10.1016/j.geomorph.2008.06.009.

Freymueller, J. T., H. Woodard, S. C. Cohen, R. Cross, J. Elliott, C. F. Larsen, H. Hreinsdottir, and C. Zweck (2008), Active deformation processes in Alaska, based on 15 years of GPS measurements, in *Active Tectonics and Seismic Potential of Alaska*, *Geophys. Monogr. Ser.*, vol. 179, edited by J. T. Freymueller et al., pp. 1–42, AGU, Washington, D. C.

Gan, W.-J., and W. H. Prescott (2001), Crustal deformation rates in central and eastern U.S. inferred from GPS, *Geophys. Res. Lett.*, 28, 3733–3736.

Gan, W., P. Zhang, Z.-K. Shen, Z. Niu, M. Wang, Y. Wan, D. Zhou, and J. Cheng (2007), Present-day crustal motion within the Tibetan Plateau inferred from GPS measurements, *J. Geophys. Res.*, 112, B08416, doi:10.1029/2005JB004120.

Garcia-Castellanos, D. (2007), The role of climate during high plateau formation: Insights from numerical experiments, *Earth Planet. Sci. Lett.*, 257, 372–390, doi:10.1016/j.epsl.2007.02.039.

Gilbert, G. K. (1904), Systematic asymmetry of crest lines in the High Sierra of California, *J. Geol.*, 12, 579–588, doi:10.1086/621182.

Grasemann, B., and N. S. Mancktelow (1993), Two-dimensional thermal modelling of normal faulting: The Simplon Fault Zone, Central Alps, Switzerland, *Tectonophysics*, 225, 155–165, doi:10.1016/0040-1951(93)90277-Q.

Griffiths, T. M. (1952), Glacial geomorphology on the Mt. McKinley massif, Alaska, paper presented at Eighth General Assembly and Seventeenth International Congress, Int. Geogr. Union, Washington, D. C.

Grujic, D., I. Coutand, B. Bookhagen, S. Bonnet, A. Blythe, and C. Duncan (2006), Climatic forcing of erosion, landscape, and tectonics in the Bhutan Himalayas, *Geology*, 34, 801–804, doi:10.1130/G22648.1.

Hack, J. T. (1960), Interpretation of erosional topography in humid temperate regions, *Am. J. Sci.*, 258-A, 80–97.

Haeuselmann, P., D. E. Granger, P. Y. Jeannin, and S. E. Lauritzen (2007), Abrupt glacial valley incision at 0.8 Ma dated from cave deposits in Switzerland, *Geology*, 35, 143–146, doi:10.1130/G23094A.

Hales, T. C., and J. J. Roering (2009), A frost "buzzsaw" mechanism for erosion of the eastern Southern Alps, New Zealand, *Geomorphology*, 107, 241–253, doi:10.1016/j.geomorph.2008.12.012.

Hampel, A., R. Hetzel, and A. L. Densmore (2007), Postglacial slip-rate increase on the Teton normal fault, northern Basin and Range Province, caused by melting of the Yellowstone ice cap and deglaciation of the Teton Range?, *Geology*, 35(12), 1107–1110.

Hay, W. W. (1996), Tectonics and climate, *Geol. Rundsch.*, 85(3), 409–437, doi:10.1007/BF02369000.

Henck, A. C., K. W. Huntington, J. O. Stone, D. R. Montgomery, and B. Hallet (2011), Spatial controls on erosion in the Three Rivers Region, southeastern Tibet and southwestern China, *Earth Planet. Sci. Lett.*, 303, 71–83, doi:10.1016/j.epsl.2010.12.038.

Herman, F., and J. Braun (2006), Fluvial response to horizontal shortening and glaciations: A study in the Southern Alps of New Zealand, *J. Geophys. Res.*, *111*, F01008, doi:10.1029/2004JF000248.

Herman, F., E. J. Rhodes, J. Braun, and L. Heiniger (2010a), Uniform erosion rates and relief amplitude during glacial cycles in the Southern Alps of New Zealand, as revealed from OSL-thermochronology, *Earth Planet. Sci. Lett.*, *297*, 183–189, doi:10.1016/j.epsl.2010.06.019.

Herman, F., et al. (2010b), Exhumation, crustal deformation, and thermal structure of the Nepal Himalaya derived from the inversion of thermochronological and thermobarometric data and modeling of the topography, *J. Geophys. Res.*, *115*, B06407, doi:10.1029/2008JB006126.

Herman, F., F. Beaud, J.-D. Champagnac, J.-M. Lemieux, and P. Sternai (2011), A mechanism for overdeepenings of glacial valleys and fjords, *Earth Planet. Sci. Lett.*, *310*, 498–508, doi:10.1016/j.epsl.2011.08.022.

Hessami, K., F. Nilforoushan, and C. J. Talbot (2006), Active deformation within the Zagros Mountains deduced from GPS measurements, *J. Geol. Soc.*, *163*, 143–148, doi:10.1144/0016-764905-031.

Hoke, G. D., B. L. Isacks, T. E. Jordan, N. Blanco, A. J. Tomlinson, and J. Ramezani (2007), Geomorphic evidence for post-10 Ma uplift of the western flank of the central Andes 18°30′–22°S, *Tectonics*, *26*, TC5021, doi:10.1029/2006TC002082.

Holmes, A. (Ed.) (1944), *Principles of Physical Geology*, 532 pp., Thomas Nelson, London.

Holmes, A. (1965), *Principles of Physical Geology*, Ronald Press, New York.

Hoskins, B. J., and D. J. Karoly (1981), The steady linear response of a spherical atmosphere to thermal and orographic forcing, *J. Atmos. Sci.*, *38*, 1179–1196, doi:10.1175/1520-0469(1981)038<1179:TSLROA>2.0. CO;2.

Hovius, N., C. P. Stark, and P. A. Allen (1997), Sediment flux from a mountain belt derived by landslide mapping, *Geology*, *25*, 231–234, doi:10.1130/0091-7613(1997)025<0231:SFFAMB>2.3.CO;2.

Hsu, Y.-J., M. Simons, S.-B. Yu, L.-C. Kuo, and H.-Y. Chen (2003), A two-dimensional dislocation model for interseismic deformation of the Taiwan mountain belt, *Earth Planet. Sci. Lett.*, *211*, 287–294, doi:10.1016/ S0012-821X(03)00203-6.

Huang, W.-J., K. M. Johnson, J. Fukuda, and S.-B. Yu (2010), Insights into active tectonics of eastern Taiwan from analyses of geodetic and geologic data, *J. Geophys. Res.*, *115*, B03413, doi:10.1029/2008JB006208.

Huybers, K., and G. H. Roe (2009), Spatial patterns of glaciers in response to spatial patterns in regional climate, *J. Clim.*, *22*(17), 4606–4620, doi:10.1175/2009JCLI2857.1.

Jade, S., B. C. Bhatt, Z. Yang, R. Bendick, V. K. Gaur, P. Molnar, M. B. Anand, and D. Kumar (2004), GPS measurements from the Ladakh Himalaya, India: Preliminary tests of plate-like or continuous deformation in Tibet, *Geol. Soc. Am. Bull.*, *116*(11), 1385–1391, doi:10.1130/ B25357.1.

Jade, S., et al. (2007), Estimates of interseismic deformation in northeast India from GPS measurements, *Earth Planet. Sci. Lett.*, *263*, 221–234, doi:10.1016/j.epsl.2007.08.031.

Kasahara, A., T. Sasamori, and W. M. Washington (1973), Simulation experiments with a 12 layer stratospheric global circulation model. I. Dynamical effect of the Earth's orography and thermal influence of continentality, *J. Atmos. Sci.*, *30*, 1229–1251, doi:10.1175/1520-0469(1973) 030<1229:SEWALS>2.0.CO;2.

Kendrick, E., M. G. Bevis, R. Smalley, and B. A. Brooks (2001), An integrated crustal velocity field for the central Andes, *Geochem. Geophys. Geosyst.*, *2*, 1066, doi:10.1029/2001GC000191.

Kendrick, E., B. A. Brooks, M. Bevis, R. J. Smalley, E. Lauria, M. Araujo, and H. Parra (2006), Active orogeny of the south-central Andes studied with GPS geodesy, *Asoc. Geol. Argent. Rev.*, *61*, 555–566.

Khazaradze, G., and J. Klotz (2003), Short- and long-term effects of GPS measured crustal deformation rates along the south central Andes, *J. Geophys. Res.*, *108*(B6), 2289, doi:10.1029/2002JB001879.

Khazaradze, G., K. Wang, J. Klotz, Y. Hu, and J. He (2002), Prolonged post-seismic deformation of the 1960 great Chile earthquake and implications for mantle rheology, *Geophys. Res. Lett.*, *29*(22), 2050, doi:10.1029/ 2002GL015986.

Kirkbride, M., and D. Matthews (1997), The role of fluvial and glacial erosion in landscape evolution: The Ben Ohau Range, New Zealand, *Earth Surf. Processes Landforms*, *22*(3), 317–327, doi:10.1002/(SICI) 1096-9837(199703)22:3<317::AID-ESP760>3.0.CO;2-I.

Klotz, J., et al. (1999), GPS-derived deformation of the central Andes including the 1995 Antofagasta Mw = 8.0 earthquake, *Pure Appl. Geophys.*, *154*, 709–730, doi:10.1007/s000240050249.

Klotz, J., G. Khazaradze, D. Angermann, C. Reigber, R. Perdomo, and O. Cifuentes (2001), Earthquake cycle dominates contemporary crustal deformation in central and southern Andes, *Earth Planet. Sci. Lett.*, *193*, 437–446, doi:10.1016/S0012-821X(01)00532-5.

Kober, F., F. Schlunegger, G. Zeilinger, and H. Schneider (Eds.) (2006), Surface uplift and climate change: The geomorphic evolution of the Western Escarpment of the Andes of northern Chile between the Miocene and present, *Spec. Pap. Geol. Soc. Am.*, *398*, 75–86.

Kogan, M. G., G. M. Steblov, R. W. King, T. A. Herring, D. I. Frolov, S. G. Egorov, V. Ye. Levin, A. Lerner-Lam, and A. Jones (2000), Geodetic constraints on the rigidity and relative motion of Eurasia and North America, *Geophys. Res. Lett.*, *27*, 2041–2044, doi:10.1029/2000GL011422.

Konstantinovskaia, E., and J. Malavieille (2005), Erosion and exhumation in accretionary orogens: Experimental and geological approaches, *Geochem. Geophys. Geosyst.*, *6*(2), Q02006, doi:10.1029/2004GC000794.

Koons, P. O. (1990), Two-sided orogen: Collision and erosion from the sandbox to the Southern Alps, New Zealand, *Geology*, *18*, 679–682, doi:10.1130/0091-7613(1990)018<0679:TSOCAE>2.3.CO;2.

Koons, P. O., R. J. Norris, D. Craw, and A. F. Cooper (2003), Influence of exhumation on the structural evolution of transpressional plate boundaries: An example from the Southern Alps, New Zealand, *Geology*, *31*, 3–6, doi:10.1130/0091-7613(2003)031<0003:IOEOTS>2.0.CO;2.

Koppes, M. N., and D. R. Montgomery (2009), The relative efficacy of fluvial and glacial erosion over modern to orogenic timescales, *Nat. Geosci.*, *2*, 644–647, doi:10.1038/ngeo616.

LaFemina, P., T. H. Dixon, R. Govers, E. Norabuena, H. Turner, A. Saballos, G. Mattioli, M. Protti, and W. Strauch (2009), Fore-arc motion and Cocos Ridge collision in Central America, *Geochem. Geophys. Geosyst.*, *10*, Q05S14, doi:10.1029/2008GC002181.

Lagabrielle, Y., M. Suárez, E. A. Rossello, G. Hérail, J. Martinod, M. Régnier, and R. de la Cruz (2004), Neogene to Quaternary tectonic evolution of the Patagonian Andes at the latitude of the Chile Triple Junction, *Tectonophysics*, *385*, 211–241, doi:10.1016/j.tecto.2004.04.023.

Lagabrielle, Y., et al. (2007), Pliocene extensional tectonics in the Eastern Central Patagonian Cordillera: Geochronological constraints and new field evidence, *Terra Nova*, *19*, 413–424, doi:10.1111/j.1365-3121. 2007.00766.x.

Lange, D., J. Cembrano, A. Rietbrock, C. Haberland, T. Dahm, and K. Bataille (2008), First seismic record for intra-arc strike-slip tectonics along the Liquiñe-Ofqui fault zone at the obliquely convergent plate margin of the southern Andes, *Tectonophysics*, *455*, 14–24, doi:10.1016/j.tecto. 2008.04.014.

Lavé, J., and J. P. Avouac (2000), Active folding of fluvial terraces across the Siwaliks Hills, Himalayas of central Nepal, *J. Geophys. Res.*, *105*, 5735–5770, doi:10.1029/1999JB900292.

Leonard, L. J., R. D. Hyndman, S. Mazzotti, L. Nykolaishen, M. Schmidt, and S. Hippchen (2007), Current deformation in the northern Canadian Cordillera inferred from GPS measurements, *J. Geophys. Res.*, *112*, B11401, doi:10.1029/2007JB005061.

Leonard, L. J., S. Mazzotti, and R. D. Hyndman (2008), Deformation rates estimated from earthquakes in the northern Cordillera of Canada and eastern Alaska, *J. Geophys. Res.*, *113*, B08406, doi:10.1029/2007JB005456.

Leopold, L. B., and T. Maddock (1953), The hydraulic geometry of stream channels and some physiographic implications, *U.S. Geol. Surv. Prof. Pap.*, *252*, 57 pp.

Lidberg, M., J. M. Johansson, H.-G. Scherneck, and J. L. Davis (2007), An improved and extended GPS derived velocity field for the glacial isostatic adjustment in Fennoscandia, *J. Geod.*, *81*, 213–230, doi:10.1007/s00190-006-0102-4.

Lucazeau, F., and J.-E. Hurtrez (1997), Length-scale dependence of relief along the southeastern border of Massif Central (France), *Geophys. Res. Lett.*, *24*, 1823–1826, doi:10.1029/97GL01673.

Lyon-Caen, H., et al. (2006), Kinematics of the North American–Caribbean-Cocos plates in Central America from new GPS measurements across the Polochic-Motagua fault system, *Geophys. Res. Lett.*, *33*, L19309, doi:10.1029/2006GL027694.

Mann, P., E. Calais, J. C. Ruegg, C. DeMets, P. E. Jansma, and G. S. Mattioli (2002), Oblique collision in the northeastern Caribbean from GPS measurements and geological observations, *Tectonics*, *21*(6), 1057, doi:10.1029/ 2001TC001304.

Mazzotti, S., and R. D. Hyndman (2002), Yakutat collision and strain transfer across the northern Canadian Cordillera, *Geology*, *30*, 495–498, doi:10.1130/0091-7613(2002)030<0495:YCASTA>2.0.CO;2.

Mazzotti, S., R. D. Hyndman, P. Flück, A. J. Smith, and M. Schmidt (2003), Distribution of the Pacific/North America motion in the Queen Charlotte Islands-S. Alaska plate boundary zone, *Geophys. Res. Lett.*, *30*(14), 1762, doi:10.1029/2003GL017586.

McCaffrey, R. (2005), Block kinematics of the Pacific-North America plate boundary in the southwestern United States from inversion of GPS, seismological, and geological data, *J. Geophys. Res.*, *110*, B07401, doi:10.1029/ 2004JB003307.

McCaffrey, R., A. I. Qamar, R. W. King, R. Wells, G. Khazaradze, C. A. Williams, C. W. Stevens, J. J. Vollick, and P. C. Zwick (2007), An update

of quaternary faults of central and eastern Oregon, *Geophys. J. Int.*, *169*(3), 1315–1340, doi:10.1111/j.1365-246X.2007.03371.x.

McClusky, S., et al. (2000), Global Positioning System constraints on plate kinematics and dynamics in the eastern Mediterranean and Caucasus, *J. Geophys. Res.*, *105*, 5695–5719.

Melnick, D., M. Rosenau, A. Folguera, and H. Echtler (2006a), Neogene tectonic evolution of the Neuquén Andes western flank (37–39°S), in *Evolution of an Andean Margin: A Tectonic and Magmatic View From the Andes to the Neuquén Basin (35°–39°S lat)*, edited by S. M. Kay and V. A. Ramos, *Spec. Pap. Geol. Soc. Am.*, *407*, 73–95.

Melnick, D., F. Charlet, H. P. Echtler, and M. De Batist (2006b), Incipient axial collapse of the Main Cordillera and strain partitioning gradient between the central and Patagonian Andes, Lago Laja, Chile, *Tectonics*, *25*, TC5004, doi:10.1029/2005TC001918.

Mitchell, S. G., and D. R. Montgomery (2006), Influence of a glacial buzzsaw on the height and morphology of the Cascade Range in central Washington State, USA, *Quat. Res.*, *65*(1), 96–107, doi:10.1016/j.yqres.2005.08.018.

Molnar, P. (1990), The rise of mountain ranges and the evolution of humans: A causal relation?, *Isr. J. Earth Sci.*, *10*(2), 199–207.

Molnar, P. (2004), Late Cenozoic increase in accumulation rates of terrestrial sediment: How might climate change have affected erosion rates?, *Annu. Rev. Earth Planet. Sci.*, *32*, 67–89, doi:10.1146/annurev.earth.32.091003.143456.

Molnar, P. (2009), The state of interactions among tectonics, erosion, and climate: A polemic, *GSA Today*, *19*(7), 44–45, doi:10.1130/GSATG00GW.1.

Molnar, P., and P. England (1990), Late Cenozoic uplift of mountain ranges and global climate change: Chicken or egg?, *Nature*, *346*, 29–34, doi:10.1038/346029a0.

Molnar, P., R. S. Anderson, and S. P. Anderson (2007), Tectonics, fracturing of rock, and erosion, *J. Geophys. Res.*, *112*, F03014, doi:10.1029/2005JF000433.

Montgomery, D. R. (1994), Valley incision and the uplift of mountain peaks, *J. Geophys. Res.*, *99*, 13,913–13,921, doi:10.1029/94JB00122.

Montgomery, D. R., and M. T. Brandon (2002), Topographic controls on erosion rates in tectonically active mountain ranges, *Earth Planet. Sci. Lett.*, *201*, 481–489, doi:10.1016/S0012-821X(02)00725-2.

Montgomery, D. R., G. Balco, and S. D. Willett (2001), Climate, tectonics, and the morphology of the Andes, *Geology*, *29*, 579–582, doi:10.1130/0091-7613(2001)029<0579:CTATMO>2.0.CO;2.

Moon, S., C. Page Chamberlain, K. Blisniuk, N. Levine, D. H. Rood, and G. E. Hilley (2011), Climatic control of denudation in the deglaciated landscape of the Washington Cascades, *Nat. Geosci.*, *4*, 469–473.

Mora, C., D. Comte, R. Russo, A. Gallego, and V. Mocanu (2010), Aysén seismic swarm (January 2007) in southern Chile: Analysis using joint hypocenter determination, *J. Seismol.*, *14*, 683–691, doi:10.1007/s10950-010-9190-y.

Moreno, M. S., J. Klotz, D. Melnick, H. Echtler, and K. Bataille (2008), Active faulting and heterogeneous deformation across a megathrust segment boundary from GPS data, south central Chile (36–39°S), *Geochem. Geophys. Geosyst.*, *9*, Q12024, doi:10.1029/2008GC002198.

Nocquet, J. M., and E. Calais (2003), Crustal velocity field of western Europe from permanent GPS array solutions, 1996–2001, *Geophys. J. Int.*, *154*(1), 72–88.

Nocquet, J. M., E. Calais, Z. Altamimi, P. Sillard, and C. Boucher (2001), Intraplate deformation in western Europe deduced from an analysis of the International Terrestrial Reference Frame 1997 (ITRF97) velocity field, *J. Geophys. Res.*, *106*, 11,239–11,257, doi:10.1029/2000JB900410.

Norabuena, E., I. Leffler-Griffin, A. Mao, T. Dixon, S. Stein, I. S. Sachs, L. Ocola, and M. Ellis (1998), Space geodetic observations of Nazca-South America convergence across the central Andes, *Science*, *279*, 358–362, doi:10.1126/science.279.5349.358.

Norabuena, E., et al. (2004), Geodetic and seismic constraints on some seismogenic zone processes in Costa Rica, *J. Geophys. Res.*, *109*, B11403, doi:10.1029/2003JB002931.

Oldow, J. S., L. Ferranti, D. S. Lewis, J. K. Campbell, B. D'Argenio, R. Catalano, G. Pappone, L. Carmignani, P. Conti, and C. L. V. Aiken (2002), Active fragmentation of Adria, the north African promontory, central Mediterranean orogen, *Geology*, *30*, 779–782, doi:10.1130/0091-7613(2002)030<0779:AFOATN>2.0.CO;2.

Parker, R. N., A. L. Densmore, N. J. Rosser, M. de Michele, Y. Li, R. Huang, S. Whadcoat, and D. N. Petley (2011), Mass wasting triggered by the 2008 Wenchuan earthquake is greater than orogenic growth, *Nat. Geosci.*, *4*, 449–452, doi:10.1038/ngeo1154.

Pedersen, V. K., D. L. Egholm, and S. B. Nielsen (2010), Alpine glacial topography and the rate of rock column uplift: A global perspective, *Geomorphology*, *122*, 129–139, doi:10.1016/j.geomorph.2010.06.005.

Penck, A. (1905), Glacial features in the surface of the Alps, *J. Geol.*, *13*, 1–19, doi:10.1086/621202.

Perron, J. T., J. W. Kirchner, and W. E. Dietrich (2009), Formation of evenly spaced ridges and valleys, *Nature*, *460*, 502–505, doi:10.1038/nature08174.

Pinet, P., and M. Souriau (1988), Continental erosion and large-scale relief, *Tectonics*, *7*, 563–582, doi:10.1029/TC007i003p00563.

Portenga, E. W., and P. R. Bierman (2011), Understanding Earth's eroding surface with [10]Be, *GSA Today*, *21*(8), 4–10, doi:10.1130/G111A.1.

Porter, S. C. (1977), The glacial ages: Late Cenozoic climatic variability on several time scales, in *Man and Nature - Makers of Climatic Variation*, pp. 1–27, Coll. of Geosci., Texas A&M Univ., College Station.

Porter, S. C. (1989), Some geological implications of average Quaternary glacial conditions, *Quat. Res.*, *32*(3), 245–261, doi:10.1016/0033-5894(89)90092-6.

Reigber, C., G. W. Michel, R. Galas, D. Angermann, J. Klotz, J.-Y. Chen, A. Papschev, R. Arslanov, V. E. Tzurkov, and M. C. Ishanov (2001), New space geodetic constraints on the distribution of deformation in Central Asia, *Earth Planet. Sci. Lett.*, *191*, 157–165, doi:10.1016/S0012-821X(01)00414-9.

Reilinger, R., et al. (2006), GPS constraints on continental deformation in the Africa-Arabia-Eurasia continental collision zone and implications for the dynamics of plate interactions, *J. Geophys. Res.*, *111*, B05411, doi:10.1029/2005JB004051.

Roe, G. (2005), Orographic precipitation, *Annu. Rev. Earth Planet. Sci.*, *33*, 645–671, doi:10.1146/annurev.earth.33.092203.122541.

Roe, G., D. R. Montgomery, and B. Hallet (2002), Effects of orographic precipitation variations on the concavity of steady-state river profiles, *Geology*, *30*, 143–146, doi:10.1130/0091-7613(2002)030<0143:EOOPVO>2.0.CO;2.

Roe, G., K. X. Whipple, and J. K. Fletcher (2008), Feedbacks among climate, erosion, and tectonics in a critical wedge orogen, *Am. J. Sci.*, *308*, 815–842, doi:10.2475/07.2008.01.

Roering, J. J., J. T. Perron, and J. W. Kirchner (2007), Functional relationships between denudation and hillslope form and relief, *Earth Planet. Sci. Lett.*, *264*, 245–258, doi:10.1016/j.epsl.2007.09.035.

Rosenau, M., D. Melnick, and H. Echtler (2006), Kinematic constraints on intra-arc shear and strain partitioning in the southern Andes between 38°S and 42°S latitude, *Tectonics*, *25*, TC4013, doi:10.1029/2005TC001943.

Ruegg, J. C., J. Campos, R. Madariaga, E. Kausel, J. B. DeChabalier, R. Armijo, D. Dimitrov, I. Georgiev, and S. Barrientos (2002), Interseismic strain accumulation in south central Chile from GPS measurements, 1996–1999, *Geophys. Res. Lett.*, *29*(11), 1517, doi:10.1029/2001GL013438.

Ruegg, J. C., A. Rudloff, A. Vigny, R. Madariaga, J. B. de Chabalier, J. Campos, E. Kausel, S. Barrientos, and D. Dimitrov (2009), Interseismic strain accumulation measured by GPS in the seismic gap between Constitución and Concepción in Chile, *Phys. Earth Planet. Inter.*, *175*, 78–85, doi:10.1016/j.pepi.2008.02.015.

Scalabrino, B., Y. Lagabrielle, J. Malavieille, S. Dominguez, D. Melnick, F. Espinoza, M. Suarez, and E. Rossello (2010), A morphotectonic analysis of central Patagonian Cordillera: Negative inversion of the Andean belt over a buried spreading center?, *Tectonics*, *29*, TC2010, doi:10.1029/2009TC002453.

Schildgen, T. F., K. V. Hodges, K. X. Whipple, P. W. Reiners, and M. S. Pringle (2007), Uplift of the western margin of the Andean plateau revealed from canyon incision history, southern Peru, *Geology*, *35*, 523–526, doi:10.1130/G23532A.1.

Schlunegger, F., G. Zeilinger, A. Kounov, F. Kober, and B. Hüsser (2006), Scale of relief growth in the forearc of the Andes of Northern Chile (Arica latitude, 18°S), *Terra Nova*, *18*, 217–223, doi:10.1111/j.1365-3121.2006.00682.x.

Seager, R., D. R. Battisti, J. Yin, N. Gordon, N. Naik, A. C. Clement, and M. A. Cane (2002), Is the Gulf Stream responsible for Europe's mild winters?, *Q. J. R. Meteorol. Soc.*, *128*, 2563–2586, doi:10.1256/qj.01.128.

Serpelloni, E., M. Anzidei, P. Baldi, G. Casula, and A. Galvani (2005), Crustal velocity and strain-rate fields in Italy and surrounding regions: New results from the analysis of permanent and non-permanent GPS networks, *Geophys. J. Int.*, *161*(3), 861–880, doi:10.1111/j.1365-246X.2005.02618.x.

Shuster, D. L., T. A. Ehlers, M. E. Rusmore, and K. A. Farley (2005), Rapid glacial erosion at 1.8 Ma revealed by 4He/3He thermochronometry, *Science*, *310*, 1668–1670, doi:10.1126/science.1118519.

Shyu, J. B. H., K. Sieh, J. P. Avouac, W. S. Chen, and Y. G. Chen (2006), Millennial slip rate of the Longitudinal Valley fault from river terraces: Implications for convergence across the active suture of eastern Taiwan, *J. Geophys. Res.*, *111*, B08403, doi:10.1029/2005JB003971.

Simoes, M., J. Braun, and S. P. Bonnet (2010), Continental-scale erosion and transport laws: A new approach to quantitatively investigate macro-scale landscapes and associated sediment fluxes over the geological past, *Geochem. Geophys. Geosyst.*, *11*, Q09001, doi:10.1029/2010GC003121.

Simons, W. J. F., et al. (2007), A decade of GPS in Southeast Asia: Resolving Sundaland motion and boundaries, *J. Geophys. Res.*, *112*, B06420, doi:10.1029/2005JB003868.

Sitchler, J. C., D. M. Fisher, T. W. Gardner, and M. Protti (2007), Constraints on inner forearc deformation from balanced cross sections, Fila Costeña thrust belt, Costa Rica, *Tectonics*, *26*, TC6012, doi:10.1029/2006TC001949.

Small, E. E., and R. S. Anderson (1998), Pleistocene relief production in Laramide mountain ranges, western United States, *Geology*, *26*, 123–126, doi:10.1130/0091-7613(1998)026<0123:PRPILM>2.3.CO;2.

Smith, R. B. (1979), The influence of mountains on the atmosphere, *Adv. Geophys.*, *27*, 87–230, doi:10.1016/S0065-2687(08)60262-9.

Snyder, N. P., K. X. Whipple, G. E. Tucker, and D. J. Merritts (2003), Importance of a stochastic distribution of floods and erosion thresholds in the bedrock river incision problem, *J. Geophys. Res.*, *108*(B2), 2117, doi:10.1029/2001JB001655.

Socquet, A., W. Simons, C. Vigny, R. McCaffrey, C. Subarya, D. Sarsito, B. Ambrosius, and W. Spakman (2006), Microblock rotations and fault coupling in SE Asia triple junction (Sulawesi, Indonesia) from GPS and earthquake slip vector data, *J. Geophys. Res.*, *111*, B08409, doi:10.1029/2005JB003963.

Spotila, J. A., J. T. Buscher, A. J. Meigs, and P. W. Reiners (2004), Long-term glacial erosion of active mountain belts: Example of the Chugach-St. Elias Range, Alaska, *Geology*, *32*, 501–504, doi:10.1130/G20343.1.

Steblov, G. M., M. G. Kogan, R. W. King, C. H. Scholz, R. Bürgmann, and D. I. Frolov (2003), Imprint of the North American plate in Siberia revealed by GPS, *Geophys. Res. Lett.*, *30*(18), 1924, doi:10.1029/2003GL017805.

Stern, T. A., A. K. Baxter, and P. J. Barrett (2005), Isostatic rebound due to glacial erosion within the Transantarctic Mountains, *Geology*, *33*, 221–224, doi:10.1130/G21068.1.

Stolar, D. B., S. Willett, and G. Roe (2006), Climatic and tectonic forcing of a critical orogen, *Spec. Pap. Geol. Soc. Am.*, *398*, 241–250.

Stolar, D. B., G. Roe, and S. Willett (2007), Controls on the patterns of topography and erosion rate in a critical orogen, *J. Geophys. Res.*, *112*, F04002, doi:10.1029/2006JF000713.

Strahler, A. N. (1950), Equilibrium theory of erosional slopes approached by frequency distribution analysis Part I, *Am. J. Sci.*, *248*, 673–696, doi:10.2475/ajs.248.10.673.

Strecker, M. R., R. N. Alonso, B. Bookhagen, B. Carrapa, G. E. Hilley, E. R. Sobel, and M. H. Trauth (2007), Tectonics and climate of the southern central Andes, *Annu. Rev. Earth Planet. Sci.*, *35*, 747–787, doi:10.1146/annurev.earth.35.031306.140158.

Stüwe, K., L. White, and R. Brown (1994), The influence of eroding topography on steady-state isotherms: Application to fission track analysis, *Earth Planet. Sci. Lett.*, *124*, 63–74, doi:10.1016/0012-821X(94)00068-9.

Sugden, D. E., and B. S. John (1969), *Glaciers and Landscape: A Geomorphological Approach*, Edward Arnold, London.

Suito, H., and J. T. Freymueller (2009), A viscoelastic and afterslip postseismic deformation model for the 1964 Alaska earthquake, *J. Geophys. Res.*, *114*, B11404, doi:10.1029/2008JB005954.

Sutherland, R., K. Berryman, and R. Norris (2006), Quaternary slip rate and geomorphology of the Alpine fault: Implications for kinematics and seismic hazard in southwest New Zealand, *Geol. Soc. Am. Bull.*, *118*, 464–474, doi:10.1130/B25627.1.

Tatar, M., D. Hatzfeld, J. Martinod, A. Walpersdorf, M. Ghafori-Ashtiany, and J. Chéry (2002), The present-day deformation of the central Zagros from GPS measurements, *Geophys. Res. Lett.*, *29*(19), 1927, doi:10.1029/2002GL015427.

Thompson, S. C., R. J. Weldon, C. M. Rubin, K. Abdarkhmatov, P. Molnar, and G. W. Berger (2002), Late Quaternary slip rates across the central Tien Shan, Kyrgyzstan, central Asia, *J. Geophys. Res.*, *107*(B9), 2203, doi:10.1029/2001JB000596.

Thomson, S. N., M. T. Brandon, J. H. Tomkin, P. W. Reiners, C. Vasquez, and N. J. Wilson (2010), Glaciation as a destructive and constructive control on mountain building, *Nature*, *467*, 313–317, doi:10.1038/nature09365.

Tomkin, J. H., and J. Braun (2002), The influence of alpine glaciation on the relief of tectonically active mountain belts, *Am. J. Sci.*, *302*, 169–190, doi:10.2475/ajs.302.3.169.

Tregoning, P. (2003), Is the Australian Plate deforming? A space geodetic perspective, *Spec. Pap. Geol. Soc. Am.*, *372*, 41–48.

Trenkamp, R., J. N. Kellogg, J. T. Freymueller, and H. P. Mora (2002), Wide plate margin deformation, southern Central America and northwestern South America, CASA GPS observations, *J. South Am. Earth Sci.*, *15*(2), 157–171, doi:10.1016/S0895-9811(02)00018-4.

Valla, P. G., D. L. Shuster, and P. A. Van Der Beek (2011), Significant increase in relief of the European Alps during Mid-Pleistocene glaciations, *Nat. Geosci.*, *4*, 688–692, doi:10.1038/ngeo1242.

Vernant, P., F. Nilforoushan, J. Chéry, R. Bayer, Y. Djamour, F. Masson, H. Nankali, J. F. Ritz, M. Sedighi, and F. Tavakoli (2004a), Deciphering oblique shortening of central Alborz in Iran using geodetic data, *Earth Planet. Sci. Lett.*, *223*, 177–185, doi:10.1016/j.epsl.2004.04.017.

Vernant, P., et al. (2004b), Present-day crustal deformation and plate kinematics in the Middle East constrained by GPS measurements in Iran and northern Oman, *Geophys. J. Int.*, *157*(1), 381–398, doi:10.1111/j.1365-246X.2004.02222.x.

Volk, T. (1987), Feedbacks between weathering and atmospheric CO_2 over the last 100 million years, *Am. J. Sci.*, *287*, 763–779, doi:10.2475/ajs.287.8.763.

von Blanckenburg, F. (2005), The control mechanisms of erosion and weathering at basin scale from cosmogenic nuclides in river sediment, *Earth Planet. Sci. Lett.*, *237*, 462–479, doi:10.1016/j.epsl.2005.06.030.

von Rotz, R., F. Schlunegger, F. Heller, and I. Villa (2005), Assessing the age of relief growth in the Andes of northern Chile: Magneto-polarity chronologies from Neogene continental sections, *Terra Nova*, *17*, 462–471, doi:10.1111/j.1365-3121.2005.00634.x.

Wager, L. R. (1937), The Arun River drainage pattern and the rise of the Himalaya, *Geogr. J.*, *89*, 239–250, doi:10.2307/1785796.

Wallace, L. M., C. Stevens, E. Silver, R. McCaffrey, W. Loratung, S. Hasiata, R. Stanaway, R. Curley, R. Rosa, and J. Taugaloidi (2004), GPS and seismological constraints on active tectonics and arc-continent collision in Papua New Guinea: Implications for mechanics of microplate rotations in a plate boundary zone, *J. Geophys. Res.*, *109*, B05404, doi:10.1029/2003JB002481.

Walpersdorf, A., D. Hatzfeld, H. Nankali, F. Tavakoli, F. Nilforoushan, M. Tatar, P. Vernant, J. Chery, and F. Masson (2006), Difference in the GPS deformation pattern of north and central zagros (Iran), *Geophys. J. Int.*, *167*(3), 1077–1088, doi:10.1111/j.1365-246X.2006.03147.x.

Wang, K., Y. Hu, M. Bevis, E. Kendrick, R. Smalley Jr., R. B. Vargas, and E. Lauría (2007), Crustal motion in the zone of the 1960 Chile earthquake: Detangling earthquake-cycle deformation and forearc-sliver translation, *Geochem. Geophys. Geosyst.*, *8*, Q10010, doi:10.1029/2007GC001721.

Weber, J., M. Vrabec, P. Pavlovčič-Prešeren, T. Dixon, Y. Jiang, and B. Stopar (2010), GPS-derived motion of the Adriatic microplate from Istria Peninsula and Po Plain sites, and geodynamic implications, *Tectonophysics*, *483*, 214–222, doi:10.1016/j.tecto.2009.09.001.

Wellman, H. W. (1979), An uplift map for the South Island of New Zealand, and a model for uplift of the Southern Alps, in *The Origin of the Southern Alps*, edited by R. I. Walcott and M. M. Cresswell, *Bull. R. Soc. N. Z.*, *18*, 13–20.

Whipple, K. X., and B. J. Meade (2006), Orogen response to changes in climatic and tectonic forcing, *Earth Planet. Sci. Lett.*, *243*, 218–228, doi:10.1016/j.epsl.2005.12.022.

Whipple, K. X., E. Kirby, and S. H. Brocklehurst (1999), Geomorphic limits to climate-induced increases in topographic relief, *Nature*, *401*, 39–43, doi:10.1038/43375.

White, S. M., R. Trenkamp, and J. N. Kellogg (2003), Recent crustal deformation and the earthquake cycle along the Ecuador-Colombia subduction zone, *Earth Planet. Sci. Lett.*, *216*, 231–242, doi:10.1016/S0012-821X(03)00535-1.

Willenbring, J. K., and F. von Blanckenburg (2010), Long-term stability of global erosion rates and weathering during late-Cenozoic cooling, *Nature*, *465*, 211–214, doi:10.1038/nature09044.

Willett, S. D. (1999), Orogeny and orography: The effects of erosion on the structure of mountain belts, *J. Geophys. Res.*, *104*, 28,957–28,981, doi:10.1029/1999JB900248.

Willett, S. D., and M. T. Brandon (2002), On steady states in mountain belts, *Geology*, *30*, 175–178, doi:10.1130/0091-7613(2002)030<0175:OSSIMB>2.0.CO;2.

Willett, S. D., C. Beaumont, and P. Fullsack (1993), Mechanical model for the tectonics of doubly vergent compressional orogens, *Geology*, *21*, 371–374, doi:10.1130/0091-7613(1993)021<0371:MMFTTO>2.3.CO;2.

Yang, S.-M., J. Li, and Q. Wang (2008), The deformation pattern and fault rate in the Tianshan Mountains inferred from GPS observations, *Sci. China D*, *51*, 1064–1080, doi:10.1007/s11430-008-0090-8.

Yu, S.-B., H.-Y. Chen, and L.-C. Kuo (1997), Velocity field of GPS stations in the Taiwan Area, *Tectonophysics*, *274*, 41–59, doi:10.1016/S0040-1951(96)00297-1.

Zeitler, P. K., et al. (2001), Crustal reworking at Nanga Parbat, Pakistan: Metamorphic consequences of thermal-mechanical coupling facilitated by erosion, *Tectonics*, *20*, 712–728, doi:10.1029/2000TC001243.

Zhang, P.-Z., P. Molnar, and W. R. Downs (2001), Increased sedimentation rates and grain sizes 2–4 Myr ago due to the influence of climate change on erosion rates, *Nature*, *410*, 891–897, doi:10.1038/35073504.

Zhang, P.-Z., Z. Shen, M. Wang, W. J. Gan, R. Burgmann, and P. Molnar (2004), Continuous deformation of the Tibetan Plateau from global positioning system data, *Geology*, *32*, 809–812, doi:10.1130/G20554.1.

Zielinski, G. A. (2000), Use of paleo-records in determining variability within the volcanism–climate system, *Quat. Sci. Rev.*, *19*, 417–438.

Zubovich, A. V., et al. (2010), GPS velocity field for the Tien Shan and surrounding regions, *Tectonics*, *29*, TC6014, doi:10.1029/2010TC002772.

Zubovich, A. V., et al. (2011), GPS velocity field for the Tien Shan and surrounding regions, *Tectonics*, *29*, TC6014, doi:10.1029/2010TC002772.

J.-D. Champagnac and F. Herman, Department of Earth Sciences, Geological Institute, Swiss Federal Institute of Technology, Sonneggstr. 5, CH-8092 Zürich, Switzerland. (jean-daniel.champagnac@erdw.ethz.ch)

P. Molnar, Department of Geological Sciences, Cooperative Institute for Research in Environmental Science, University of Colorado at Boulder, Benson Earth Sciences Building, Campus Box 399, Rm. 462C, Boulder, CO 80309, USA.

C. Sue, Laboratoire Chrono-Environnement, UMR 6249, Université de Franche-Comté, 16 route de Gray, F-25030 Besançon CEDEX, France.